

# **Pharmaceutically relevant protein-protein interactions for controlled drug delivery**

Dissertation zur Erlangung des naturwissenschaftlichen Doktorgrades der  
Julius-Maximilians-Universität Würzburg

vorgelegt von

Vera Werner  
aus Werneck

Würzburg 2015

Eingereicht bei der Fakultät für Chemie und Pharmazie am

\_\_\_\_\_

Gutachter der schriftlichen Arbeit

1. Gutachter: \_\_\_\_\_

2. Gutachter: \_\_\_\_\_

Prüfer des öffentlichen Promotionskolloquiums

1. Prüfer: \_\_\_\_\_

2. Prüfer: \_\_\_\_\_

3. Prüfer: \_\_\_\_\_

Datum des öffentlichen Promotionskolloquiums

\_\_\_\_\_

Doktorurkunde ausgehändigt am

\_\_\_\_\_

Die vorliegende Arbeit wurde in der Zeit von März 2011 bis März 2015 am Institut für Pharmazie und Lebensmittelchemie der Bayerischen Julius-Maximilians-Universität Würzburg unter der  
Anleitung von  
**Herr Prof. Dr. Dr. Lorenz Meinel**  
angefertigt.



# TABLE OF CONTENTS

SUMMARY .....	1
ZUSAMMENFASSUNG .....	3
CHAPTER I.....	7
<i>From silk spinning in insects and spiders to advanced silk fibroin drug delivery systems</i>	
CHAPTER II .....	31
<i>The effects of Hofmeister salts on silk fibroin and its interaction pattern</i>	
CHAPTER III.....	59
<i>Immobilizing of interleukin-4 for permanent M2-activation of macrophages</i>	
GENERAL CONCLUSIONS AND OUTLOOK .....	101
ABBREVIATIONS .....	109
Data from this dissertation thesis was published or presented before as follows .....	111
CURRICULUM VITAE .....	113
ACKNOWLEDGMENTS .....	115



## SUMMARY

Protein-protein interactions play a crucial role in the development of drug delivery devices for the increasingly important biologicals, including antibodies, growth factors and cytokines. The understanding thereof might offer opportunities for tailoring carriers or drug proteins specifically for this purpose and thereby allow controlled delivery to a chosen target. The possible applications range from trigger-dependent release to sustained drug delivery and possibly permanently present stimuli, depending on the anticipated mechanism.

Silk fibroin (SF) is a biomaterial that is suitable as a carrier for protein drug delivery devices. It combines processability under mild conditions, good biocompatibility and stabilizing effects on incorporated proteins.

As SF is naturally produced by spiders and silkworms, the understanding of this process and its major factors might offer a blueprint for formulation scientists, interested in working with this biopolymer. The natural process of silk spinning covers a fascinating versatility of aggregate states, ranging from colloidal solutions through hydrogels to solid systems. The transition among these states is controlled by a carefully orchestrated process *in vivo*. Major players within the natural process include the control of spatial pH throughout passage of the silk dope, the composition and type of ions, and fluid flow mechanics within the duct, respectively. The function of these input parameters on the spinning process is reviewed before detailing their impact on the design and manufacture of silk based drug delivery systems (DDS). Examples are reported including the control of hydrogel formation during storage or significant parameters controlling precipitation in the presence of appropriate salts, respectively. The review details the use of silk fibroin to develop liquid, semiliquid or solid DDS with a focus on the control of SF crystallization, particle formation, and drug-SF interaction for tailored drug load.

Although we were able to show many examples for SF drug delivery applications and there are many publications about the loading of biologics to SF systems, the mechanism of interaction between both in solution was not yet extensively explored. This is why we made this the subject of our work, as it might allow for direct influence on pharmaceutical parameters, like aggregation and drug load.

In order to understand the underlying mechanism for the interaction between SF and positively charged model proteins, we used isothermal titration calorimetry for thermodynamic characterization. This was supported by hydrophobicity analysis and by colloidal characterization

methods including static light scattering, nanoparticle tracking analysis and zeta potential measurements. We studied the effects of three Hofmeister salts – NaCl (neutral), NaSCN (chaotropic) and Na<sub>2</sub>SO<sub>4</sub> (cosmotropic) – and the pH on the interaction of SF with the model proteins in dependence of the ratio from one to another. The salts impacted the SF structure by stabilizing (cosmotropic) or destabilizing (chaotropic) the SF micelles, resulting in completely abolished (cosmotropic) or strongly enhanced (chaotropic) interaction. These effects were responsible for different levels of loading and coacervation when varying type of salt and its concentration. Additionally, NaCl and NaSCN were able to prolong the stability of aqueous SF solution during storage at 25°C in a preliminary study.

Another approach to influence protein-protein interactions was followed by covalent modification. Interleukin-4 (IL-4) is a cytokine driving macrophages to M2 macrophages, which are known to provide anti-inflammatory effects. The possibility to regulate the polarization of macrophages to this state might be attractive for a variety of diseases, like atherosclerosis, in which macrophages are involved. As these cases demand a long-term treatment, this polarization was supposed to be maintained over time and we were planning to achieve this by keeping IL-4 permanently present in an immobilized way. In order to immobilize it, we genetically introduced an alkyne-carrying, artificial amino acid in the IL-4 sequence. This allowed access to a site-specific click reaction (Cu(I)-catalyzed Huisgen azide-alkyne cycloaddition) with an azide partner. This study was able to set the basis for the project by successful expression and purification of the IL-4 analogue and by proving the availability for the click reaction and maintained bioactivity. The other side of this project was the isolation of human monocytes and the polarization and characterization of human macrophages. The challenge here was that the majority of related research was based on murine macrophages which was not applicable to human cells and the successful work was so far limited to establishing the necessary methods.

In conclusion, we were able to show two different methods that allow the influence of protein-protein interactions and thereby the possible tailoring of drug loading. Although the results were very promising for both systems, their applicability in the development of drug delivery devices needs to be shown by further studies.



## ZUSAMMENFASSUNG

Die Wechselwirkungen zwischen Proteinen spielen eine entscheidende Rolle in der Entwicklung von Freigabesystemen für die immer wichtiger werdenden Protein-Therapeutika, wie Antikörper, Wachstumsfaktoren und Zytokine. Das Verständnis dieser Mechanismen würde die Möglichkeit eröffnen, sowohl die Träger, als auch die zu verabreichenden Proteine so zu verändern und zu steuern, dass sie auf kontrollierte Weise an einem bestimmten Ort freigesetzt werden. Die Anwendungen hierfür reichen von Trigger gesteuerter Freisetzung, über verzögerte Freigabe bis zur permanenten Präsentation von Stimuli, abhängig davon was für die jeweilige Applikation gewünscht ist.

Seidenfibroin (SF) ist ein Biomaterial, welches verschiedene positive Eigenschaften für die Anwendung als Trägermaterial in sich vereint, indem es unter sehr milden Bedingungen verarbeitet werden kann, gut biokompatibel ist und stabilisierend auf eingebettete Proteine wirken kann.

Da SF in der Natur von Spinnen und Seidenraupen produziert wird, könnte das Verständnis dieses Prozesses, sowie seiner wichtigsten Faktoren eine Vorlage für die Formulierung dieses Biopolymers geben. Der natürliche Prozess des Seidenspinnens vereint eine faszinierende Vielfalt von Aggregatzuständen, die von kolloidalen Lösungen über Hydrogele bis hin zu festen System reichen. Die Übergänge zwischen diesen Zuständen sind *in vivo* sehr sorgfältig kontrolliert. Die Hauptfaktoren dieses Prozesses sind der pH-Wert während der Passage der Spinnlösung durch die Drüse, sowie die Art und Zusammensetzung der Ionen und die herrschenden Scherkräfte. Die Funktion dieser einzelnen Faktoren auf den Spinnprozess wurde recherchiert und wird beschrieben, bevor ihr Einfluss auf die Entwicklung und Herstellung von seidenbasierten Freigabesystemen untersucht wird. Es werden Beispiele vorgestellt, die die Kontrolle der Hydrogelbildung während der Lagerung untersuchen oder signifikante Parameter für die kontrollierte Präzipitation in Gegenwart bestimmter Salze zeigen. Der Review betrachtet den Einsatz von Seidenfibroin in der Entwicklung von flüssigen, halbfesten oder festen Freigabesystemen und legt besonderen Fokus auf die Kontrolle der SF Kristallisation, Partikelbildung und Interaktion mit dem Arzneistoff für steuerbare Beladung.

Obwohl wir viele Beispiele für die Anwendung von SF in Freigabesystemen zeigen konnten und viele Publikationen die Beladung von Proteinen auf SF-Systeme behandeln, wurde der Mechanismus der Interaktion zwischen beiden bisher nicht detailliert untersucht. Es gibt wenige Studien die einige Aspekte abdecken, aber keines beschäftigte sich spezifisch mit dieser

Fragestellung. Darum machen wir dies zum Gegenstand unserer Arbeit, da dies einen direkten Einfluss auf pharmazeutische Parameter, wie Aggregation und Beladung, erlauben würde.

Um den zugrundeliegenden Mechanismus der Wechselwirkung zwischen SF und einem positiv geladenen Modellprotein zu verstehen, nutzten wir isotherme Titrationskalorimetrie für eine thermodynamische Charakterisierung. Diese wurde durch kolloidale Charakterisierungsmethoden wie Statische Lichtstreuung, nanoparticle tracking analysis und Zeta-potentialmessungen, sowie Hydrophobitätsbestimmungen unterstützt. Wir untersuchten die Effekte von drei verschiedenen Hofmeister Salzen - NaCl (neutral), NaSCN (chaotrop) und Na<sub>2</sub>SO<sub>4</sub> (kosmotrop) – und des pH Wertes auf die Interaktion von SF mit dem Modellprotein in Abhängigkeit vom Verhältnis der beiden zueinander. Die Salze beeinflussten die SF Struktur, indem sie die SF Mizellen entweder stabilisierten (kosmotrop) oder destabilisierten (chaotrop) und dadurch die Interaktion entweder vollständig unterbanden (kosmotrop) oder verstärkten (chaotrop). Diese Effekte waren verantwortlich für verschiedene Level des Loadings und der Koazervation, wenn Salzart und –konzentration variiert wurden. Außerdem waren NaCl und NaSCN in der Lage die Stabilität einer wässrigen SF-Lösung während der Lagerung bei 25°C zu verlängern.

Ein andere Ansatz um die Wechselwirkung zwischen Proteinen zu beeinflussen wurde mit kovalenter Modifikation verfolgt. Interleukin-4 (IL-4) ist ein Zytokin und kann Makrophagen zu M2 Makrophagen polarisieren, welche dann anti-inflammatorische Wirkungen haben. Die Möglichkeit diese Polarisation zu regulieren wäre für verschiedene Krankheiten, wie Arteriosklerose, bei denen Makrophagen eine Rolle spielen interessant. Da in diesen Fällen eine Langzeitbehandlung von Nöten ist sollte die Polarisation über die Zeit erhalten bleiben. Wir planten dies durch die Immobilisation von IL-4 zu erreichen, die für eine permanente Präsenz sorgen würde. Um IL-4 zu immobilisieren haben wir eine künstliche Aminosäure in die Sequenz eingeführt, die eine Alkingruppe trägt. Diese ermöglicht den Zugang zu einer Kupfer vermittelten, spezifischen Click-Reaktion (Cu(I)-catalyzed Huisgen azide-alkyne cycloaddition) mit einem Azid-Partner. Diese Studie war in der Lage die Basis für dieses Projekt zu erstellen, indem wir eine erfolgreiche Expression und Aufreinigung des IL-4 Analogons leisten konnten und dieses sowohl erhaltene Bioaktivität als auch Verfügbarkeit für die Clickreaktion zeigte.

Die andere Seite dieses Projekts bestand aus der Isolation von humanen Monozyten und der Polarisation und Charakterisierung von humanen Makrophagen. Die Herausforderung hierbei lag darin dass die meiste Forschung auf diesem Gebiet an murinen Makrophagen durchgeführt wurde und dies nicht auf humane Zellen übertragbar war, und die erfolgreiche Arbeit bisher, beschränkte sich auf die Etablierung der nötigen Methoden.

Zusammenfassend lässt sich sagen, dass wir in der Lage waren zwei verschiedene Methoden zur Beeinflussung der Protein-Protein Wechselwirkungen und damit der Beladung zu zeigen. Obwohl die Ergebnisse für beide Systeme vielversprechend waren muss ihre Anwendbarkeit in der Entwicklung von Freigabesystemen noch durch weitere Studien belegt werden.



# CHAPTER I

## FROM SILK SPINNING IN INSECTS AND SPIDERS TO ADVANCED SILK FIBROIN DRUG DELIVERY SYSTEMS

Full text literally transferred from:

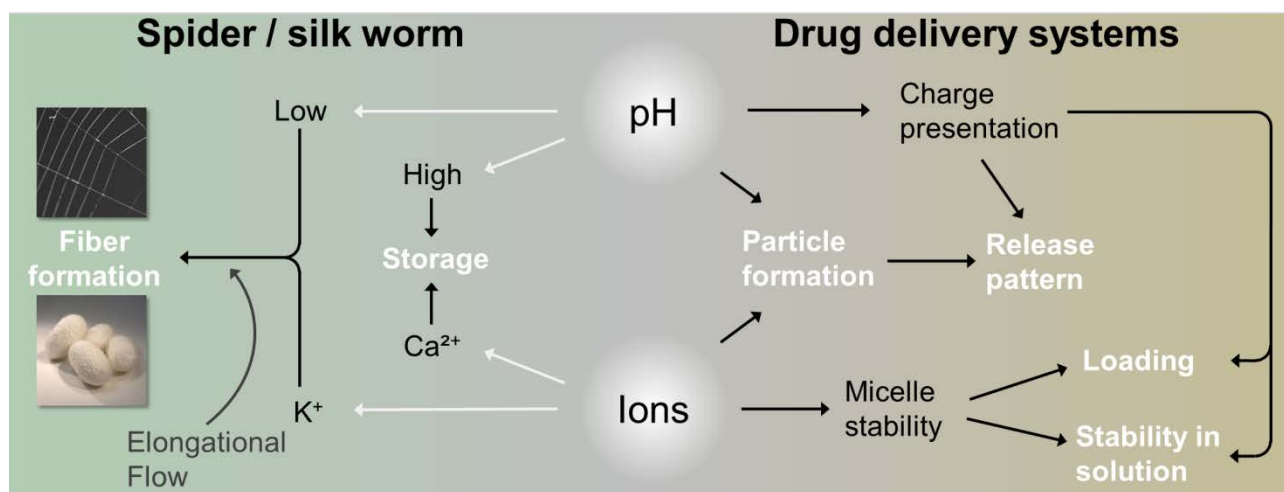
V. Werner, L. Meinel, From silk spinning in insects and spiders to advanced silk fibroin drug delivery systems, *European Journal of Pharmaceutics and Biopharmaceutics*, (2015), 10.1016/j.ejpb.2015.03.016.

With permission of Elsevier (License number: 3596990165187, License date: Mar 27, 2015)

This review was written by me, with supporting and improving work provided by Prof. Dr. Dr. Lorenz Meinel.

**Abstract**

The natural process of silk spinning covers a fascinating versatility of aggregate states, ranging from colloidal solutions through hydrogels to solid systems. The transition among these states is controlled by a carefully orchestrated process *in vivo*. Major players within the natural process include the control of spatial pH throughout passage of the silk dope, the composition and type of ions, and fluid flow mechanics within the duct, respectively. The function of these input parameters on the spinning process is reviewed before detailing their impact on the design and manufacture of silk based drug delivery systems (DDS). Examples are reported including the control of hydrogel formation during storage or significant parameters controlling precipitation in the presence of appropriate salts, respectively. The review details the use of silk fibroin (SF) to develop liquid, semiliquid or solid DDS with a focus on the control of SF crystallization, particle formation, and drug - SF interaction for tailored drug load.



## Introduction

Silk either from spiders or from silkworms has been of high research interest during the last decades in a variety of scientific fields due to extraordinary properties, ranging from inkjet applications [1], bio-resorptive optics [2], implants [3], or drug delivery of proteins [4] and small molecules [5, 6] in various application forms [7]. The silk fibers have a high toughness [8] comparable to high-performance polymers such as Kevlar [9] leading to the use of these fibers as suture material and for textiles since ancient times. Early studies linked the extraordinary mechanical properties of some silk threads to Nylon and reported linear mass density of the silk fiber from the cribellate spider genus *Araneus* of 7.8 den (den = mass in grams per 9 km) and 8.7 den for Nylon [10]. A distinguishing feature of these silk threads from Nylon, however, is the tensile strength and ductility. One colorful description was that these threads could be extended up to a length of 80 km before these would break under their own weight [11]. The mechanical properties of processed silk differ from the wild-type fibers [12-14] and are variable upon different treatment [15], but still make it an attractive material for musculoskeletal use and tissue engineering [16-22]. In contrast to manufacturing conditions of synthetic polymers, the natural process leading to silk is confined to physiologic conditions, i.e. all-aqueous processes at ambient temperatures, ambient pressure and within a moderate range of pH values. It is for these benign conditions that scaffolds, implants, or drug delivery systems (DDS) made from silk circumvent challenges arising from residual organic solvent or harsh conditions leading to stability challenges e.g. of co-formulated drugs [23-29]. Furthermore, the general cell- and biocompatibility has been demonstrated for sericin-free silk [30-33]. Another advantage is the stabilizing effect during storage and processing of co-formulated biologics in a silk matrix. This successful stabilization has particularly been shown for silk fibroin (SF) – the major component of whole silk for different proteins, as well as for small molecules [4, 23, 26, 29, 34-37] with excellent tolerability as demonstrated in pre-clinical studies [16, 38, 39]. The ability to tailor the biodegradability of silk [40] allows the balancing of mechanical stability and degradation rate, with SF being proteolytically degraded into uncritical degradation products [4, 41-44].

## Molecular structure and function of silk fibroin building blocks

The SF primary sequence, conformation and inter-molecular interaction allow for a perplexing self-assembly pattern which is key to understand the remarkable characteristics of this protein. This is based on a rather unusual amino acid composition, dominated by short side chained alanine, glycine, and serine, accounting for about 50–65% of SF [45-47]. Upon spinning, most of these are present in crystalline parts of SF, which was attributed to the tensile strength of the

material, whereas intermediate amorphous regions account for the rubber like properties and ductility [48, 49]. These properties are a function of absorbed water with a plasticizing effect [50]. The primary sequence is composed of hydrophobic blocks, combined with terminal and intermediate hydrophilic parts. The *in vivo* spinning process is tightly controlling the interaction of these hydrophobic blocks, thereby controlling the  $\beta$ -sheet formation and overall crystallinity. This control is at least in part by hydrophilic linkers positioned between the hydrophobic blocks. The charge of these linkers is a function of pH, ionic strength and composition of the surrounding phase. Furthermore, these linkers provide chain flexibility for protein folding and water solubility [51], allowing for micellar structures in which the larger and charged terminal blocks are discussed to point outside and interact with the surrounding phase [52]. The formation of micelles is favored by a folding of the SF molecules into loosely assembled structures allowing better interaction of the terminal hydrophilic blocks with the continuous phase and interaction of the hydrophobic blocks within the same molecules and/or with other SF molecules. At this stage, the molecules are still flexible and processes are reversible. With increasing interaction of these hydrophobic blocks the formation of  $\beta$ -sheets at least in part irreversibly locks the resulting structures. Increasing micelle concentration allows for increasing inter-micellar interaction, eventually leading to the formation of nanofibrils and liquid crystalline phases. These nanofibrils are further organized to fibers by stretching and progressing  $\beta$ -sheet formation. SFs from various species allow for this mechanism in spite of differences in their crystal forming regions, with e.g. *Bombyx mori* (*B.mori*) SF having glycine-alanine-glycine-alanine-glycine-serine repeats (GAGAGS)<sub>n</sub> and spider SF being composed of repeated poly(alanine) regions [53]. Each of these steps is governed by the composition of the surrounding phases, including pH, ionic strength of selected ions and protein composition comprising silk concentration. Aspects of these gained insights into the fascinating natural processes were recapitulated in laboratory experiments. The focus of this review is to delineate insights of the natural process in an effort to translate these for application in the design and manufacture of SF based DDS.

### **Silk processing in insects and spiders**

Insects and spiders have developed highly specialized glands in evolution. Some spiders produce up to seven different types of silks [54-56]. The focus of the following mechanistic description is on the gland for major ampullate silk, from which dragline and radial web fibers are built. This gland is divided into three main functional zones A to C (proximal to distal). In spiders' A-zone the core of the fiber is formed from spidroin 2 (spidroins are fibroins in spiders), which is secreted by tall cells from granules [57]. In these granules, Spidroin 2 is in a predominantly random



coil conformation, already showing some  $\beta$ -sheet and  $\alpha$ -turn patterns [54]. This dope solution containing small spherical droplets is transported to the B-zone. In the B-zone, spidroin 1 is secreted and coating the spidroin 2. Morphologically, the duct is now narrowing, which in turn increases the shear forces on the colloidal solution and pressure difference. It is this increase in pressure favoring conformational change to a  $\beta$ -sheet structure along with controlled acidification (*vide infra*). The spidroin pre-formed fiber is now progressing into a segment within which water and sodium are further removed from the lumen and potassium, surfactants and lubricants are added [55]. Additionally, proton pumps are further decreasing the pH and the morphology of the duct is changing into small tube like, tapered structures. The liquid phase is exposed to low and uniform stress within this channel like part of the duct, allowing a careful orientation of the SF molecules along the gradient. Once the solution reaches the drawdown taper, the force required for moving the dope along the wall becomes larger than the force of drawing the thread and the dope detaches to form a narrow thread. A valve is located distally, through which a broken thread can be gripped, the spinning process can be restarted and the thread is repaired [58]. The spigot positioned at the distal outlet is further removing residual water and forcing the fiber outside. The morphology of the *B. mori* silk gland is different from spiders (*vide supra*) and divided into three anatomical units [59]. The thin and flexuous posterior part of the synthesizing unit is responsible for SF production and synthesis of the P25 accessory protein which are then transported to a wider middle part where they are stored as a concentrated hydrogel. In the following distal part the expression of sericin, which is coating the SF core, peaks. The fluids entering the subsequently tapered duct are exposed to a low and constant extensional flow. Furthermore, pumps are located in the proximal duct for the regulation of pH and ion type as well as ion concentration. By these means and in analogy to what was described above for spider silk processing, the interplay of precisely controlled fluid mechanics as well as appropriately balanced ion types, ion concentrations, and pH is responsible for the orientation of liquid crystalline phases. Continuing active removal of water and proceeding  $\beta$ -sheet formation lead to a thread at the exit of the spigot. These exciting insights as well as recent advancements in the understanding of the natural spinning processes prompted us to select three major input parameters, critically impacting the formation of silk threads *in vivo*. We translate the role of these parameters within the *in vivo* spinning process to the application for the manufacture of drug delivery systems. The factors are the (i) pH, (ii) ion composition and (iii) fluid flow of the dope in the natural spinning process (**Figure 1**).

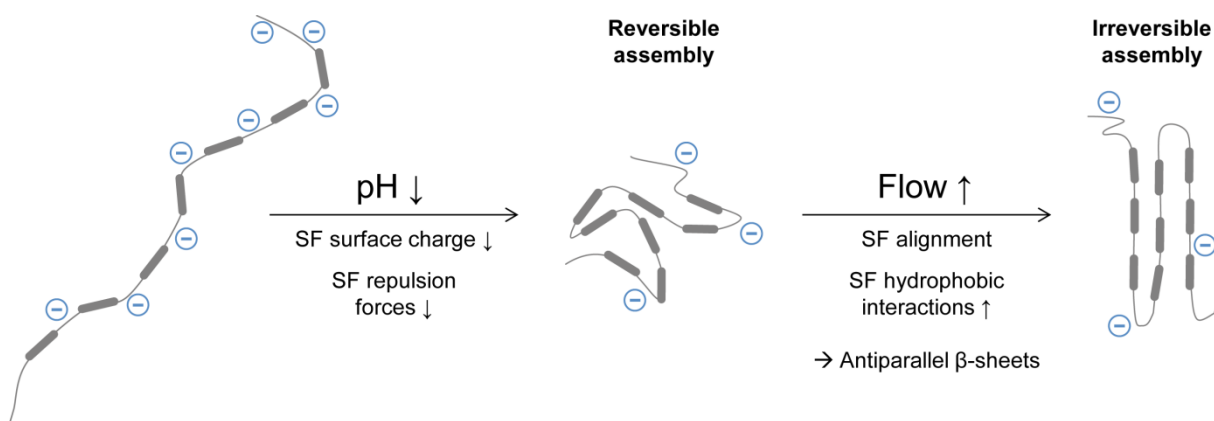


**Figure 1:** Schematic overview of the natural spinning process with a focus on the impact of pH and elongational flow on a single SF molecule. SF = Silk fibroin

## *pH*

A thorough understanding of the molecular structure of the SF molecule (*vide supra*) is key to unlock the biopolymer's responsiveness to pH gradients. As pointed out before, hydrophobic blocks are positioned between hydrophilic spacers and this “block polymer” like structure is flanked N- and C- terminally by a hydrophilic head and tail, respectively. The hydrophobic (and crystal forming) blocks do not carry charges and are not responsive to pH. However, the hydrophilic spacers are acidic as are the N-terminal head group and the C-terminally bound light chain of SF, leading to a negative net charge at neutral pH and as reflected by an isoelectric point (*pI*) of about 4 [4, 60]. The role of the N-terminal domain is particularly well documented for the pH-dependent control of fiber formation, preventing premature formation of  $\beta$ -sheets at neutral pH and guiding fiber formation during acidification [61-63] and has been reviewed before [64, 65]. The role of the C-terminus includes influence on both, storage and ordered assembly [66, 67].

The pH in the gland of spiders can be actively adjusted by using different mechanisms [60]. In the A-zone the pH is approximately neutral, followed by gradual acidification in the B-zone by virtue of proton pumps as well as by the secretion of acidic polysaccharides, resulting in a pH of 6.3 in the duct [54, 68]. Acidification lowers charges on the acidic SF, which lowers repulsive forces among molecules. Thereby, the hydrophobic blocks may reassemble leading to increased  $\beta$ -sheet content eventually leading to gelation. Structural studies using circular dichroism detailed conformational changes of SF as a function of acidification [60]. Another model emphasized the impact of potassium ion concentrations along with pH changes leading to an unfolding of the spider SF molecule through breakage of its water shell and facilitating molecular alignment along the flow gradient leading to the formation of antiparallel chains [69]. The pH further impacts the liquid crystalline state of SF and a transition from nematic to cholesteric phases was observed under fluid

flow, ultimately leading to phase separation with one phase rich in SF and one phase rich in solvent as a result of the formation of SF threads [55, 69, 70]. The phase separation was further detailed for SF from *B. mori* silk, studying the shear response of SF under a variety of different input parameters, including purity and concentration. Phase separation was observed at a critical shear rate at which  $\beta$ -sheet formation was induced. The critical shear rate was a function of SF concentration, intermolecular interaction and pH, more specifically when operating close to the critical micelle concentration (CMC) at which shear sensitivity reached its maximum [71]. Subsequent studies detailed these findings, corroborating the impact of pH on the conformation of spider and silkworm SF and stressing the importance for precise pH control for proper thread formation [72].

### ***Ion composition***

Ion composition and ion concentration play a pivotal role in silk spinning in spiders [68, 69]. Along the duct, a gradual decrease is observed for sodium and chloride ions parallel to a gradual increase for potassium, phosphor and sulfur containing ions. Sodium and potassium have opposing gradients in the duct. Potassium ions are chaotropic, hence affecting the structure of water and facilitating unfolding. Thereby, increased potassium cation concentrations may prime the silk for unfolding, which is facilitated at decreasing pH and leading to the formation of crystalline  $\beta$ -sheets [60]. In contrast, calcium, and magnesium were suggested to stabilize SF in its disordered state, thereby reducing intermolecular interaction,  $\beta$ -sheet content, crystallinity, and aggregation [60].

The impact of ions on *B. mori* silk was also detailed [73]. The finding of increasing copper concentrations at distal sites of the duct correlated with the facilitated formation of  $\beta$ -sheets. Similarly, the increase of sodium and potassium along the duct increased crystallization priming thread formation during spinning. In spite of the fact that potassium had only minor impact on SF conformation, the cation was suggested to support *in vivo* fiber formation during spinning by destabilizing the gel structure, which in return increases the mobility of SF as a prerequisite for the formation of  $\beta$ -sheets. The impact of calcium was detailed to result in a stabilizing effect of SF hydrogels. Mechanistically, this stabilization was linked to electrostatic interaction between the bivalent cation and deprotonated carboxyl groups on SF [74]. Evidence was collected for this hypothesis by complexing the bivalent cations with EDTA, which resulted in SF hydrogel collapse [72].

***Fluid flow***

The control of fluid flow/shear forces of the dope solution is of essential importance for successful spinning, requiring a precise interplay with other factors, including pH, ions, and gradients of larger molecules. A prerequisite of proper alignment is partial unfolding of SF as triggered by potassium cations and acidification. Thereby, a molecular chain rearrangement along the flow vectors of the fluid is facilitated. Upon alignment, inter-molecular hydrogen bonds are formed, resulting in anti-parallel arrangement and some parts may form hairpin loops. Also, the hydrophobic blocks get closer and van der Waals forces lead to  $\beta$ -pleated structures [69]. Anatomically,  $\beta$ -sheets were found at the beginning of the draw-down taper, a site at which shear stress suddenly increases [75]. Proximal to this site, a constant but slow flow rate is maintained and it is these mechanics which in concert with the other factors mentioned before prevent premature crystallization. Spherical silk structures are found in zone A [58], elongating into ellipsoid structures in the distal B-zone [70]. This carefully orchestrated state is priming the silk dope for the last step of fibril formation, acidification in addition to the precisely tailored fluid flow, as deduced from studies using genetically engineered SF variants [76]. In spite of the fact that these observations were made on spider silks, striking analogy has been presented for *B. mori* silk [59]. An anatomical difference between spiders and the silkworm is the longer duct for the latter. Previous reports linked the constant and slow flow in the proximal part of the duct in the silkworm to the necessity to provide the dope with appropriate cation concentrations facilitating an effective spinning process [68].

In summary, the fluid flow facilitates the assembly of SF molecules and their pre-formed structures, aligning these parallel to the flow field vectors and resulting in antiparallel arrangement within fibrillar structures. These observations also illustrate the fact that the spinning process is the result of many carefully orchestrated input parameters, of which pH, ion type, ion concentrations as well as the tightly controlled flow field gradients are major players.

**Transfer to drug delivery applications**

Biomimicry of many aspects of the natural spinning process serves as a blueprint for the formulation scientist interested in SF based drug delivery. Advantages when processing silk include the water based manufacture and hence the absence of organic solvent by-products in the resulting DDS [4, 29, 77]. Similarly, the entire manufacture is under benign conditions rendering a translation of the natural spinning process into the manufacture of DDS particularly attractive for sensitive molecules including biologics. Another fascinating feature is the tight control of micelle

formation as well as control of micelle transition as observed throughout passage *in vivo*, which may be exploited for the solubilization of drugs [78]. On the other hand, the silk spinning process is designed to ultimately lead into controlled molecular assembly resulting in a stable thread. This potential translates into a stability challenge during storage for liquid SF systems, as dynamic changes such as continuing crystallization during storage are unacceptable from a pharmaceutical perspective. Nature has provided a blueprint to formulation scientists detailing approaches meeting this challenge. Viscous and concentrated SF solutions are stored in the glands of insects and spiders and biomimicry of selected aspects of these storage conditions may provide the necessary insight to control continuing crystallization during storage. Independent of the intended DDS - hydrogels [79], microparticles [27, 80], films [81], nanoparticles [82, 83] or three-dimensional scaffolds [26, 41, 84, 85] – the formulation scientist interested in working with SF will be challenged by this control of  $\beta$ -sheet content during manufacture, storage, and application [4, 86]. On the other hand, this feature has been exploited for sustained, controlled drug delivery, which has been demonstrated for many drugs, including biologics [27, 84, 87] and a direct correlation has been postulated for the overall  $\beta$ -sheet content and the diffusion coefficient through the SF biopolymer [81].

### ***Crystallinity***

Conformation changes are typically studied by FTIR and changes to  $\beta$ -sheets are typically discussed in light of shifts of the amide I absorption band (from  $\sim 1656\text{ cm}^{-1}$  to  $\sim 1628\text{ cm}^{-1}$ ) and of the amide II band (from  $\sim 1543\text{ cm}^{-1}$  to  $\sim 1516\text{ cm}^{-1}$ ) [41]. Reported values may differ [29, 88-90]. FTIR results on  $\beta$ -sheets are often corroborated by a diffractometric assessment of overall crystallinity [29]. Alternative approaches have been described including solid-state  $^{13}\text{C}$  NMR spectroscopy [89], e.g. identifying chemical shifts of alanine residues in random coil versus  $\beta$ -sheet conformation, respectively [91]. Furthermore, circular dichroism was used (*vide supra*) [90]. Additionally, morphological changes of solid SF scaffolds or particles can be observed upon crystallization, typically including shrinkage of scaffolds, changes in porosity [41] or altered surface roughness [29, 92]. Methanol is typically used to induce the crystallinity [90] through SF dehydration and conformational destabilizing leading to  $\beta$ -sheet formation [41]. In spite of the general use of methanol it has been challenged by potential disadvantageous impact on incorporated drugs and the formation of brittle materials if not formulated along with other excipients [88, 89]. Alternative strategies for crystallization deploy water vapor [89] and current protocols deviate in some aspects from each other with exposure lasting for up to 24 h [93] whereas others describe 6 hours only [89]. The formation of  $\beta$ -sheet is a function of temperature and a direct relationship

between crystallinity and temperature was postulated [94]. In addition, other protocols using water were described [88].

### ***pH***

The pH responsiveness of SF was deployed in many manufacturing protocols for DDS. In one contribution, the impact of the pH of the continuous phase during mixing of the drug and the SF in solution was tested [26]. Mixing of the liquid SF – drug solution was conducted at pH 4, which is close to the isoelectric point of SF hence minimizing electrostatic interaction between drug and SF and compared to pH 7, at which the SF was negatively charged and the biologic positively charged. No qualitative impact of the formulation pH on crystallinity was observed before and after methanol treatment by FTIR. Differences in release profiles as a function of solution pH were observed for scaffolds before methanol treatment but not thereafter, suggesting that drug release patterns are not impacted by the pH during the mixing step when followed by methanol induced crystallization. However, structural differences of the solid SF were reported for particles [95]. The experiments were conducted at pH 4-9 and particles were salted out for collection. Manufacture at the higher pH reduced the initial burst release. These experiments on particles outlined the impact of pH on formulation success. For example, at pH 4 SF is nearly uncharged, favoring intermolecular interaction. The micelles were salted out to form particles, which were analyzed. From these studies it was concluded, that at pH 4 the micelles were densely packed, and the surface charge was minimal whereas at pH 9 these were loosely packed. These examples demonstrate the design space within which the properties of SF can be tailored. Pending on the intended drug, the versatility of the SF based DDS platforms allows a precise tailoring of drug – SF interaction. The pH dependency of SF was also deployed for the design of pH responsive systems within the context of cancer therapy [96]. These nanoparticles were designed to release doxorubicin at accelerated rates at lysosomal pH, at which – with lysosomal pH being close to the isoelectric point of SF – drug/SF interactions were minimal as a result of neutralized overall charge on SF. Therefore, the pH of the continuous phase may be deployed to tailor the charge of SF colloids in solution as well as on solid particles. Depending on the drug intended for delivery, these charges are optimized through pH adaptation to maximize binding sites for the drug on SF [4, 93].

### ***Ion composition***

Protein stability is effectively impacted by the type of ion and its concentration. For example,  $K_3PO_4$  is priming a solution favoring inter-molecular SF hydrophobic interactions. Henceforth, supplementing the salt to a SF solution favors micelle and particle formation,

respectively. Previous reports using SF defined a ‘critical ionic strength’ which when exceeded resulted in the formation of particles, whereas hydrogel gelation was observed below this threshold level [95]. The ion type and ion concentration can be effectively used to modulate the properties of SF microspheres. For example, SF microspheres were prepared on lipid vesicle templates and exposed to methanol or sodium chloride, thereafter [27]. The particle size depended on the duration of exposure to sodium chloride and smoother surfaces were found. Lastly, NaCl induced crystallinity as efficiently as methanol, thereby providing means to induce  $\beta$ -sheet formation with an alternative method. This was corroborated by other studies within which SF microparticles were prepared directly on NaCl crystals serving as templates and as inducers of  $\beta$ -sheets alike [97]. In contrast to these salts, hydrogel formation is disfavored in the presence of calcium or magnesium cations – a finding which is in analogy to the aforementioned role of calcium cations in the *in vivo* spinning process (*vide supra*) [74].

Another approach, leading to a better understanding of the effects of selected salt and its concentration was performed by using adhesion experiments of spider silk proteins to solid substrates [98, 99]. These studies used recombinant abbreviated spider silk proteins approximating the properties of full length silk fibroin, and their results gave insights into the mentioned effects. The resulting desorption forces in different liquids (salt, concentration thereof, etc.) were quantified by using AFM tip immobilized abbreviated spider silk protein and pulling it from a hydrophobic surface (diamonds and other). They were correlated directly with the cosmotropicity of the selected salt, a finding which was observed for quite high salt concentrations of 5 or 1 M respectively. Similar studies addressed the impact of the aqueous phase composition on SF, focussing on the effects of salt and shear, in an effort to improve our understanding of the natural storage and spinning process in spiders [100]. These studies linked SF aggregation to the presence of cosmotropic salt ( $\text{NaH}_2\text{PO}_4$ ; not observed when replaced by NaCl) and detailed the concentration dependence for  $\text{NaH}_2\text{PO}_4$ .

The impact of different salts and their concentration was systematically addressed in another study focussing on the pattern of SF assembly in solution [78]. Salts were selected based on cosmotropic/chaotropic properties –  $\text{Na}_2\text{SO}_4$  (cosmotropic), NaCl (neutral), NaSCN (chaotropic) - and the impact on micelle formation and protein interaction was studied thermodynamically and regarding colloidal properties [78]. All studies were conducted at a neutral pH, at which the acidic SF carries negative charges. Interaction studies were conducted with protamine (model for biologic), a positively charged model protein at pH 7. The unfolding of *in situ* present SF micelles was observed in histidine buffer at low ionic strength (0.3 mM) and endothermic when minute

amounts of protamine were titrated into SF solutions. Nanoparticle tracking analysis linked the endothermic heat signal for the first titration steps of protamine into the SF solution to structural changes of micelles, an energy consuming rearrangement. With increasing protamine concentration, the interaction became exothermic and the formation of negatively charged nanocomplexes was demonstrated followed by phase separation. These studies detailed that interaction of SF with a basic model protein in solution is particularly effective, once the micellar structures of SF are impacted. This was observed in low ionic strength histidine buffer and instrumental to maximize the interaction between the biopolymer and the basic protein. Conceptually, new binding sites on the SF molecules are continuously opening up, firstly by liberation of SF molecules from micelles and secondly by continuing unfolding of the biopolymer for each titration step. This process is observed until protamine – SF interaction produced the most exothermic signal coinciding with phase separation. Thereafter, the exothermic signals decreased from titration to titration, suggesting that binding sites for protamine decreased accordingly. Supplementing NaCl into the solution resulted in qualitatively similar but much smaller heat signals at each protamine titration step. NaCl negatively impacted the association process of protamine to SF and the free enthalpy was insufficient to effectively liberate SF from micelles or to induce SF unfolding to the same extent as seen for the plain histidine buffer. This pattern in the presence of NaCl is translating into reduced protamine loading, reflecting the relative paucity of binding sites for protamine as compared to histidine buffer alone. In the presence of NaSCN, each titration of protamine resulted in increasing exothermic signals, suggesting over-proportional protamine binding from titration step to titration step. This was discussed such that each titration step resulted in over-proportional generation of novel binding sites for protamine on the biopolymer. In contrast, the use of Na<sub>2</sub>SO<sub>4</sub> stabilized SF micelles through favoring hydrophobic interaction and to an extent that protamine binding with SF was minimal. Further studies detailed these findings regarding physico-chemical and galenical properties including colloidal surface charge ( $\zeta$ -potential), particle formation and protamine load on SF colloids as a function of pH and the ionic strength of a selected salt. The  $\zeta$ -potential of the colloid particles was significantly impacted by pH and the protamine to SF ratio (referred to as ‘ratio’), a finding which was made in the presence of three salts (Na<sub>2</sub>SO<sub>4</sub>, NaCl, NaSCN) when protamine was titrated into a SF solution. Particle formation was monitored photometrically at  $\lambda = 600$  nm (**Figure 2**). In the presence of NaCl, significant parameters impacting particle formation included the ratio and pH of the continuous phase, with the ratio having a larger impact as compared to pH (**Figure 2 A**). Replacing NaCl by NaSCN rendered ionic strength and the ratio significant parameters impacting particle formation, with the ratio having a substantially larger effect as



compared to the ionic strength (**Figure 2 B**). The supplementation of  $\text{Na}_2\text{SO}_4$  resulted in ratio and ionic strength as significant input parameters. Interestingly, the impact of the ratio was low for  $\text{Na}_2\text{SO}_4$  solutions, reflecting the generally poor binding of protamine to SF in the presence of this salt [78]. Similarly, the impact of the ionic strength on particle formation is reflecting the fact that from a certain concentration onwards,  $\text{Na}_2\text{SO}_4$  is effectively suppressing particle formation (**Figure 2 C**). Protein loading of the colloids in the presence of NaCl showed a similar trend as observed for particle formation, but only the ratio and not the pH had a significant impact. Most effective loading among salts was observed in the presence of NaSCN, for which the ratio was significant. The loading of protamine on SF in the presence of  $\text{Na}_2\text{SO}_4$  – no protamine interaction was observed apart from very low ionic strengths/concentrations of  $\text{Na}_2\text{SO}_4$  – was significantly and strongly impacted by the ionic strength and was lowest among the conditions tested.

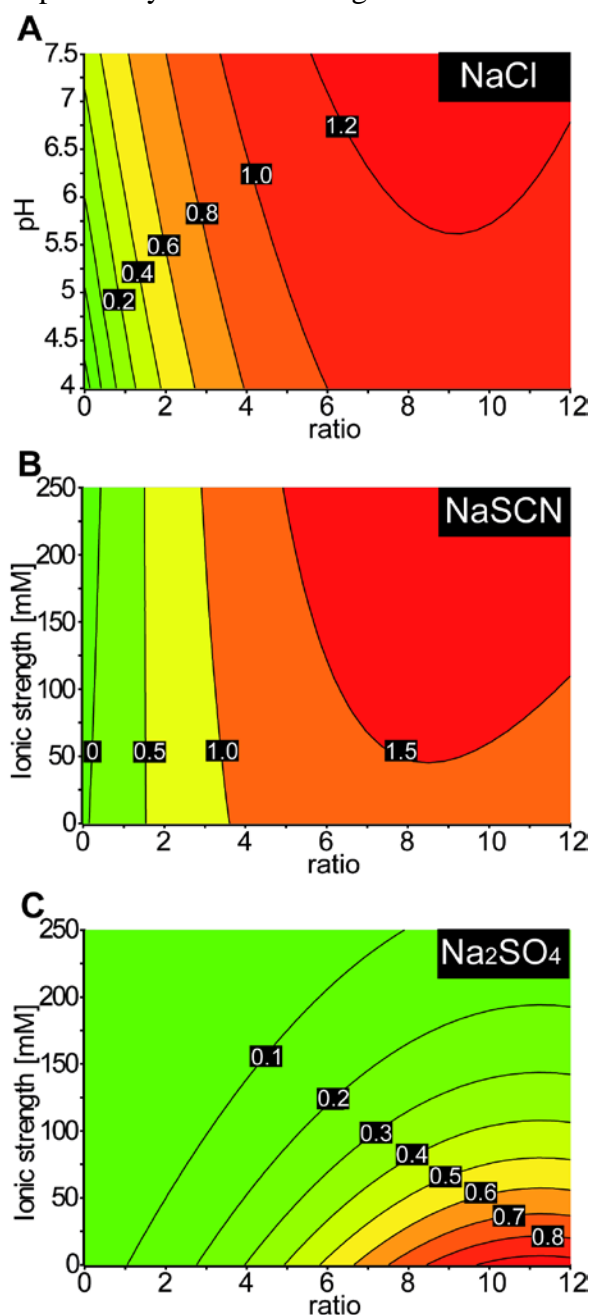


**Figure 2:** Particle formation as a function of significant input parameters. Histidine buffer was supplemented and the ionic strength was adapted with different salts. (A) Significant input parameters in histidine buffer with NaCl were buffer pH and the ratio of protamine given to the SF solution ('ratio'). The impact of the ratio exceeded the impact of the buffer pH. (B) Particle formation in the presence of NaSCN was a function of the ionic strength of the salt and the ratio but not the solution pH. The impact of the ratio exceeded the impact of the ionic strength. This indicated that the presence of this chaotropic salt effectively opened SF binding sites for protamine. (C) In the presence of  $\text{Na}_2\text{SO}_4$ , the ionic strength and the ratio were the significant input parameters affecting particle formation. Binding of protamine to SF was almost independent of the ratio apart from low ionic strengths of  $\text{Na}_2\text{SO}_4$ , reflecting the suppression of protamine to SF binding and particle formation, respectively. Numbers within the panels indicate the absorption by particles as monitored at  $\lambda = 600$  nm.

These data sets demonstrated the versatility of SF as a platform for drug delivery. Loading, colloid charge and size and the propensity for particle formation can be effectively tailored by selecting appropriate salts for manufacture. The data also demonstrated the need to carefully optimize the buffer compositions in the liquid phase, such that effective drug loading and reproducible outcome are guaranteed. The selection of salts is also a strategy to control the self-assembly of SF as a prerequisite to control particle formation/precipitation. As outlined before, spiders and insects store SF hydrogels in glands and  $\beta$ -sheet formation is prevented. However, in laboratory settings, plain SF solutions tend to precipitate with time particularly when stored at room temperature [4]. The control of this precipitation – typically leading to hydrogel formation in initial states – was studied (**Figure 3**). For that the  $\beta$ -sheet formation of SF solutions was tested after 90 days when stored at different concentrations (1%, 3%, 5%; m/V), temperatures (5 °C, 25 °C) and in solutions containing different salts in histidine buffer ( $\text{Na}_2\text{SO}_4$ , NaCl, NaSCN), histidine buffer without salts and as compared to water. At the end of the study, all samples in plain water and histidine buffer alone had formed a hydrogel regardless of the SF concentration and when stored at 25 °C.  $\text{Na}_2\text{SO}_4$  reduced the tendency for hydrogel formation and was restricted to solutions with 3% and 5% SF. No hydrogels were observed in the presence of NaCl or NaSCN. Hydrogel formation correlated strongly with the formation of  $\beta$ -sheets as determined by FTIR, which showed a shift (1637–1620  $\text{cm}^{-1}$ ) to a conformation reflecting the crystalline state for the formed hydrogels for water, plain histidine buffer, and histidine buffer with  $\text{Na}_2\text{SO}_4$  (**Figure 3 A-C**). However, no relevant changes in the transmission bands were observed for histidine buffer with NaCl or NaSCN, reflecting the fact that crystallization was effectively suppressed (**Figure 3 D and E**). These findings are particularly interesting for future liquid SF pharmaceutical images, which were challenged in the past by their propensity for  $\beta$ -sheet formation during storage. Such unacceptable changes may be controlled by means of proper salt selection and salt concentration, respectively, thereby opening SF for the formulation of liquid systems. The study presented here is preliminary and real time stability studies lasting for 24 months or more are required to corroborate these findings before final conclusions may be drawn. Suitable applications of liquid SF solutions include topical forms, sprays, eye drops (thixotropic hydrogels) and other applications.

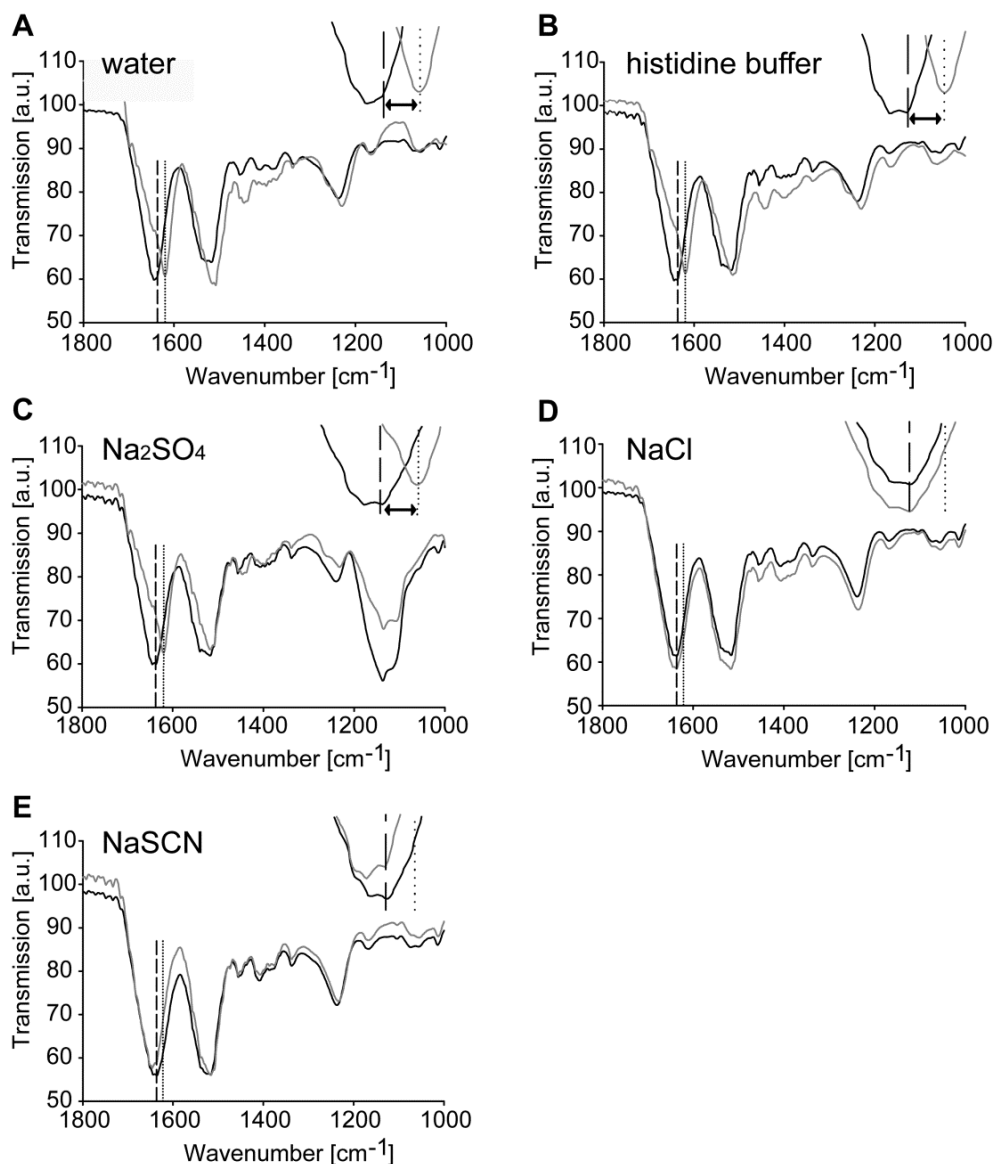


**Figure 3:** FTIR transmission spectra of selected samples at the beginning of the testing period (black line) and after 90 days (gray line) when stored at 25°C and an SF concentration of 5% (m/V). The dashed line marks 1637  $\text{cm}^{-1}$ , indicative for random coil conformation and the dotted line marks 1620  $\text{cm}^{-1}$ , indicating  $\beta$ -sheets. Experiments were conducted in (A) water, or (B) histidine buffer. The histidine buffer was further supplemented with salts at an ionic strength of 0.19 M using (C)  $\text{Na}_2\text{SO}_4$  or (D)  $\text{NaCl}$  or (E)  $\text{NaSCN}$ , respectively. The 1637 - 1620  $\text{cm}^{-1}$  shift was observed for water, histidine buffer and  $\text{Na}_2\text{SO}_4$  in histidine buffer and not in the presence of  $\text{NaSCN}$  and  $\text{NaCl}$ . The data indicated that in the presence of these salts, stable formulations were obtained. [a.u.] = arbitrary units. Inserts highlight the wave numbers 1637 - 1620  $\text{cm}^{-1}$ .

**Conclusion**

The carefully orchestrated natural process of *in vivo* silk spinning includes different aggregate states, including colloidal solutions, hydrogels, or solid structures. Thereby, nature is providing a blueprint outlining the perplexing versatility of SF and the translational potential for pharmaceutical application. Examples were provided how aspects of the natural process can be successfully delineated such that improved pharmaceutical formulations of protein-drugs can be developed deploying SF as a biomaterial carrier.

## References

- [1] R. Suntivich, I. Drachuk, R. Calabrese, D.L. Kaplan, V.V. Tsukruk, Inkjet Printing of Silk Nest Arrays for Cell Hosting, *Biomacromolecules*, 15 (2014) 1428-1435.
- [2] H. Tao, J.M. Kainerstorfer, S.M. Siebert, E.M. Pritchard, A. Sassaroli, B.J.B. Panilaitis, M.A. Brenckle, J. Amsden, J. Levitt, S. Fantini, D.L. Kaplan, F.G. Omenetto, Implantable, multifunctional, bioresorbable optics, *Proc. Natl. Acad. Sci. U. S. A.*, 109 (2012) 19584-19589, S19584/19581-S19584/19531.
- [3] C. Vepari, D.L. Kaplan, Silk as a Biomaterial, *Progress in polymer science*, 32 (2007) 991-1007.
- [4] E. Wenk, H.P. Merkle, L. Meinel, Silk fibroin as a vehicle for drug delivery applications, *Journal of controlled release : official journal of the Controlled Release Society*, 150 (2011) 128-141.
- [5] P. Wu, Q. Liu, R. Li, J. Wang, X. Zhen, G. Yue, H. Wang, F. Cui, F. Wu, M. Yang, X. Qian, L. Yu, X. Jiang, B. Liu, Facile preparation of paclitaxel loaded silk fibroin nanoparticles for enhanced antitumor efficacy by locoregional drug delivery, *ACS applied materials & interfaces*, 5 (2013) 12638-12645.
- [6] B. Subia, S.C. Kundu, Drug loading and release on tumor cells using silk fibroin-albumin nanoparticles as carriers, *Nanotechnology*, 24 (2013) 035103.
- [7] A.J. Meinel, O. Germershaus, T. Luhmann, H.P. Merkle, L. Meinel, Electrospun matrices for localized drug delivery: current technologies and selected biomedical applications, *European journal of pharmaceutics and biopharmaceutics : official journal of Arbeitsgemeinschaft fur Pharmazeutische Verfahrenstechnik e.V*, 81 (2012) 1-13.
- [8] A. Nova, S. Ketten, N.M. Pugno, A. Redaelli, M.J. Buehler, Molecular and nanostructural mechanisms of deformation, strength and toughness of spider silk fibrils, *Nano letters*, 10 (2010) 2626-2634.
- [9] F.G. Omenetto, D.L. Kaplan, New opportunities for an ancient material, *Science*, 329 (2010) 528-531.
- [10] F. Lucas, Spiders and their silks, *Discovery*, 25 (1976) 20-26.
- [11] R. Foelix, *Biologie der Spinnen*, Stuttgart: Thieme, 1992.
- [12] J. Pérez-Rigueiro, C. Viney, J. Llorca, M. Elices, Mechanical properties of single-brin silkworm silk, *Journal of Applied Polymer Science*, 75 (2000) 1270-1277.
- [13] C. Holland, A.E. Terry, D. Porter, F. Vollrath, Natural and unnatural silks, *Polymer*, 48 (2007) 3388-3392.
- [14] F. Vollrath, D. Porter, Silks as ancient models for modern polymers, *Polymer*, 50 (2009) 5623-5632.
- [15] G. Zhou, Z. Shao, D.P. Knight, J. Yan, X. Chen, Silk Fibers Extruded Artificially from Aqueous Solutions of Regenerated Bombyx mori Silk Fibroin are Tougher than their Natural Counterparts, *Advanced Materials*, 21 (2009) 366-370.
- [16] L. Uebersax, T. Apfel, K.M. Nuss, R. Vogt, H.Y. Kim, L. Meinel, D.L. Kaplan, J.A. Auer, H.P. Merkle, B. von Rechenberg, Biocompatibility and osteoconduction of macroporous silk fibroin implants in cortical defects in sheep, *European journal of pharmaceutics and biopharmaceutics : official journal of Arbeitsgemeinschaft fur Pharmazeutische Verfahrenstechnik e.V*, 85 (2013) 107-118.

- [17] S. Hofmann, M. Hilbe, R.J. Fajardo, H. Hagenmuller, K. Nuss, M. Arras, R. Muller, R.B. von, D.L. Kaplan, H.P. Merkle, L. Meinel, Remodeling of tissue-engineered bone structures in vivo, *Eur. J. Pharm. Biopharm.*, 85 (2013) 119-129.
- [18] T. Luhmann, O. Germershaus, J. Groll, L. Meinel, Bone targeting for the treatment of osteoporosis, *J. Controlled Release*, 161 (2012) 198-213.
- [19] N. Kasoju, U. Bora, Silk fibroin in tissue engineering, *Advanced healthcare materials*, 1 (2012) 393-412.
- [20] B. Kundu, R. Rajkhowa, S.C. Kundu, X. Wang, Silk fibroin biomaterials for tissue regenerations, *Adv Drug Deliv Rev*, 65 (2013) 457-470.
- [21] N. Kuboyama, H. Kiba, K. Arai, R. Uchida, Y. Tanimoto, U.K. Bhawal, Y. Abiko, S. Miyamoto, D. Knight, T. Asakura, N. Nishiyama, Silk fibroin-based scaffolds for bone regeneration, *Journal of biomedical materials research. Part B, Applied biomaterials*, 101 (2013) 295-302.
- [22] L. Meinel, R. Fajardo, S. Hofmann, R. Langer, J. Chen, B. Snyder, G. Vunjak-Novakovic, D. Kaplan, Silk implants for the healing of critical size bone defects, *Bone*, 37 (2005) 688-698.
- [23] E. Wenk, A.R. Murphy, D.L. Kaplan, L. Meinel, H.P. Merkle, L. Uebersax, The use of sulfonated silk fibroin derivatives to control binding, delivery and potency of FGF-2 in tissue regeneration, *Biomaterials*, 31 (2010) 1403–1413.
- [24] X. Wang, E. Wenk, X. Zhang, L. Meinel, G. Vunjak-Novakovic, D.L. Kaplan, Growth factor gradients via microsphere delivery in biopolymer scaffolds for osteochondral tissue engineering, *J. Controlled Release*, 134 (2009) 81-90.
- [25] A.J. Meinel, K.E. Kubow, E. Klotzsch, M. Garcia-Fuentes, M.L. Smith, V. Vogel, H.P. Merkle, L. Meinel, Optimization strategies for electrospun silk fibroin tissue engineering scaffolds, *Biomaterials*, 30 (2009) 3058-3067.
- [26] L. Uebersax, H.P. Merkle, L. Meinel, Insulin-like growth factor I releasing silk fibroin scaffolds induce chondrogenic differentiation of human mesenchymal stem cells, *J Control Release*, 127 (2008) 12-21.
- [27] X. Wang, E. Wenk, A. Matsumoto, L. Meinel, C. Li, D.L. Kaplan, Silk microspheres for encapsulation and controlled release, *J Control Release*, 117 (2007) 360-370.
- [28] L. Uebersax, M. Mattotti, M. Papaloizos, H.P. Merkle, B. Gander, L. Meinel, Silk fibroin matrices for the controlled release of nerve growth factor (NGF), *Biomaterials*, 28 (2007) 4449-4460.
- [29] S. Hofmann, P.F.C.T. Wong, F. Rossetti, M. Textor, G. Vunjak-Novakovic, D.L. Kaplan, H.P. Merkle, L. Meinel, Silk fibroin as an organic polymer for controlled drug delivery, *J. Controlled Release*, 111 (2006) 219-227.
- [30] G.H. Altman, F. Diaz, C. Jakuba, T. Calabro, R.L. Horan, J. Chen, H. Lu, J. Richmond, D.L. Kaplan, Silk-based biomaterials, *Biomaterials*, 24 (2002) 401-416.
- [31] Y. Yang, X. Chen, F. Ding, P. Zhang, J. Liu, X. Gu, Biocompatibility evaluation of silk fibroin with peripheral nerve tissues and cells in vitro, *Biomaterials*, 28 (2007) 1643-1652.
- [32] J. Wang, Y. Wei, H. Yi, Z. Liu, D. Sun, H. Zhao, Cytocompatibility of a silk fibroin tubular scaffold, *Materials science & engineering. C, Materials for biological applications*, 34 (2014) 429-436.

- [33] T.L. Liu, J.C. Miao, W.H. Sheng, Y.F. Xie, Q. Huang, Y.B. Shan, J.C. Yang, Cytocompatibility of regenerated silk fibroin film: a medical biomaterial applicable to wound healing, *Journal of Zhejiang University. Science. B*, 11 (2010) 10-16.
- [34] S. Hofmann, S. Knecht, R. Langer, D.L. Kaplan, G. Vunjak-Novakovic, H.P. Merkle, L. Meinel, Cartilage-like Tissue Engineering Using Silk Scaffolds and Mesenchymal Stem Cells, *Tissue Eng.*, 12 (2006) 2729-2738.
- [35] S. Hofmann, H. Hagenmüller, A.M. Koch, R. Müller, G. Vunjak-Novakovic, D.L. Kaplan, H.P. Merkle, L. Meinel, Control of in vitro tissue-engineered bone-like structures using human mesenchymal stem cells and porous silk scaffolds, *Biomaterials*, 28 (2007) 1152–1162.
- [36] E.M. Pritchard, P.B. Dennis, F. Omenetto, R.R. Naik, D.L. Kaplan, Review physical and chemical aspects of stabilization of compounds in silk, *Biopolymers*, 97 (2012) 479-498.
- [37] M. Demura, T. Asakura, E. Nakamura, H. Tamura, Immobilization of peroxidase with a Bombyx mori silk fibroin membrane and its application to biophotosensors, *Journal of Biotechnology*, 10 (1989) 113-119.
- [38] L. Meinel, D.L. Kaplan, Silk constructs for delivery of musculoskeletal therapeutics, *Adv. Drug Delivery Rev.*, 64 (2012) 1111-1122.
- [39] L. Meinel, S. Hofmann, V. Karageorgiou, C. Kirker-Head, J. McCool, G. Gronowicz, L. Zichner, R. Langer, G. Vunjak-Novakovic, D.L. Kaplan, The inflammatory responses to silk films in vitro and in vivo, *Biomaterials*, 26 (2005) 147-155.
- [40] J.H. Kim, C.H. Park, O.J. Lee, J.M. Lee, J.W. Kim, Y.H. Park, C.S. Ki, Preparation and in vivo degradation of controlled biodegradability of electrospun silk fibroin nanofiber mats, *Journal of biomedical materials research. Part A*, 100 (2012) 3287-3295.
- [41] E. Wenk, A.J. Meinel, S. Wildy, H.P. Merkle, L. Meinel, Microporous silk fibroin scaffolds embedding PLGA microparticles for controlled growth factor delivery in tissue engineering, *Biomaterials*, 30 (2009) 2571-2581.
- [42] M. Li, M. Ogiso, N. Minoura, Enzymatic degradation behavior of porous silk fibroin sheets, *Biomaterials*, 24 (2003) 357-365.
- [43] G. Guan, L. Wang, M. Li, L. Bai, In vivo biodegradation of porous silk fibroin films implanted beneath the skin and muscle of the rat, *Bio-medical materials and engineering*, 24 (2014) 789-797.
- [44] Y. Cao, B. Wang, Biodegradation of silk biomaterials, *International journal of molecular sciences*, 10 (2009) 1514-1524.
- [45] D.B. Peakall, Synthesis of Silk Mechanism and Location, *Am Zool*, 9 (1969) 71-79.
- [46] R.W. Work, C.T. Young, The Amino-Acid Compositions of Major and Minor Ampullate Silks of Certain Orb-Web-Building Spiders (Araneae, Araneidae), *J Arachnol*, 15 (1987) 65-80.
- [47] S. Lombardi, D. Kaplan, The *Nephila clavipes* major ampullate gland silk protein, amino acid composition and detection of silk gene-related nucleic acids in the genome, *Acta Zool Fennica*, 190 (1991) 243.
- [48] J.M. Gosline, M.W. Denny, M.E. DeMont, Spider silk as rubber, *Nature*, 309 (1984) 551-552.
- [49] J.M. Gosline, M.E. DeMont, M.W. Denny, The structure and properties of spider silk, *Endeavour*, 10 (1986) 37-43.
- [50] R.W. Work, Dimensions, Birefringences, and Force-Elongation Behavior of Major and Minor Ampullate Silk Fibers from Orb-Web-Spinning Spiders - Effects of Wetting on These Properties, *Text Res J*, 47 (1977) 650-662.

- [51] H.-J. Jin, D.L. Kaplan, Mechanism of silk processing in insects and spiders, *Nature*, 424 (2003) 1057–1061.
- [52] Q. Lu, H. Zhu, C. Zhang, F. Zhang, B. Zhang, D.L. Kaplan, Silk Self-Assembly Mechanisms and Control From Thermodynamics to Kinetics, *Biomacromolecules*, 13 (2012) 826–832.
- [53] M.E. Rousseau, T. Lefevre, L. Beaulieu, T. Asakura, M. Pezolet, Study of protein conformation and orientation in silkworm and spider silk fibers using Raman microspectroscopy, *Biomacromolecules*, 5 (2004) 2247–2257.
- [54] C. Dicko, F. Vollrath, J.M. Kenney, Spider silk protein refolding is controlled by changing pH, *Biomacromolecules*, 5 (2004) 704–710.
- [55] F. Vollrath, D.P. Knight, Liquid crystalline spinning of spider silk, *Nature*, 410 (2001) 541–548.
- [56] F. Vollrath, Strength and structure of spiders' silks, *Reviews in Molecular Biotechnology*, 74 (2000) 67–83.
- [57] M. Andersson, L. Holm, Y. Ridderstrale, J. Johansson, A. Rising, Morphology and composition of the spider major ampullate gland and dragline silk, *Biomacromolecules*, 14 (2013) 2945–2952.
- [58] F. Vollrath, D.P. Knight, Structure and function of the silk production pathway in the spider *Nephila edulis*, *Int. J. Biol. Macromol.*, 24 (1999) 243–249.
- [59] T. Asakura, K. Umemura, Y. Nakazawa, H. Hirose, J. Higham, D. Knight, Some observations on the structure and function of the spinning apparatus in the silkworm *Bombyx mori*, *Biomacromolecules*, 8 (2007) 175–181.
- [60] C. Dicko, J.M. Kenney, D. Knight, F. Vollrath, Transition to a beta-sheet-rich structure in spidroin in vitro: the effects of pH and cations, *Biochemistry*, 43 (2004) 14080–14087.
- [61] R. Silvers, F. Buhr, H. Schwalbe, Der molekulare Mechanismus der Bildung von Spinnenseide, *Angewandte Chemie*, 122 (2010) 5538–5540.
- [62] Y.-X. He, N.-N. Zhang, W.-F. Li, N. Jia, B.-Y. Chen, K. Zhou, J. Zhang, Y. Chen, C.-Z. Zhou, N-Terminal Domain of *Bombyx mori* Fibroin Mediates the Assembly of Silk in Response to pH Decrease, *Journal of Molecular Biology*, 418 (2012) 197–207.
- [63] F. Hagn, C. Thamm, T. Scheibel, H. Kessler, pH-dependent dimerization and salt-dependent stabilization of the N-terminal domain of spider dragline silk--implications for fiber formation, *Angewandte Chemie (International ed. in English)*, 50 (2011) 310–313.
- [64] A. Rising, Controlled assembly: A prerequisite for the use of recombinant spider silk in regenerative medicine?, *Acta Biomater.*, 10 (2014) 1627–1631.
- [65] N. Kronqvist, M. Otkovs, V. Chmyrov, G. Chen, M. Andersson, K. Nordling, M. Landreh, M. Sarr, H. Jornvall, S. Wennmalm, J. Widengren, Q. Meng, A. Rising, D. Otzen, S.D. Knight, K. Jaudzems, J. Johansson, Sequential pH-driven dimerization and stabilization of the N-terminal domain enables rapid spider silk formation, *Nat. Commun.*, 5 (2014) 4254/4251–4254/4211.
- [66] L. Eisoldt, C. Thamm, T. Scheibel, Review the role of terminal domains during storage and assembly of spider silk proteins, *Biopolymers*, 97 (2012) 355–361.
- [67] F. Hagn, L. Eisoldt, J.G. Hardy, C. Vendrely, M. Coles, T. Scheibel, H. Kessler, A conserved spider silk domain acts as a molecular switch that controls fibre assembly, *Nature*, 465 (2010) 239–242.



- [68] D.P. Knight, F. Vollrath, Changes in element composition along the spinning duct in a *Nephila* spider, *Naturwissenschaften*, 88 (2001) 179-182.
- [69] D.P. Knight, F. Vollrath, Biological liquid crystal elastomers, *Philosophical transactions of the Royal Society of London. Series B, Biological sciences*, 357 (2002) 155-163.
- [70] D.P. Knight, F. Vollrath, Liquid crystals and flow elongation in a spider's silk production line, *Proceedings of the Royal Society B: Biological Sciences*, 266 (1999) 519-523.
- [71] A. Matsumoto, A. Lindsay, B. Abedian, D.L. Kaplan, Silk fibroin solution properties related to assembly and structure, *Macromol Biosci*, 8 (2008) 1006-1018.
- [72] A.E. Terry, D.P. Knight, D. Porter, F. Vollrath, pH induced changes in the rheology of silk fibroin solution from the middle division of *Bombyx mori* silkworm, *Biomacromolecules*, 5 (2004) 768-772.
- [73] L. Zhou, X. Chen, Z. Shao, Y. Huang, D.P. Knight, Effect of metallic ions on silk formation in the Mulberry silkworm, *Bombyx mori*, *The journal of physical chemistry. B*, 109 (2005) 16937-16945.
- [74] A. Ochi, K.S. Hossain, J. Magoshi, N. Nemoto, Rheology and Dynamic Light Scattering of Silk Fibroin Solution Extracted from the Middle Division of *Bombyx mori* Silkworm, *Biomacromolecules*, 3 (2002) 1187-1196.
- [75] D.P. Knight, M.M. Knight, F. Vollrath, Beta transition and stress-induced phase separation in the spinning of spider dragline silk, *International journal of biological macromolecules*, 27 (2000) 205-210.
- [76] S. Rammensee, U. Slotta, T. Scheibel, A.R. Bausch, Assembly mechanism of recombinant spider silk proteins, *Proceedings of the National Academy of Sciences of the United States of America*, 105 (2008) 6590-6595.
- [77] L. Uebersax, H.P. Merkle, L. Meinel, Biopolymer-Based Growth Factor Delivery for Tissue Repair: From Natural Concepts to Engineered Systems, *Tissue Eng., Part B*, 15 (2009) 263-289.
- [78] O. Germershaus, V. Werner, M. Kutscher, L. Meinel, Deciphering the mechanism of protein interaction with silk fibroin for drug delivery systems, *Biomaterials*, 35 (2014) 3427-3434.
- [79] F.P. Seib, E.M. Pritchard, D.L. Kaplan, Self-assembling doxorubicin silk hydrogels for the focal treatment of primary breast cancer, *Advanced functional materials*, 23 (2013) 58-65.
- [80] P.C. Bessa, E.R. Balmayor, J. Hartinger, G. Zanoni, D. Dopler, A. Meinel, A. Banerjee, M. Casal, H. Redl, R.L. Reis, M. van Griensven, Silk fibroin microparticles as carriers for delivery of human recombinant bone morphogenetic protein-2: in vitro and in vivo bioactivity, *Tissue engineering. Part C, Methods*, 16 (2010) 937-945.
- [81] D.J. Hines, D.L. Kaplan, Mechanisms of Controlled Release from Silk Fibroin Films, *Biomacromolecules*, 12 (2011) 804-812.
- [82] A.B. Mathur, V. Gupta, Silk fibroin-derived nanoparticles for biomedical applications, *Nanomedicine*, 5 (2010) 807-820.
- [83] J. Kundu, Y.I. Chung, Y.H. Kim, G. Tae, S.C. Kundu, Silk fibroin nanoparticles for cellular uptake and control release, *International journal of pharmaceuticals*, 388 (2010) 242-250.
- [84] T. Yucel, M.L. Lovett, D.L. Kaplan, Silk-based biomaterials for sustained drug delivery, *J Control Release*, 190 (2014) 381-397.
- [85] K. Zhang, X. Mo, C. Huang, C. He, H. Wang, Electrospun scaffolds from silk fibroin and their cellular compatibility, *Journal of biomedical materials research. Part A*, 93 (2010) 976-983.

- [86] K. Numata, D.L. Kaplan, Silk-based delivery systems of bioactive molecules, *Adv. Drug Delivery Rev.*, 62 (2010) 1497-1508.
- [87] J. Zhou, B. Zhang, L. Shi, J. Zhong, J. Zhu, J. Yan, P. Wang, C. Cao, D. He, Regenerated silk fibroin films with controllable nanostructure size and secondary structure for drug delivery, *ACS applied materials & interfaces*, 6 (2014) 21813-21821.
- [88] H.J. Jin, J. Park, V. Karageorgiou, U.J. Kim, R. Valluzzi, P. Cebe, D.L. Kaplan, Water-Stable Silk Films with Reduced  $\beta$ -Sheet Content, *Advanced functional materials*, 15 (2005) 1241-1247.
- [89] B.-M. Min, L. Jeong, K.Y. Lee, W.H. Park, Regenerated Silk Fibroin Nanofibers: Water Vapor-Induced Structural Changes and Their Effects on the Behavior of Normal Human Cells, *Macromolecular Bioscience*, 6 (2006) 285-292.
- [90] D. Wilson, R. Valluzzi, D. Kaplan, Conformational Transitions in Model Silk Peptides, *Biophysical Journal*, 78 (2000) 2690-2701.
- [91] T. Asakura, Y. Nakazawa, E. Ohnishi, F. Moro, Evidence from  $^{13}\text{C}$  solid-state NMR spectroscopy for a lamella structure in an alanine-glycine copolyptide: a model for the crystalline domain of *Bombyx mori* silk fiber, *Protein Sci*, 14 (2005) 2654-2657.
- [92] I. Schultz, F. Vollmers, T. Lühmann, J.C. Rybak, R. Wittmann, K. Stank, H. Steckel, B. Kardziej, M. Schmidt, P. Högger, L. Meinel, Pulmonary Insulin-like growth factor I delivery from trehalose and silk-fibroin microparticles, *ACS Biomaterials Science & Engineering* accepted (2015).
- [93] E. Wenk, A.J. Wandrey, H.P. Merkle, L. Meinel, Silk fibroin spheres as a platform for controlled drug delivery, *Journal of Controlled Release*, 132 (2008) 26–34.
- [94] F.P. Seib, D.L. Kaplan, Doxorubicin-loaded silk films: drug-silk interactions and in vivo performance in human orthotopic breast cancer, *Biomaterials*, 33 (2012) 8442-8450.
- [95] A.S. Lammel, X. Hu, S.-H. Park, D.L. Kaplan, T.R. Scheibel, Controlling silk fibroin particle features for drug delivery, *Biomaterials*, 31 (2010) 4583–4591.
- [96] F.P. Seib, G.T. Jones, J. Rnjak-Kovacina, Y. Lin, D.L. Kaplan, pH-dependent anticancer drug release from silk nanoparticles, *Advanced healthcare materials*, 2 (2013) 1606-1611.
- [97] U.J. Kim, J. Park, H.J. Kim, M. Wada, D.L. Kaplan, Three-dimensional aqueous-derived biomaterial scaffolds from silk fibroin, *Biomaterials*, 26 (2005) 2775-2785.
- [98] M. Geisler, T. Pirzer, C. Ackerschott, S. Lud, J. Garrido, T. Scheibel, T. Hugel, Hydrophobic and Hofmeister effects on the adhesion of spider silk proteins onto solid substrates: an AFM-based single-molecule study, *Langmuir*, 24 (2008) 1350-1355.
- [99] T. Pirzer, M. Geisler, T. Scheibel, T. Hugel, Single molecule force measurements delineate salt, pH and surface effects on biopolymer adhesion, *Physical Biology*, 6 (2009) 025004.
- [100] L. Eisoldt, J.G. Hardy, M. Heim, T.R. Scheibel, The role of salt and shear on the storage and assembly of spider silk proteins, *Journal of structural biology*, 170 (2010) 413–419.





## CHAPTER II

### THE EFFECTS OF HOFMEISTER SALTS ON SILK FIBROIN AND ITS INTERACTION PATTERN

The following passages were literally transferred or only slightly modified from:

- \*O. Germershaus, \*V. Werner, M. Kutscher, L. Meinel, Deciphering the mechanism of protein interaction with silk fibroin for drug delivery systems, *Biomaterials*, 35 (2014) 3427-3434.

\* shared first authorship

#### **Methods**

(Preparation of SF solution, ITC, Static Light Scattering,  $\zeta$ -potential, NTA, Fluorescence spectroscopy, Fluorescent labeling protamine, Fluorescence microscopy)

With permission of Elsevier (License number: 3585901108401, License date: Mar 11, 2015)

#### **Figures 1-6, 8 and 11**

With permission of Elsevier (License number: 3554160955980, License date: Jan 22, 2015)

- V. Werner, L. Meinel, From silk spinning in insects and spiders to advanced silk fibroin drug delivery systems, *European Journal of Pharmaceutics and Biopharmaceutics*, (2015), 10.1016/j.ejpb.2015.03.016.

#### **Figures 7 and 9 (with additional data added)**

With permission of Elsevier (License number: 3596990165187, License date: Mar 27, 2015)

All experimental work described in the following chapter was done by me, with support in NTA measurements by Marika Kutscher. The experiments were planned and discussed by me in collaboration with Prof. Dr. Dr. Lorenz Meinel and Prof. Dr. Oliver Germershaus.

**Abstract**

Silk fibroin (SF) is a biomaterial which is suitable as a carrier for protein drug delivery devices. It combines processability under mild conditions, good biocompatibility and stabilizing effects on incorporated proteins. In order to understand the underlying mechanism for the interaction between SF and positively charged model proteins, we used isothermal titration calorimetry for thermodynamic characterization. This was supported by hydrophobicity analysis and by colloidal characterization methods including static light scattering, nanoparticle tracking analysis and zeta potential measurements. We studied the effects of three Hofmeister salts – NaCl (neutral), NaSCN (chaotropic) and Na<sub>2</sub>SO<sub>4</sub> (cosmotropic) – and the pH on the interaction of SF with the model proteins in dependence of the ratio from one to another. The salts impacted the SF structure by stabilizing (cosmotropic) or destabilizing (chaotropic) the SF micelles, resulting in completely abolished (cosmotropic) or strongly enhanced (chaotropic) interaction. These effects were responsible for different levels of loading and coacervation, when varying type of salt and its concentration. Additionally, NaCl and NaSCN were able to prolong the stability of aqueous SF solution during storage at 25°C in a preliminary study.

## Introduction

Silk fibroin (SF) finds increasing interest in the research of drug delivery devices [1-6] and carrier materials, as it has many desirable properties for this use. First of all it can be processed under very mild and all-aqueous conditions, thereby only having minor effects on possible drug proteins' integrity. It has already been shown that SF has stabilizing effects on biologicals [3] and is suitable to develop delivery systems for many therapeutically relevant proteins [5, 7]. Although there are many positive experiences with SF, the underlying mechanism for the binding between the carrier and the drug in solution remains unclear, leading to unavoidably empirical approaches for the development of such systems. Therefore, this study aims to investigate the mechanism for the interaction between SF and model proteins, carrying positive charges at neutral pH to allow electrostatic forces to the negatively charged SF ( $pI \approx 4.5$  [8]). We chose two different ones to include the effect of their structural differences, with polylysine being strongly and evenly charged, and therefore developing a random coil conformation [9] and protamine representing a more complex molecule containing, besides the numerous charges, some hydrophobic domains [10]. These properties made protamine the more interesting subject for our experiments and we explored its interaction with SF in more detail. The second variable parameter in this study was the choice of salt, being supplemented during the interaction process. We were interested in the effect of Hofmeister salts [11] and chose one for each possible Hofmeister property. In detail the used salts were NaCl as Hofmeister neutral to study the simple ionic strength effect, NaSCN as chaotropic and  $Na_2SO_4$  as kosmotropic representative [12].

A major drawback for the use of SF as a solution is its tendency to precipitate and form hydrogels during storage, especially when not stored under the right conditions [3]. The control thereof by supplementing the above-mentioned salts was studied, as this might open the possibility for liquid SF formulations.

## Material and Methods

### Materials

Cocoons of <i>B.mori</i>	Trudel AG (Zurich, Switzerland)
Protamine sulfate salt from salmon grade x, amorphous powder	Sigma Aldrich (Schnelldorf, Germany)
Polylysine hydrobromide	Sigma Aldrich (Schnelldorf, Germany)
SpectraPor dialysis membrane (MWCO 6-8000Da)	Spectrum labs (Rancho Dominguez, CA, USA)
5 µm syringe filter (Versapor)	Pall Life Sciences (Washington, NY, USA)
0.22 µm syringe filter, Rotilabo, CME, sterile	Carl Roth GmbH&Co KG (Karlsruhe, Germany)
3.5 ml quartz cuvette type 101-QS	Hellma (Müllheim, Germany)

(All other chemicals were at least of analytical grade and from Sigma Aldrich)

### Instruments

LS 50B luminescence spectrometer	Perkin Elmer (Waltham, MA, USA)
Delsa Nano HC	Beckmann Coulter (Brea, CA, USA)
NanoSight NS 500	NanoSight (Wiltshire, UK)
Freeze dryer Alpha 1-4	Christ (Osterrode, Germany)
FT/IR-6100	JASCO (Frankfurt, Germany)
MicroCal iTC200	GE Healthcare (Buckinghamshire, GB)
Axio Observer Z1	Carl Zeiss (Oberkochen, Germany)
+ camera: AxioCam MRm3	
+ objective: Plan-Apochromat 40x/ 0.95	



---

## *Methods*

### Preparation of SF solution

SF solutions were prepared from silk cocoons as previously described with modification [13]. Cocoons were boiled in a stirred aqueous solution of 0.02 M Na<sub>2</sub>CO<sub>3</sub> twice for 1 h each, and then washed with water 10 times. The dried fibers were dissolved in 9 M aqueous LiBr solution at 55 - 60°C until completely dissolved, yielding a concentration of 20% (w/v) SF which was filtered through a 5 µm syringe filter and dialyzed against ultrapure water for 2 days, changing the water 5 times and using SpectraPor dialysis membranes (MWCO 6-8000 Da). The SF solution had a final concentration of 1.5-2% (w/v) and was stored at 2-8°C. Prior to use, the SF solution was filtered through a 5 µm syringe filter. In later experiments the solution was dialyzed against borate buffer (300 mM borate, 150 mM NaCl, pH 9.0) for 24 h prior to ultrapure water.

### ITC

The ITC titrations were performed using a MicroCal iTC200 to measure the heat of reaction when a protamine solution (1.622 mM) was titrated into an SF solution (32 µM) or a polylysine solution (98 µM) was titrated into an SF solution (19 µM) at 25°C and stirred at 400 rpm. Both, SF and titrant (protamine or polylysine) were dissolved in the same medium, composed of a 25 mM histidine buffer (ionic strength 0.31 mM), pH 7.6 supplemented with NaCl, NaSCN, or Na<sub>2</sub>SO<sub>4</sub> yielding an ionic strength of 0.19 M, respectively. Each injection consisted of 2 µl of titrant injected during 4 s each (first titration at 0.2 µl of titrant injected during 0.4 s), with a spacing of 150 s between each of a total of 20 injections. The cell volume was 200 µl. The first injection was always omitted to minimize the impact of equilibration artifacts, following the manufacturer's recommendations. All curves were corrected by a blank titration, performed by titrating the respective model protein (protamine or polylysine) in buffer/salt solution without SF.

## SLS

Light scattering was performed using an LS 50B luminescence spectrometer at a fixed angle of 90°. Excitation- and emission wavelength and -slits were set to 638 nm and 2.5 nm, respectively. Scattered light was observed for 60 s with an integration time of 0.1 s and a data interval of 1.2 s. The samples were produced as described before but volumes were increased by a factor of 10 to allow reliable measurements in a 3.5 ml quartz cuvette.

## Zeta potential ( $\zeta$ -potential)

The surface charge was determined by a Delsa Nano HC using a 658 nm laser and a scattering angle of 15°. The samples were produced as described before but were diluted 1:12.5 for protamine and 1:7.5 for polylysine with ultrapure water immediately before each measurement.

## NTA

The colloid kinetics of SF and protamine alone, as well as of SF/protamine mixtures at different mixing ratios, were determined by nanoparticle tracking analysis (NTA) with a NanoSight NS 500 instrument using a 40 mW laser at 638 nm and the NTA Software Version 2.3 (NanoSight, Wiltshire, UK). All samples were prepared as described before, and were diluted 1:10 using the respective buffer/salt solution immediately before each experiment. Movies were cut using Movie Maker (Microsoft, Redmont, WA).

## Fluorescence spectroscopy

Fluorescence intensities were recorded using an LS 50B luminescence spectrometer setting excitation at 490 nm and emission at 570 nm. Samples were prepared as follows: 2036  $\mu$ l of an SF solution at 3.2  $\mu$ M in the respective buffer/salt solution were mixed with 4  $\mu$ l of a Sypro Orange (SO) solution, diluted 1:10 in DMSO from a stock solution (total dilution of working solution 50,000x). The protamine solution was added in steps of 20  $\mu$ l each, measuring the fluorescence spectrum at each titration point (*vide supra*). Relative fluorescence was calculated by setting the

fluorescence of the SF solution without protamine as reference (corresponding to a relative fluorescence of 1).

For the stability test (*vide infra*) the samples were prepared by diluting the SF solution to 0.125% (w/v) with the particular medium to a total volume of 2 ml and adding 4  $\mu$ l of the described SO solution.

### Fluorescent labeling of protamine

8 ml of a 1.0 mg/ml solution of Fluorescein isothiocyanate were added drop-wise to 100 ml of a stirred 2.0 mg/ml solution of protamine in 0.1 M Na<sub>2</sub>CO<sub>3</sub> buffer, pH 9.0. The mixture was stirred for 8 h at 4°C protected from light. Afterwards the solution was dialyzed against ultrapure water for 36 h, using a SpectraPor dialysis membrane (MWCO 6-8000 Da) and the solution was freeze-dried for 24 h at 5°C and 0.16 mbar using the freeze dryer Alpha 1-4.

### Fluorescence microscopy

A 32  $\mu$ M SF solution was mixed with a 1.622 mM solution of fluorescent labeled protamine at a molar ratio of 10.4 (corresponding to the last point of titration). An Axio Observer.Z1 microscope equipped with a Plan-Apochromat 40x/0.95 objective and an AxioCam MRm3 camera was used. Excitation wavelength was set to 450-490 nm and emission wavelength to 500-550 nm.

### Design of Experiments

In order to further understand the influences on the interaction between SF and protamine as model protein we performed a Design of Experiments, for each salt (NaCl, NaSCN and Na<sub>2</sub>SO<sub>4</sub>) independently. As factors we chose the pH (4 – 7.5), the ionic strength of particular salt (0 – 250 mM) and the ratio (molar ratio of protamine to SF (0 -12)). We used Modde 9.0 (Umetrics, Umeå, Sweden) to create the experimental plan (**Table 1**) plan by underlying an Onion D-Optimal design (quadratic model).

Experiment	Run Order	pH	Ionic strength [mM]	ratio
1	17	6.33327	83.3375	4.0002
2	13	5.16673	166.663	4.0002
3	9	5.16673	83.3375	7.9998
4	6	6.33327	166.663	7.9998
5	15	6.91673	41.6625	1.9998
6	12	4.58327	208.337	1.9998
7	21	4.58327	41.6625	10.0002
8	19	6.91673	208.337	10.0002
9	3	4	0	0
10	1	4	250	0
11	24	7.5	250	0
12	2	4	0	12
13	11	7.5	0	12
14	4	4	250	12
15	5	7.5	250	12
16	20	7.5	0	4
17	23	7.5	83.3333	0
18	22	6.33333	0	0
19	16	4	125	6
20	7	5.75	250	6
21	8	5.75	125	12
22	10	5.75	125	6
23	18	5.75	125	6
24	14	5.75	125	6

**Table 1:** Experimental plan for Design of Experiments

As responses we were investigating the particle formation in terms of UV absorption at  $\lambda=600$  nm, the surface charge of developed complexes in terms of  $\zeta$ -potential and the loading of protamine on SF in terms of % of initially added protamine, by determining the free portion.

In detail we prepared a particular SF and FITC-labeled protamine solution with the given properties and combined them in the default ratio. Afterwards, the suspension was directly measured in UV/Vis at 600 nm, diluted 1 to 12.5 with ultrapure water for  $\zeta$ -potential and centrifuged at 12800xg for 15 min for loading measurements. All formed particles were thereby

removed and the free protamine in the supernatant was detectable by measuring the fluorescence using an LS 50B luminescence spectrometer setting excitation to 490 nm (slit 2.5) and emission to 514 nm (slit 15.0). The resulting fluorescence value was divided by a reference value, where the same mixture was performed without SF and then the bound content (loading) was calculated based on a FITC calibration curve in the same medium.

The analysis was done using Modde 9.0 and outliers were repeated to confirm their values.

### Stability test of SF solutions

To evaluate if the Hofmeister salts do have an impact on SF structure itself we performed a stability test with the following setup. The SF concentration was set to 1, 3 and 5% (w/v), the temperature was either 5°C or 25°C, as solvents we used water, a 25 mM histidine buffer, pH 7.6 pure and histidine buffer supplemented with NaCl, NaSCN, or Na<sub>2</sub>SO<sub>4</sub> yielding an ionic strength of 0.19 M, respectively. We measured the samples immediately and after 2, 7, 14, 28 and 90 days of storage in closed HPLC vials.

As parameters for the structural changes we used UV/Vis at 600 nm for turbidity, fluorescence with Sypro Orange for hydrophobicity and FTIR for conformation.

The samples were prepared by proper dilution of SF solution, sterile filtration using 0.22 µm syringe filters and filling in HPLC vials under laminar flow to avoid any microbiological influences. They were used directly for UV and fluorescence measurements, and were freeze-dried for 2 days at 3°C, 0.16 mbar and for half a day at 25°C, 0.16 mbar using freeze dryer Alpha 1-4 prior to FTIR analysis.

### FTIR

Freeze-dried samples were measured directly by attenuated total reflectance FTIR. For each measurement, 16 scans were combined with a resolution of 4 cm<sup>-1</sup>, and a wavenumber range from 600 to 4000 cm<sup>-1</sup>. The SpectraManager IR software (JASCO, Frankfurt, Germany) was used for measurement and further analysis.

## Results

### *Interaction SF - protamine*

ITC results of the titration of protamine into an SF solution in histidine buffer (**Figure 1**) showed an initially endothermic pattern with decreasing intensity until a molar ratio of 1.5, where the reaction became exothermic. The heat development increased until reaching its maximum at a molar ratio of 3 and diminished afterwards (**Figure 1 A**). The hydrophobicity of the system was determined by Sypro Orange fluorescence throughout the same titration as performed in the ITC. It increased until a ratio of 2.2 and decreased subsequently, thereby indicating the highest hydrophobicity at the mentioned ratio (**Figure 1 A**). The right angle light scattering showed a slight increase until a molar ratio of 2.6, followed by a very steep step for the next titration point. Afterwards the signal decreased with shrinking speed (**Figure 1 B**). The maximal light scattering matches the charge neutralization, indicated by the  $\zeta$ -potential crossing the value of zero after strongly increasing until the molar ratio of 3. Finally, the  $\zeta$ -potential plateaued at slightly positive values (**Figure 1 B**).

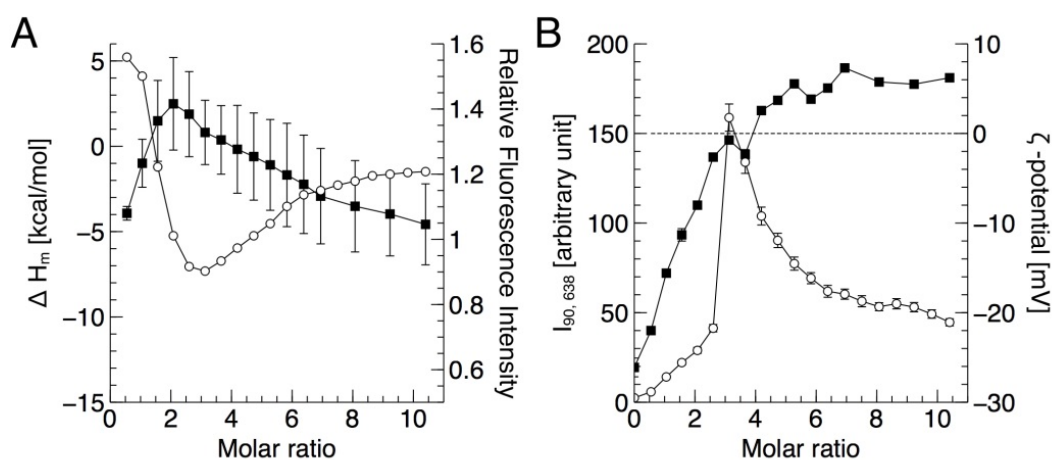


**Figure 1:** Interaction of SF and protamine in histidine buffer. (A) Development of isothermal enthalpy (open circles) and SO fluorescence (filled squares) during addition of increasing amount of protamine to SF. (B) Development of right angle light scattering at 638 nm (open circles) and  $\zeta$ -potential (filled squares) during titration of SF with protamine.

In the presence of 0.19 M NaCl (**Figure 2**), a Hofmeister neutral salt, the ITC curve already started with exothermic signals, which reached their maximum at a ratio of 1.6 and decreased thereafter (**Figure 2 A**). The hydrophobicity showed a small maximum at a ratio of 1.1 and

continuously decreased at higher ratios (**Figure 2 A**). The light scattering results were lower compared to histidine buffer and showed a peak at a ratio of 6.3 (**Figure 2 B**). The  $\zeta$ -potential showed generally lower values and charge neutralization was found later, with its definite point being difficult to determine (**Figure 2 B**).

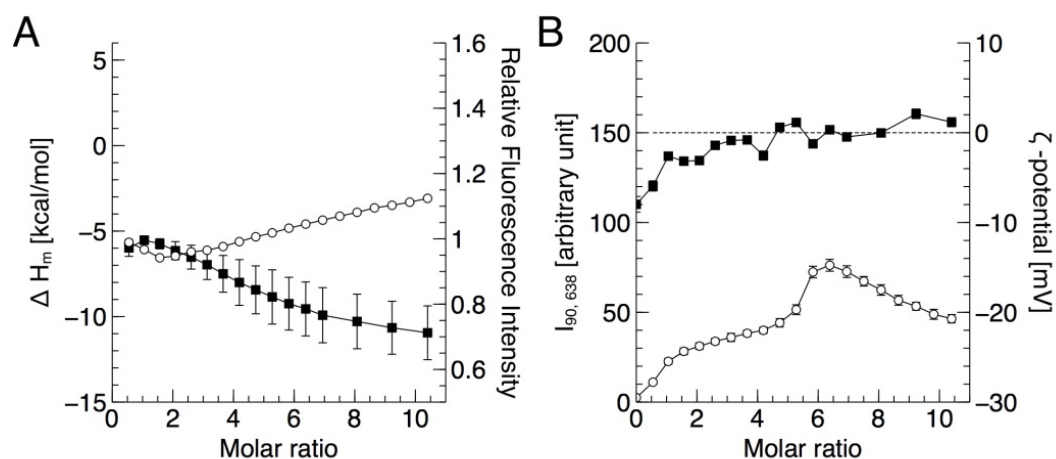


**Figure 2:** Interaction of SF and protamine in histidine buffer containing 0.19 M NaCl. (A) Development of isothermal enthalpy (open circles) and SO fluorescence (filled squares) during addition of increasing amount of protamine to SF. (B) Development of right angle light scattering at 638 nm (open circles) and  $\zeta$ -potential (filled squares) during titration of SF with protamine.

Substitution of NaCl by the chaotropic NaSCN (**Figure 3**) resulted in permanently exothermic ITC signals as well, but the signal kept on increasing throughout the studied molar ratio region (**Figure 3 A**). The hydrophobicity peaked at a ratio of 2.6 and its initial part was steeper, compared to NaCl (**Figure 3 A**). The light scattering intensity increased slightly until a ratio of 5.9, then it got steeper and finally plateaued. The absolute scattering intensity was the highest for all compared conditions (**Figure 3 B**). The  $\zeta$ -potential developed very similar to the titration in the presence of NaCl (**Figure 3 B**).

Finally, Na<sub>2</sub>SO<sub>4</sub> was supplemented to histidine buffer in order to explore the influence of a kosmotropic salt (**Figure 4**). The ITC signals were dramatically reduced and did not indicate any observable reaction heat (**Figure 4 A**). The hydrophobicity decreased throughout the whole titration (**Figure 4 A**), whereas the light scattering showed a slight increase until a ratio of 6.5 and plateaued at higher ratios (**Figure 4 B**). The  $\zeta$ -potential developed almost parallelly, but reached its maximum at a ratio of 5, in contrast to the three other conditions no charge neutralization was detectable (**Figure 4 B**).

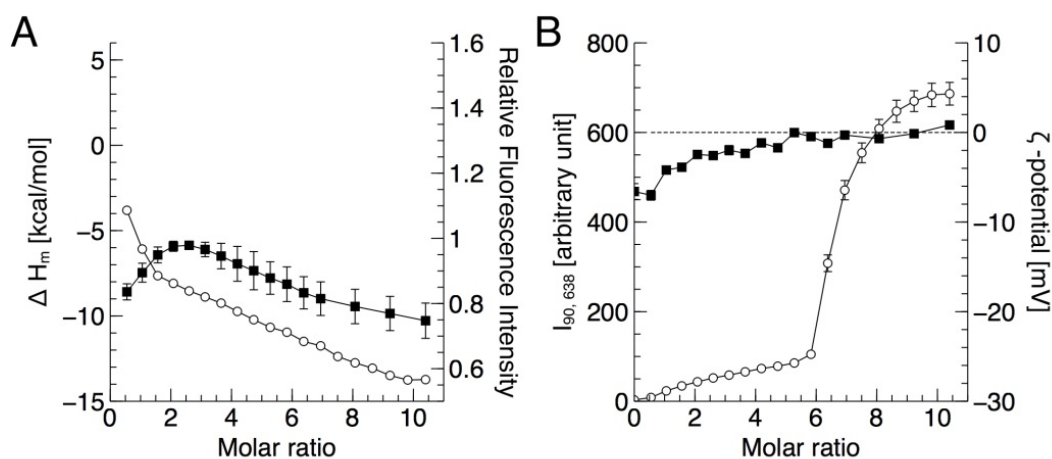


**Figure 3:** Interaction of SF and protamine in histidine buffer containing 0.19 M NaSCN. (A) Development of isothermal enthalpy (open circles) and SO fluorescence (filled squares) during addition of increasing amount of protamine to SF. (B) Development of right angle light scattering at 638 nm (open circles) and  $\zeta$ -potential (filled squares) during titration of SF with protamine.

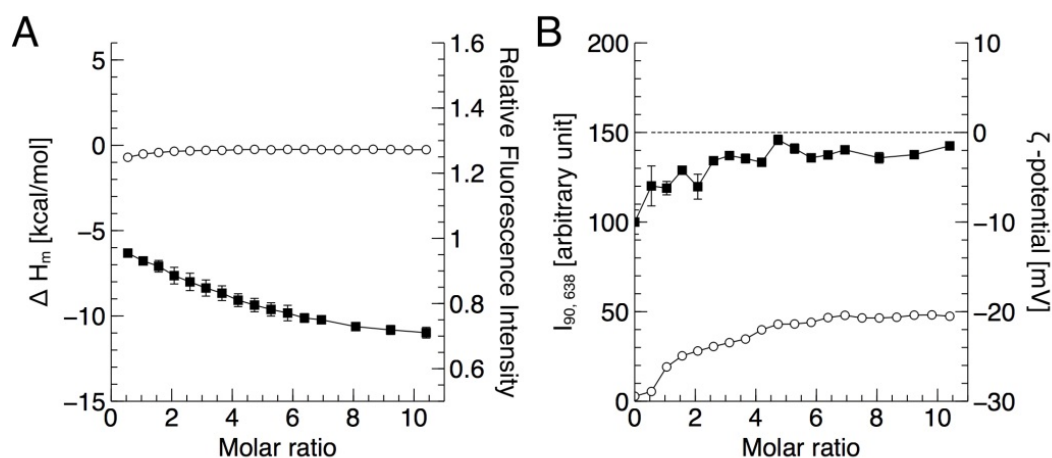


**Figure 4:** Interaction of SF and protamine in histidine buffer containing 64 mM  $\text{Na}_2\text{SO}_4$  (identical ionic strength as 0.19 M NaCl). (A) Development of isothermal enthalpy (open circles) and SO fluorescence (filled squares) during addition of increasing amount of protamine to SF. (B) Development of right angle light scattering at 638 nm (open circles) and  $\zeta$ -potential (filled squares) during titration of SF with protamine.

For a further characterization of formed particles we used nanoparticle tracking analysis (**Figure 5**). As the particle sizes were very diverse, i.e. the particle size in pure SF solution ranged from 100 to 400 nm (data not shown), their analysis was very difficult, and we decided to evaluate particle morphology and pattern upon interaction instead.



In histidine buffer we observed an increasing number of fast moving particles at molar ratios below 2, indicating the formation of smaller particles. Afterwards, larger, slower moving particles, as well as duplet or triplet particles were detected (**Figure 5 A1-4**). In the presence of NaCl small particles were formed at molar ratios from 1.1 to 3.2, again followed by interaction and the formation of duplex particles (**Figure 5 B1-4**). For NaSCN the outcome was very similar as for NaCl, with a lower amount of larger particles (**Figure 5 C1-4**). However, the substitution by Na<sub>2</sub>SO<sub>4</sub> resulted in no observable changes in particle size or pattern throughout the whole titration (**Figure 5 D1-4**).

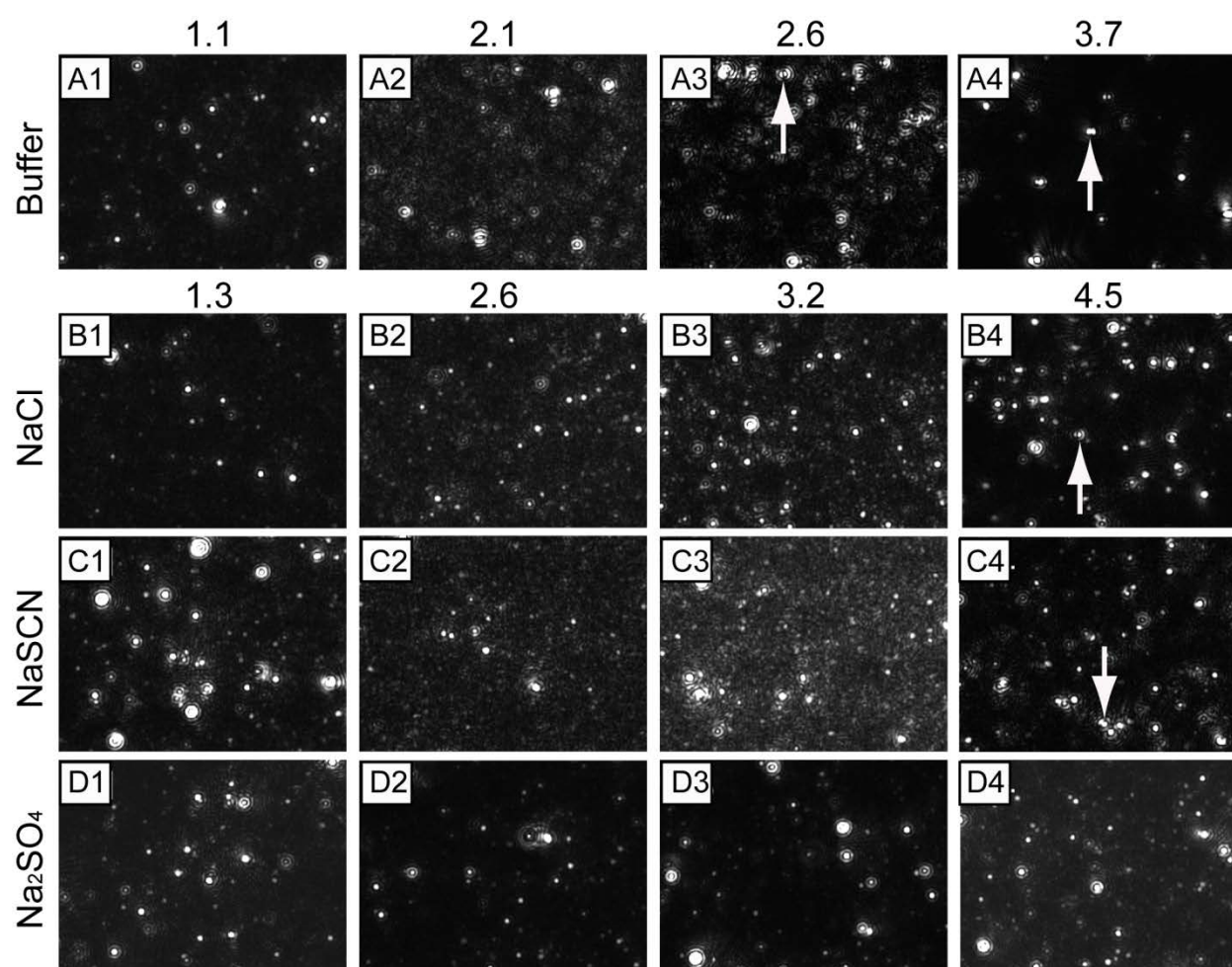


**Figure 5:** Evaluation of nanoparticle characteristics during the titration in different buffer and salt solutions using nanoparticle tracking analysis. Titrations were performed in histidine buffer, NaCl, NaSCN and Na<sub>2</sub>SO<sub>4</sub>, respectively. Representative video stills are shown for the SF to protamine ratio of 1.1, 2.1, 2.6 and 3.7 for histidine buffer and 1.3, 2.6, 3.2, and 4.5 for all other salts deployed, respectively. Arrows highlight duplex particles.

In the presence of histidine buffer, NaCl and NaSCN we could detect particles in micrometer size at the ratio 10.4 of fluorescent labeled protamine to SF. These were characterized by fluorescence microscopy and following analysis of Ferret diameter and revealed many small particles for the NaSCN conditions, and fewer but bigger particles in the presence of NaCl (**Figure 6**).

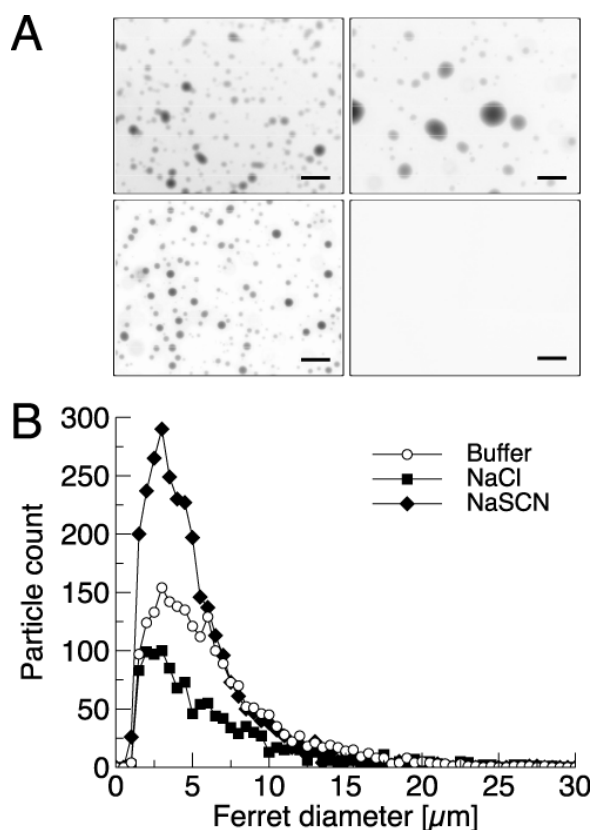


**Figure 6:** Microscopic analysis of complex coacervate at a protamine/SF mixing ratio of 10.4. (A) Representative micrographs of particles formed in histidine buffer (top left), NaCl (top right), NaSCN (bottom left) and  $\text{Na}_2\text{SO}_4$  (bottom right). Scale bar represents 25 mm. (B) Analysis of Ferret diameter of particles in histidine buffer (open circles), NaCl (filled squares) and NaSCN (filled diamonds).

For the DOE, we chose 3 factors (i) pH value, (ii) ionic strength of selected salt and (iii) ratio of protamine to SF for each salt to study physico-chemical and galenical properties including (i) particle formation, which was followed photometrically at  $\lambda = 600$  nm, (ii) loading of protamine in percent of initially applied protamine and (iii) the  $\zeta$ -potential (**Figure 7**). The particle formation was significantly influenced by the pH and the ratio in the presence of NaCl. For NaSCN the significant parameters were the ionic strength and the ratio. For both salts the ratio was the more

important factor. The replacement by  $\text{Na}_2\text{SO}_4$  revealed the same significant parameters as for NaSCN, but showed the opposite impact order (**Figure 7 A-C**).

The loading, in the presence of NaCl and NaSCN was only impacted by the ratio, whereas for  $\text{Na}_2\text{SO}_4$  the only significant parameter was the ionic strength (**Figure 7 D-F**). The absolute loading values differed between the salts. When NaSCN was supplemented, the highest loading was achieved with up to 70%. In the presence of NaCl only 40% were maximum and for  $\text{Na}_2\text{SO}_4$  only 25%.

The  $\zeta$ -potential results were significantly influenced by all three factors, regardless which salt was supplemented. As the ionic strength directly influenced the measurement itself, only pH and ratio are shown in the figure (**Figure 7 G-I**).

As the underlying analysis is only feasible with the prerequisite of normally distributed deleted studentized residuals, a Shapiro-Wilk test was performed and showed a normal distribution for all data (**Table 2**).

	<b>salt type</b>	<b>p-value</b>	<b>distribution</b>
<b>UV</b>	NaCl	0.897	normal
	NaSCN	0.066	normal
	$\text{Na}_2\text{SO}_4$	0.163	normal
<b>Loading</b>	NaCl	0.09	normal
	NaSCN	0.107	normal
	$\text{Na}_2\text{SO}_4$	0.939	normal
<b><math>\zeta</math>-potential</b>	NaCl	0.124	normal
	NaSCN	0.457	normal
	$\text{Na}_2\text{SO}_4$	0.065	normal

**Table 2:** Shapiro-Wilk test for normal distribution of the deleted studentized residuals for each set of experiments

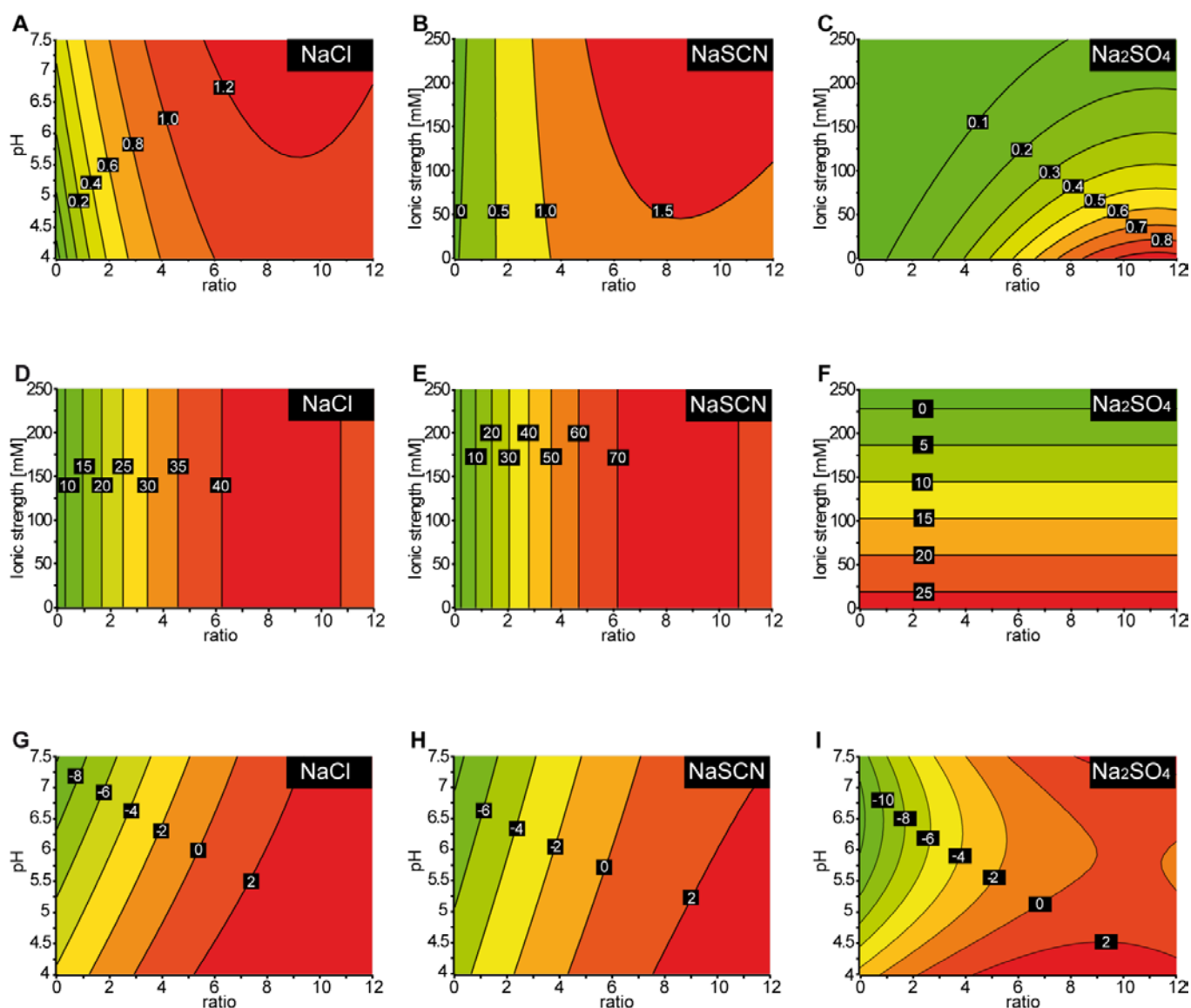


**Figure 7:** (A-C) Particle formation as a function of significant input parameters. (A) Significant input parameters in the presence of NaCl were pH and the ratio of protamine to SF ('ratio'). (B) Particle formation in the presence of NaSCN was impacted by the ionic strength of the salt and the ratio but not the solution pH. (C) With Na<sub>2</sub>SO<sub>4</sub>, the ionic strength and the ratio were significant input parameters. Numbers within the panels indicate the absorption by particles as monitored at  $\lambda = 600$  nm

(D-F) Loading of protamine to SF as a function of significant input parameters. (D, E) For both NaCl and NaSCN the only significant input parameter was the ratio, whereas for Na<sub>2</sub>SO<sub>4</sub> (F) only the ionic strength was significant. Numbers within panels indicate the loading in % of initially applied protamine.

(G-I)  $\zeta$ -potential as a function of significant parameters. For all 3 salts ionic strength, ratio and pH were significant parameters, but only pH and ratio are shown here, because the ionic strength had an impact on the measurement itself. (G) NaCl, (H) NaSCN, (I) Na<sub>2</sub>SO<sub>4</sub>. Numbers within panels indicate the  $\zeta$ -potential in mV.

### Interaction SF- polylysine

The ITC results showed mainly endothermic signals for all examined conditions, which was in contrast to protamine, where we only observed a small endothermic part in histidine buffer. Additionally, the enthalpy signal was a lot higher compared to protamine, especially in buffer, and the whole interaction process took place at considerably lower molar ratios (**Figure 8 A**). By comparing the chosen conditions we could observe a decreasing interaction intensity from buffer, over NaCl and NaSCN to Na<sub>2</sub>SO<sub>4</sub>. The pattern of the static light scattering showed plateau regions for all conditions at higher molar ratios, with the end of increasing signal depending on buffer composition, as it was 0.37 for pure buffer, 0.16 for NaCl, 0.37 for NaSCN and 0.32 for Na<sub>2</sub>SO<sub>4</sub> (**Figure 8 B**). The  $\zeta$ -potential did not show a definite trend in the presence of salt, but a slope from -19 mV to 9 mV in buffer. The charge neutralization happened at a molar ratio of 0.6, which is not consistent with the maximal light scattering as it was for protamine (**Figure 8 C**).

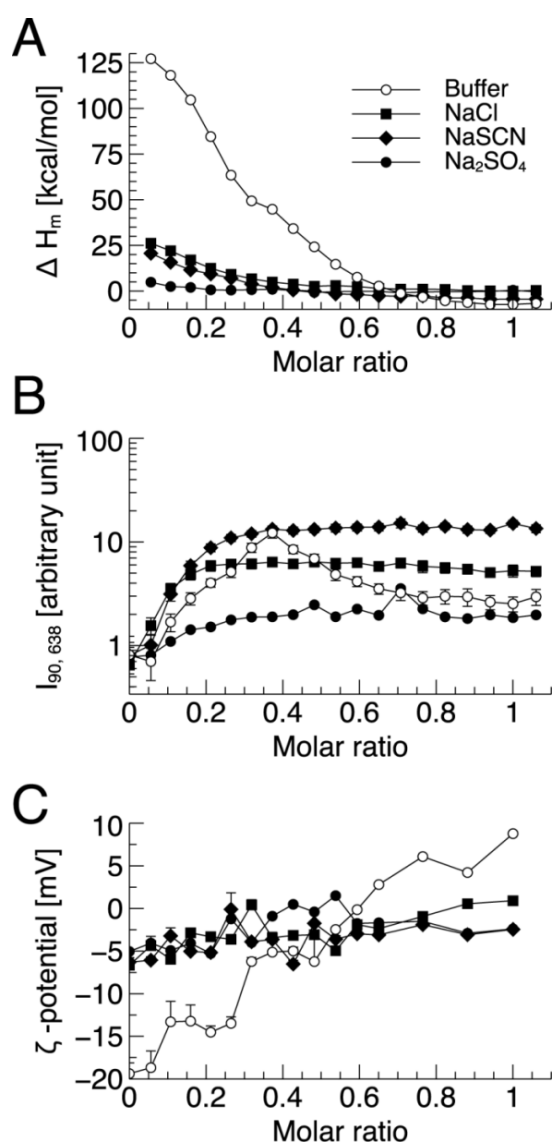


**Figure 8:** Analysis of interaction of polylysine and SF. (A) Isothermal titration calorimetry, (B) right angle light scattering at 638 nm and (C)  $\zeta$ -potential obtained upon mixing of polylysine to SF in histidine buffer (open circles), NaCl (filled squares), NaSCN (filled diamonds), and Na<sub>2</sub>SO<sub>4</sub> (filled circles).

***Stability***

We stored SF solutions in different media (pure water, histidine buffer and histidine buffer supplemented with NaCl, NaSCN and Na<sub>2</sub>SO<sub>4</sub> at an ionic strength of 0.19 M, respectively) and concentrations (1, 3 and 5% (w/v)) for up to 90 days. After 90 days all samples in pure water and histidine buffer formed hydrogels, independently of the SF concentration. In Na<sub>2</sub>SO<sub>4</sub> the hydrogel formation was only observable at 3 and 5% (w/v) SF. The FTIR results for 5% solutions after 90 days of storage (**Figure 9**) showed a shift to  $\beta$ -sheet structure (1637 to 1620 cm<sup>-1</sup>) for water, histidine buffer and Na<sub>2</sub>SO<sub>4</sub> (**Figure 9 A-C**), and preserved random coil structure (1637 cm<sup>-1</sup>) in NaCl and NaSCN (**Figure 9 D, E**).

The UV absorption at  $\lambda = 600$  nm was determined at each time point in order to observe possible particle formation due to aggregation of SF (**Figure 10 A**) and showed no detectable turbidity throughout the whole testing period for all of the chosen solutions.

The hydrophobicity, tested by Sypro Orange fluorescence (**Figure 10 B**) did not show a definite trend for the conformation development over time.

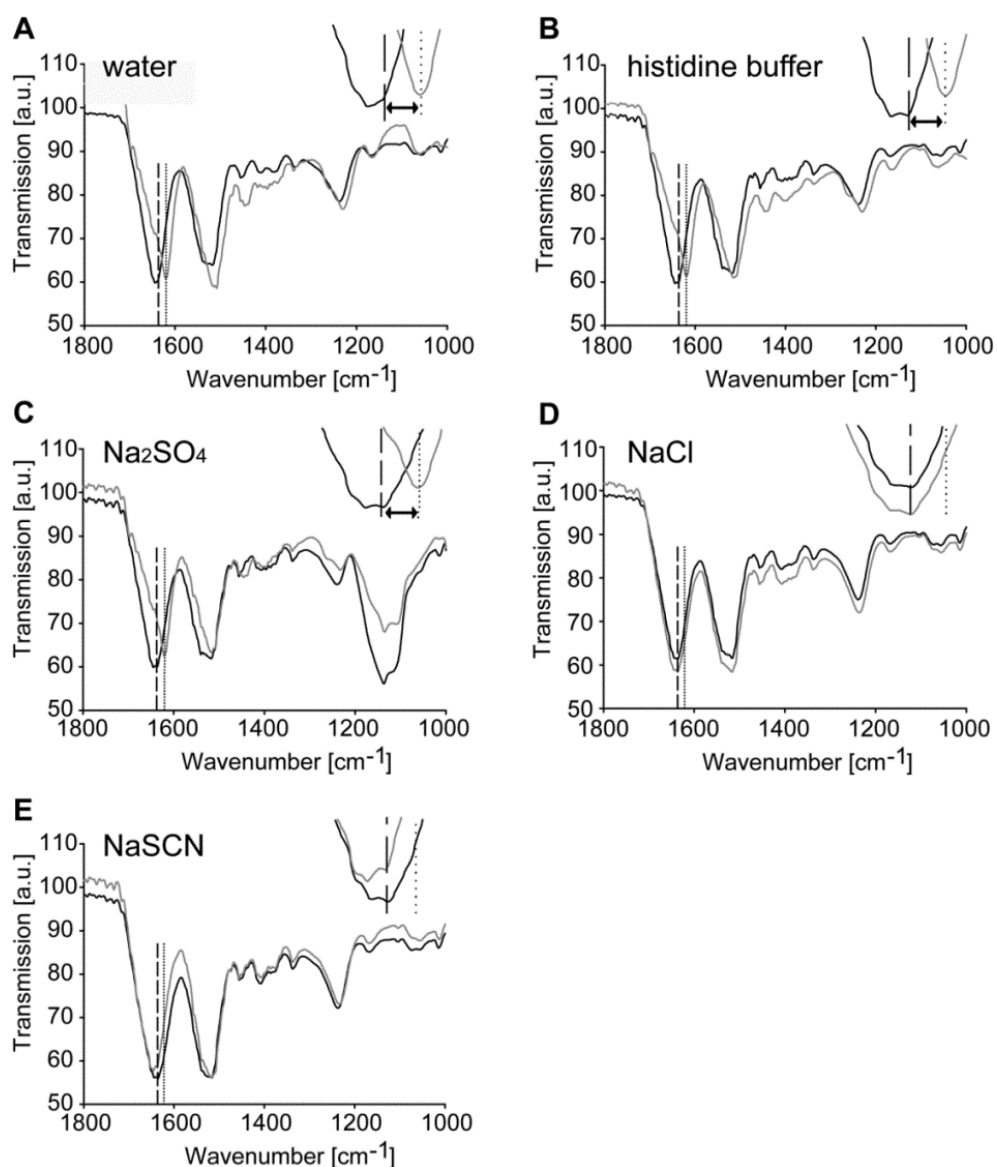


**Figure 9:** FTIR transmission spectra of selected samples at the beginning of the testing period (black line) and after 90 days (gray line) when stored at 25°C and an SF concentration of 5% (m/V). The dashed line marks 1637  $\text{cm}^{-1}$ , indicative for random coil conformation and the dotted line marks 1620  $\text{cm}^{-1}$ , indicating  $\beta$ -sheets. Experiments were conducted in (A) water, (B) histidine buffer, (C)  $\text{Na}_2\text{SO}_4$ , (D)  $\text{NaCl}$  or (E)  $\text{NaSCN}$ , respectively. The 1637 - 1620  $\text{cm}^{-1}$  shift was observed for water, histidine buffer and  $\text{Na}_2\text{SO}_4$  in histidine buffer and not in the presence of  $\text{NaSCN}$  and  $\text{NaCl}$ . [a.u.] = arbitrary units. Inserts highlight the wave numbers 1637 - 1620  $\text{cm}^{-1}$ .

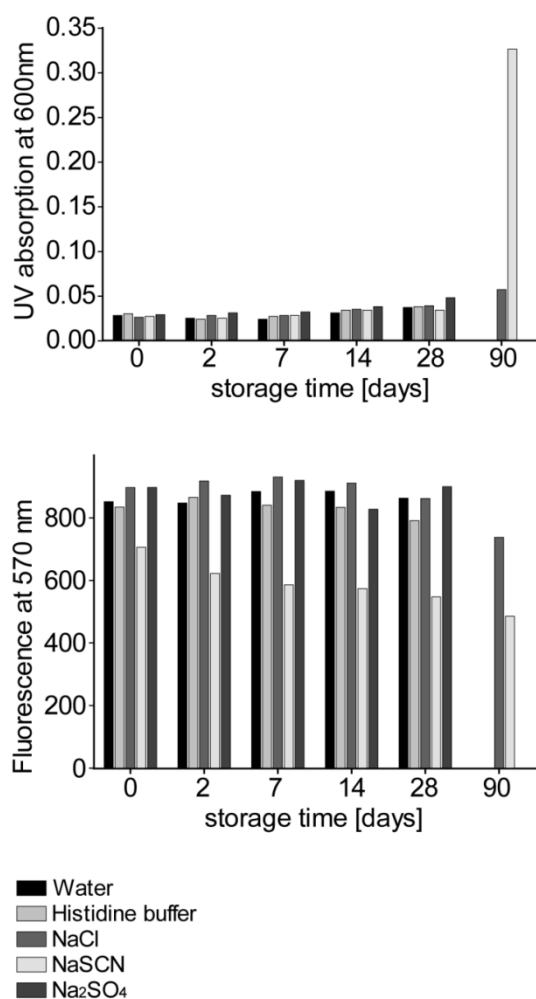


**Figure 10:** Particle formation in SF solution when stored at 25°C and an SF concentration of 5% (m/V) was determined by UV absorption at  $\lambda = 600$  nm and hydrophobicity was determined by Sypro Orange fluorescence at  $\lambda_{em} = 570$  nm. Experiments were conducted in water, histidine buffer or histidine buffer supplemented with salts at an ionic strength of 0.19 M using Na<sub>2</sub>SO<sub>4</sub>, NaCl or NaSCN, respectively. The gray shades indicate the different media (compare legend) and the experiments were performed at the beginning of the storage period, and after 2, 7, 14, 28 and 90 days. After 90 days the samples in water, histidine buffer and Na<sub>2</sub>SO<sub>4</sub> formed hydrogels, therefore, no data points were measured here.



## Discussion

Initially, the interaction between SF and protamine in pure histidine buffer, which stands for almost no further influence factors than the two proteins themselves, is studied.

SF in solution contains free molecules and additionally forms micelles [14]. Both structures contribute to the process and allow interaction with protamine. At low molar ratios, the binding of protamine to free SF molecules resulted in the formation of nanocomplexes, which can be observed in SLS (**Figure 1 B**) and NTA (**Figure 5 A 1, 2**) and continued until reaching charge neutrality. At this point the nanocomplexes started to aggregate and phase separation occurred (**Figure 1 B; 5 A 3, 4**). The nanocomplex formation typically is an entropical process, mainly driven by release of counterions as it was described elsewhere [15]. This is supported by our observations of decreasing interactions with increasing ionic strength of the system (**Figure 2 A**) and prior results for comparable setups [16-18]. The simple interaction between polycations (protamine) and polyanions (SF), which seems to manifest itself in ion pairing during the first part of the interaction, accompanied by endothermic ITC signals, is followed by coacervation and phase separation at higher ratios [19, 20]. The above-mentioned SF micelles might also have an impact, mainly on the endothermic signals observed at low molar ratios. While the free molecules contribute to the general process by entropically driven association of protamine to SF, the micelles were probably destroyed and the folding of SF was changed, which is supported by the observation of increasing hydrophobicity (**Figure 1 A**). These structural changes probably were a main reason for the endothermic signals [21] at low molar ratios, as very similar titration curves were recorded for other studies including the role of micelles [22], although their system differed from ours, with the micelle-containing partner being placed in the ITC syringe and not in the cell as for our experiments, resulting in completely different excess proportions. At ratios above two, the signal became exothermic and increased until entering a phase of decreasing signal strength, indicating reduced interactions at this part. As we could parallelly observe a decreasing hydrophobicity, we assume shielding effects of already adsorbed protamine being responsible for decreased interactions in means of a saturation of binding sites.

The ability of protamine to induce the unfolding of SF, respectively the stability of its micelles was highly influenced by the present salt and its ionic strength, which was expectable as the right choice of salt is very important during the natural spinning process [23]. In the presence of 0.19 M NaCl the ITC curve looked similar to histidine buffer, but lacked the initial endothermic part, which was probably due to the higher ionic strength, lowering the entropy gain by counterion

release. Additionally, the  $\zeta$ -potential was reduced, which further decreased electrostatic interactions. However, the principle was maintained and the micelle stability was only marginally influenced, as supported by the DOE results (**Figure 7 A, D**), not showing a significant influence of ionic strength for both loading and particle formation. The pH effect on particle formation was smaller than the impact of the ratio and is simply explainable by a higher charge density with increasing distance to the pI ( $\approx 4.5$  [8]), allowing more electrostatic interaction and a more elongated conformation [24], easing the access of interaction partners. The effect of pH on the  $\zeta$ -potential was again due to the different charge densities while the effect of the ratio was due to the shielding of these charges, comparable as explained before for the saturation of the ITC curve (*vide supra*). This is true for all three salts, with only minor differences in the exact figure (**Figure 7 G-I**).

In contrast, the other salts influenced the interaction between SF and protamine, by their Hofmeister properties. We assume that they are able to affect the micellar structure of SF comparable to experiences with other protein and micellar systems [25-27] and as already similarly indicated for SF [28, 29].

The chaotropic NaSCN led to a completely different pattern of ITC signals, with increasing exothermic signals throughout the whole tested molar ratio. Additionally, it showed a different pattern in NTA measurements, with the formation of many smaller particles (**Figure 5 C 3**), and of coacervates at a smaller size, than the other conditions (**Figure 6**). Altogether, this indicates the destabilization of SF micelles and thereby an easier approaching of protamine, which was then able to open up more binding sites for itself, resulting in a more efficient interaction. This finding is supported by the DOE data (**Figure 7 B, E**), where we could find the highest loading efficiency for NaSCN, although ionic strength has not been a significant factor for this response. However, the ionic strength had a significant, but weak impact on the particle/nanocomplex formation.

Finally,  $\text{Na}_2\text{SO}_4$  as the kosmotropic salt was able to completely abolish the interaction between SF and protamine at 0.19 M ionic strength, as we could not detect any heat signals (**Figure 4 A**), nor nanocomplex formation (**Figure 4 B, 5 D**), nor coacervation tendencies (**Figure 6**). The DOE results showed a huge impact of the ionic strength on both particle formation and loading (**Figure 7 C, F**), whereas the maximal loading was the lowest compared to the other two salts. As the loading was solely impacted by the ionic strength, we assume the existence of a threshold-concentration of  $\text{Na}_2\text{SO}_4$ , above which no interaction is possible. The mechanism of interaction is probably, similar to NaSCN, influenced by impacting the SF micelle structure, but in a stabilizing manner.

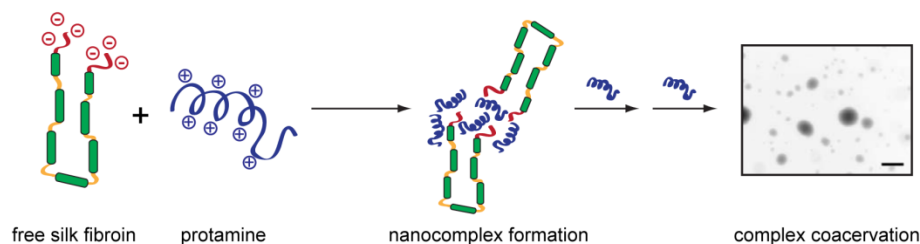
In conclusion, it is possible to improve and control the interaction between protamine and SF by controlling the environmental properties, like salt type, ionic strength and pH (**Figure 11**). In terms of application as drug delivery device, this could provide the possibility of tailored drug loading with reproducible results.

When replacing protamine with polylysine, the ITC results in all chosen media initially showed endothermic signals (**Figure 8 A**). Especially for pure histidine buffer, they were a lot higher compared to protamine and did not reach a noteworthy shift to exothermic signals at higher ratios. A very similar outcome was found by Chang et al. [30], who also reacted polylysine with a polyanion, but chose a polysaccharide for this purpose. The principle of an entropically motivated process already presented for protamine, is also visible for polylysine, as an increase in ionic strength dramatically reduced the heat signal. However, this happened almost independently of the chosen salt type.

As we found both, conformity and discrepancy, when comparing the observed effects for protamine and polylysine, we can assume that the environmental effects (salt type, ionic strength, pH) on SF are generally not sufficient to explain and regulate the interaction process. The nature and structure of the interaction partner also has an impact, probably mainly due to its capability to interfere with the SF structure and thereby opening more binding sites for themselves. In our case, protamine, which consists of positively charged as well as hydrophobic sections, seems to fulfill this task better than polylysine, which lacks molecular parts that can potentially interact with the hydrophobic core of SF micelles.

The influence of Hofmeister salts on the SF structure was further studied, to find a way to store SF solution without precipitation and hydrogel formation. The FTIR results showed no  $\beta$ -sheet formation in the presence of NaCl and NaSCN (**Figure 9 D, E**), which allows the conclusion of stable storage over the tested 90 days. Similar to our reasoning for the salt-influence on the interaction, this is probably due to the SF structure itself, including its micelles. The chaotropic NaSCN decreased the hydrophobic interactions, which would lead to  $\beta$ -sheet formation in the SF molecule, and kept it in solution instead. The conformational change of SF to its precipitating form was successfully suppressed for NaCl and NaSCN, opening the possibility for storage of liquid formulations by addition of proper salts. As the effect is observable for NaCl and even for Na<sub>2</sub>SO<sub>4</sub> to a lesser extent, as, at least the lower SF concentrations did not form a hydrogel, the pure ionic strength of the systems seems to influence the stability. However, these results are preliminary as the testing period and sample size was not sufficient and further studies are necessary before a final statement can be made.

## Complex coacervation of free silk fibroin:



## Specific ion effects on micelle stability:

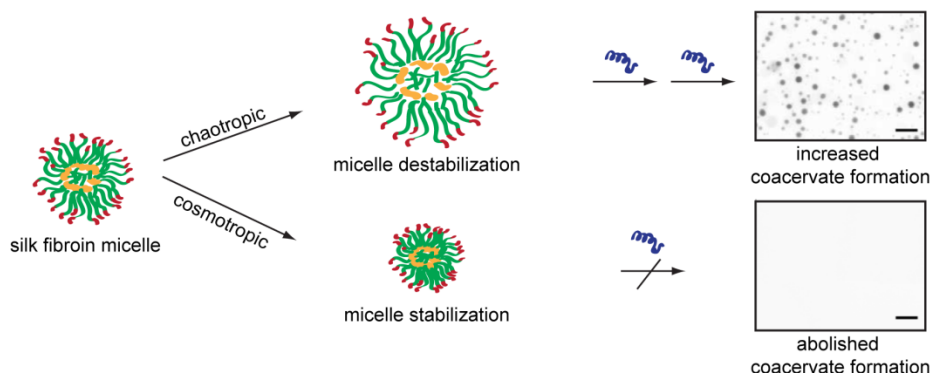


**Figure 11:** Mechanism of drug load of free SF molecules by complex coacervation and deployment of chaotropic and kosmotropic salts to impact SF micelle stability for tailored drug load.

## Conclusion

Our experiments delivered evidence for the possibility to change the stability of SF micelles by choosing the right environmental conditions, especially the proper salt. This has an impact on the pattern in solution as well as on the interaction with a partner. In solution we were able to prolong the stability of SF solutions and avoid the formation of  $\beta$ -sheets and thereby hydrogels. This may allow the future development of liquid SF formulations, if our results are confirmed over a longer time and in formulations. The influence on the interaction was possible through the destabilization of SF micelles or the stabilization thereof to avoid any further association. This might offer a tool for controlled drug loading and release, although it still needs to be studied how our results can be transferred to a general technique.

## References

- [1] L. Uebersax, T. Apfel, K.M. Nuss, R. Vogt, H.Y. Kim, L. Meinel, D.L. Kaplan, J.A. Auer, H.P. Merkle, B. von Rechenberg, Biocompatibility and osteoconduction of macroporous silk fibroin implants in cortical defects in sheep, *European journal of pharmaceutics and biopharmaceutics : official journal of Arbeitsgemeinschaft fur Pharmazeutische Verfahrenstechnik e.V.*, 85 (2013) 107-118.
- [2] A.J. Meinel, O. Germershaus, T. Luhmann, H.P. Merkle, L. Meinel, Electrospun matrices for localized drug delivery: current technologies and selected biomedical applications, *European journal of pharmaceutics and biopharmaceutics : official journal of Arbeitsgemeinschaft fur Pharmazeutische Verfahrenstechnik e.V.*, 81 (2012) 1-13.
- [3] E. Wenk, H.P. Merkle, L. Meinel, Silk fibroin as a vehicle for drug delivery applications, *Journal of controlled release : official journal of the Controlled Release Society*, 150 (2011) 128-141.
- [4] S. Hofmann, H. Hagenmüller, A.M. Koch, R. Müller, G. Vunjak-Novakovic, D.L. Kaplan, H.P. Merkle, L. Meinel, Control of in vitro tissue-engineered bone-like structures using human mesenchymal stem cells and porous silk scaffolds, *Biomaterials*, 28 (2007) 1152-1162.
- [5] L. Uebersax, H.P. Merkle, L. Meinel, Insulin-like growth factor I releasing silk fibroin scaffolds induce chondrogenic differentiation of human mesenchymal stem cells, *J Control Release*, 127 (2008) 12-21.
- [6] E. Wenk, A.J. Wandrey, H.P. Merkle, L. Meinel, Silk fibroin spheres as a platform for controlled drug delivery, *Journal of Controlled Release*, 132 (2008) 26-34.
- [7] N.A. Guzewicz, A.J. Massetti, B.J. Perez-Ramirez, D.L. Kaplan, Mechanisms of monoclonal antibody stabilization and release from silk biomaterials, *Biomaterials*, 34 (2013) 7766-7775.
- [8] A. Matsumoto, J. Chen, A.L. Collette, U.J. Kim, G.H. Altman, P. Cebe, D.L. Kaplan, Mechanisms of silk fibroin sol-gel transitions, *The journal of physical chemistry. B*, 110 (2006) 21630-21638.
- [9] J.J. Grigsby, H.W. Blanch, J.M. Prausnitz, Effect of secondary structure on the potential of mean force for poly-L-lysine in the alpha-helix and beta-sheet conformations, *Biophysical chemistry*, 99 (2002) 107-116.
- [10] D. Awotwe-Otoo, C. Agarabi, D. Keire, S. Lee, A. Raw, L. Yu, M.J. Habib, M.A. Khan, R.B. Shah, Physicochemical characterization of complex drug substances: evaluation of structural similarities and differences of protamine sulfate from various sources, *The AAPS journal*, 14 (2012) 619-626.
- [11] W. Kunz, P. Lo Nostro, B.W. Ninham, The present state of affairs with Hofmeister effects, *Current Opinion in Colloid & Interface Science*, 9 (2004) 1-18.
- [12] Y. Zhang, P. Cremer, Interactions between macromolecules and ions: the Hofmeister series, *Current Opinion in Chemical Biology*, 10 (2006) 658-663.
- [13] L. Meinel, S. Hofmann, V. Karageorgiou, L. Zichner, R. Langer, D. Kaplan, G. Vunjak-Novakovic, Engineering cartilage-like tissue using human mesenchymal stem cells and silk protein scaffolds, *Biotechnology and bioengineering*, 88 (2004) 379-391.
- [14] H.-J. Jin, D.L. Kaplan, Mechanism of silk processing in insects and spiders, *Nature*, 424 (2003) 1057-1061.

- [15] A.L. Becker, K. Henzler, N. Welsch, M. Ballauff, O. Borisov, Proteins and polyelectrolytes: A charged relationship, *Current Opinion in Colloid & Interface Science*, 17 (2012) 90-96.
- [16] R. Chollakup, J.B. Beck, K. Dirnberger, M. Tirrell, C.D. Eisenbach, Polyelectrolyte Molecular Weight and Salt Effects on the Phase Behavior and Coacervation of Aqueous Solutions of Poly(acrylic acid) Sodium Salt and Poly(allylamine) Hydrochloride, *Macromolecules*, 46 (2013) 2376-2390.
- [17] C.G. de Kruijff, F. Weinbreck, R. de Vries, Complex coacervation of proteins and anionic polysaccharides, *Current Opinion in Colloid & Interface Science*, 9 (2004) 340-349.
- [18] S.L. Turgeon, C. Schmitt, C. Sanchez, Protein-polysaccharide complexes and coacervates, *Current Opinion in Colloid & Interface Science*, 12 (2007) 166-178.
- [19] D. Priftis, N. Laugel, M. Tirrell, Thermodynamic characterization of polypeptide complex coacervation, *Langmuir*, 28 (2012) 15947-15957.
- [20] S.L. Turgeon, M. Beaulieu, C. Schmitt, C. Sanchez, Protein-polysaccharide interactions: phase-ordering kinetics, thermodynamic and structural aspects, *Current Opinion in Colloid & Interface Science*, 8 (2003) 401-414.
- [21] T. Ooi, Thermodynamics of protein folding: effects of hydration and electrostatic interactions, *Advances in biophysics*, 30 (1994) 105-154.
- [22] A.D. Nielsen, L. Arleth, P. Westh, Analysis of protein-surfactant interactions—a titration calorimetric and fluorescence spectroscopic investigation of interactions between *Humicola insolens* cutinase and an anionic surfactant, *Biochimica et Biophysica Acta (BBA) - Proteins and Proteomics*, 1752 (2005) 124-132.
- [23] D.P. Knight, F. Vollrath, Changes in element composition along the spinning duct in a *Nephila* spider, *Naturwissenschaften*, 88 (2001) 179-182.
- [24] A.S. Lammel, X. Hu, S.-H. Park, D.L. Kaplan, T.R. Scheibel, Controlling silk fibroin particle features for drug delivery, *Biomaterials*, 31 (2010) 4583-4591.
- [25] D.A. Chiappetta, A. Sosnik, Poly(ethylene oxide)-poly(propylene oxide) block copolymer micelles as drug delivery agents: improved hydrosolubility, stability and bioavailability of drugs, *European journal of pharmaceutics and biopharmaceutics : official journal of Arbeitsgemeinschaft fur Pharmazeutische Verfahrenstechnik e.V*, 66 (2007) 303-317.
- [26] M. Malmsten, B. Lindman, Self-assembly in aqueous block copolymer solutions, *Macromolecules*, 25 (1992) 5440-5445.
- [27] M.T. Record, Jr., E. Guinn, L. Pegram, M. Capp, Introductory lecture: interpreting and predicting Hofmeister salt ion and solute effects on biopolymer and model processes using the solute partitioning model, *Faraday discussions*, 160 (2013) 9-44; discussion 103-120.
- [28] M. Geisler, T. Pirzer, C. Ackerschott, S. Lud, J. Garrido, T. Scheibel, T. Hugel, Hydrophobic and Hofmeister effects on the adhesion of spider silk proteins onto solid substrates: an AFM-based single-molecule study, *Langmuir*, 24 (2008) 1350-1355.
- [29] L. Eisoldt, J.G. Hardy, M. Heim, T.R. Scheibel, The role of salt and shear on the storage and assembly of spider silk proteins, *Journal of structural biology*, 170 (2010) 413-419.
- [30] Y. Chang, L. McLandsborough, D.J. McClements, Interactions of a cationic antimicrobial (epsilon-polylysine) with an anionic biopolymer (pectin): an isothermal titration calorimetry, microelectrophoresis, and turbidity study, *Journal of agricultural and food chemistry*, 59 (2011) 5579-5588.







---

## CHAPTER III

### IMMOBILIZING OF INTERLEUKIN-4 FOR PERMANENT M2-ACTIVATION OF MACROPHAGES

The data in this Chapter is unpublished.

All experimental work described in the following chapter was done by me, except for the following:

- Cloning  
The strategy was discussed and planned by me in collaboration with Prof. Dr. Dr. Lorenz Meinel and Dr. Tessa Lühmann, and the technical work was performed by Cornelia Heindl (former technical assistant at the Chair of Pharmaceutics and Biopharmaceutics, University of Wuerzburg).
- MALDI-MS  
The experiments were discussed and planned by me in collaboration with Prof. Dr. Dr. Lorenz Meinel, Dr. Tessa Lühmann and Dr. Jennifer Ritzer. The preparing steps were performed by me, and the technical work of the analytical part was performed by Dr. Jennifer Ritzer (Post Doc at the Chair of Pharmaceutics and Biopharmaceutics, University of Wuerzburg).
- Trypsin digestion and NanoLC-MS/MS analysis  
The strategy was discussed and planned by me in collaboration with Prof. Dr. Dr. Lorenz Meinel, Dr. Tessa Lühmann, and the technical work, analysis of data and method description was provided by Stephanie Lamer (Rudolf-Virchow-Zentrum, University of Wuerzburg).

**Abstract**

Interleukin-4 (IL-4) is a cytokine driving macrophages to M2 macrophages, which are known to provide anti-inflammatory effects. The possibility to regulate the polarization of macrophages to this state might be attractive for a variety of diseases, like atherosclerosis, in which macrophages are involved. As these cases demand a long-term treatment, this polarization was supposed to be maintained over time and we were planning to achieve this by keeping IL-4 permanently present in an immobilized way. In order to immobilize it, we genetically introduced an alkyne-carrying, artificial amino acid in the IL-4 sequence. This allowed access to a site-specific click reaction (Cu(I)-catalyzed Huisgen azide-alkyne cycloaddition) with an azide partner. This study was able to set the basis for the project by successful expression and purification of the IL-4 analogue and by proving maintained bioactivity and the availability for the click reaction. The other side of this project was the isolation of human monocytes and the polarization and characterization of human macrophages. The challenge here was that the majority of related research was based on murine macrophages which was not applicable to human cells and the successful work was so far limited to establishing the necessary methods.

## Introduction

This research is driven by the effort to polarize macrophages into the M2 state by exposure to a stimulating cytokine, which we aimed to immobilize on a surface, to ensure the maintenance of activation over time. M2 macrophages are, in contrast to M1 macrophages, fulfilling the trophic role of this cell type. They have a positive impact on wound healing and other repair processes in the human body [1-3]. The control of the polarization of macrophages could be attractive in many diseases, where macrophages are involved in inflammation, including rheumatoid arthritis [4], obesity [5, 6] and atherosclerosis [7, 8]. In order to reach this target, we started the experimental work on this project from two different sides.

The first was the expression of an immobilizable stimulus, able to activate macrophages to their M2 state. We chose the cytokine interleukin-4 (IL-4) to fulfill this task, as it is known to be a major inducer for M2 activation [2]. Its structure includes four alpha-helices, arranged in an antiparallel way and connected by two  $\beta$ -sheet parts [9] (**Figure 1**). We introduced an artificial amino acid, namely a propargyl-protected lysine derivate (Plk) (**Figure 2**), in its sequence in order to insert an alkyne group. We chose to substitute Lysine 42 by Plk, as this is not involved in any receptor binding activities [10] (**Figure 1**) and is directed outwards, which should allow it to be reachable by the corresponding partner. The necessary modification of the IL-4 gene was done by introducing an amber codon in position 42 [11]. This codon (TAG) usually works as a stop codon, and would not allow the expression by *E.coli* without further intervention. Therefore, we co-transformed a second vector, carrying pyrrolysine tRNA synthetase pylS [12] from *Methanosarcina barkeri* and the gene for the pyrrolysine tRNA was harbored by the IL-4-containing vector. In combination, the two additionally introduced genes enabled the synthesis of Plk-loaded pyrrolysine tRNA, thereby the continued translation and eventually the expression of Plk IL-4 in *E.coli*.

Plk, more precisely its alkyne group, offers the opportunity for a site-specific click reaction (Cu(I)-catalyzed Huisgen azide-alkyne cycloaddition) with an azide partner [11, 13-15]. We planned to immobilize the cytokine to a surface using this reaction, but firstly we investigated the ability of the expressed Plk IL-4 to react this way (“Clickability”) using a fluorescent dye and further optimized the necessary conditions. The click reaction is based on Cu(I), which needs to be created in situ by reduction of a Cu(II) salt by a pair of redox helpers, with one reducing Cu(II) to Cu(I) and the other preventing the further reduction to Cu(0). There are different possibilities published, and we chose sodium ascorbate as reducing agent, and Tris(3-hydroxypropyltriazolylmethyl)amine (THPTA) as protecting reagent both for the protein and Cu(I). This is the standard pair as ascorbate outperforms Tris(2-carboxyethyl)phosphine (TCEP) concerning the interference of

the reaction, and THPTA allows, in contrast to Tris[(1-benzyl-1H-1,2,3-triazol-4-yl)methyl]amine (TBTA) the reaction in an all-aqueous medium [14, 16, 17].

The second side was the isolation of monocytes from human blood, their successful activation to macrophages and finally their polarization to M2 macrophages, combined with the development of corresponding characterization methods. An enormous body of work has been done on characterizing murine macrophages and their experimentally available properties, but there are huge differences to the human macrophages we were working with [18, 19]. The latter are less explored and the possible methods were limited, but we found a reliable way of characterization by the use of known marker genes, and the study of their expression by qPCR [20-22].

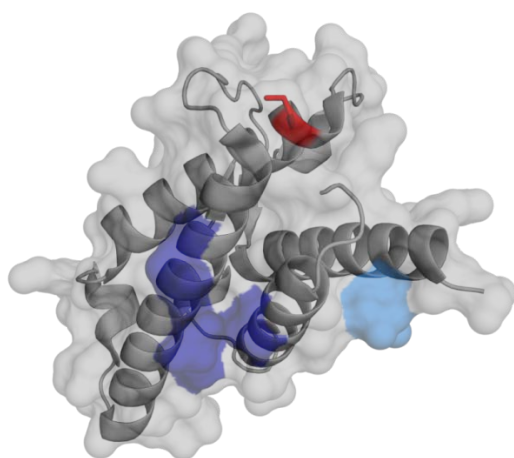


**Figure 1:** Wild-type human IL-4 as PDB rendering by PyMOL Molecular Graphics System version 1.5.0.3, Schrödinger, LLC based on 2B8U (x-ray diffraction with resolution of 1.80 Å) showing IL-4R $\alpha$  binding site (dark blue), IL-13R $\alpha$ 1 binding site (light blue) and Lysine 42 (red) [10].

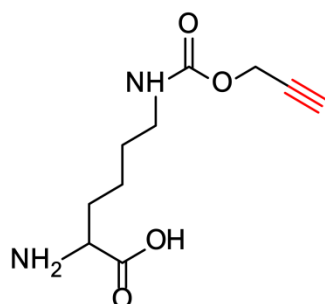


**Figure 2:** Structure of Plk, highlighting the introducible alkyne group (red).

## Materials and Methods

### *Materials*

#### *Chemicals*

Chromeo 488-Azide	Iris Biotech (Marktredwitz, Germany)
WST reagent	Roche (Basel, Switzerland)
Coomassie Brilliant Blue G250	Pierce (Rockford, USA)
Super Signal® West Pico Luminescent Substrate	Thermo Scientific (Waltham, MA, USA)
IPTG (Isopropyl- $\beta$ -D-thiogalactopyranosid)	Sigma Aldrich (Schnelldorf, Germany)
Kanamycin	Sigma Aldrich (Schnelldorf, Germany)
Carbenicillin	Sigma Aldrich (Schnelldorf, Germany)
Percoll	GE Healthcare (Buckinghamshire, GB)
Histopaque-1077	Sigma Aldrich (Schnelldorf, Germany)
Boc-protected lysine	NovaBiochem/Merck Millipore (Darmstadt, Germany)
Propargyl-chloroformate	Sigma Aldrich (Schnelldorf, Germany)
Propargyl protected lysine (Plk)	
TFA salt	self-synthesized
HCl salt	kindly provided by Dr. J.-C. Rybak

(All other chemicals were at least of analytical grade and from Sigma Aldrich)

#### *Microbiologicals*

ImmunoPure Rabbit Anti-Goat IgG, (H+L), Peroxidase Conjugated	Thermo Scientific (Waltham, MA, USA)
Human IL-4 Antibody, polyclonal goat IgG	R&D (Minneapolis, MN, USA)

Human IL-4	R&D (Minneapolis, MN, USA)
Macrophage colony-stimulating factor (M-CSF)	kindly provided by Novartis AG
Recombinant Human Interferon $\gamma$ (IFN $\gamma$ )	GIBCO life technologies (Carlsbad, CA, USA)
Lipopolysaccharides (LPS) from E.coli 0111:B4	Sigma Aldrich (Schnelldorf, Germany)
TaqMan probes	Applied Biosystems (Foster City, CA, USA)
GAPDH (Hs02758991_g1)	
M1: IRF7 (Hs01014809_g1)	
relB (Hs00232399_m1)	
CCR7 (Hs01013469_m1)	
M2: SCARB 1 (HS00969821_m1)	
ALOX 15 (Hs00993765_g1)	
PPAR $\gamma$ (HS01115513_m1)	
TaqMan Gene Expression Master Mix	Applied Biosystems (Foster City, CA, USA)
Pure Link $\text{\textcircled{R}}$ RNA Mini Kit	Life technologies (Carlsbad, CA, USA)
RNAse free water	Sigma Aldrich (Schnelldorf, Germany)
High Capacity cDNA Reverse Transcriptase Kit	Applied Biosystems (Foster City, CA, USA)
Anti-CD14 antibody [MEM-15] (FITC)	Abcam (Cambridge, UK)
Buffy coat	Blutspendedienst des bayerischen Roten Kreuzes (München, Germany)
NuPAGE LDS sample buffer	Life technologies (Carlsbad, CA, USA)
Protein standard I	Bruker Daltonics Inc (Billerica, MA, USA)
Fetal bovine serum	GIBCO life technologies (Carlsbad, CA, USA)

*Consumables*

HiTrap SP XL ÄKTA column (5ml)	GE Healthcare (Buckinghamshire, GB)
SpectraPor dialysis membrane (MWCO 6-8000Da)	Spectrum labs (Rancho Dominguez, CA, USA)
Nucleosil 300-3 C4 HPLC column	Macherey-Nagel (Düren, Germany)
ZipTip <sub>C18</sub> -tips	Millipore Merck (Darmstadt, Germany)
CD14 MicroBeads, human	Miltenyi Biotec (Bergisch Gladbach, Germany)
Auto-MACS columns	Miltenyi Biotec (Bergisch Gladbach, Germany)
Tray Cell, Typ 105.800 cuvette	Hellma (Müllheim, Germany)
96-well optical reactron plate with barcode	Applied Biosystems (Foster City, CA, USA)
Adhesive qPCR seal	Sarstedt (Nürmbrecht, Germany)
MTP 384 target plate, ground steel BC	Bruker Daltonics Inc (Billerica, MA, USA)
24-well tissue culture polystyrole plate	Greiner Bio One (Frickenhausen, Germany)
Microtest Plate, 96 Well, F	Sarstedt (Nürmbrecht, Germany)

*Plasmids*- **pET11a (Novagen)**

containing the pyrrolysine tRNA and the lipoprotein promotor lpp and the terminator RRN b/c as described by Eger et al. [11].

*Kindly provided by Dr. Marina Rubini*

- **pRSF-Duet (Novagen)**

containing the gene for the pyrrolysine tRNA synthetase pylS in the MCS II as described by Eger et al. [11]

*Kindly provided by Dr. Marina Rubini*

*Bacteria***BL21DE3 E coliK12**

**Genotype:** *fhuA2* [Ion] *ompT gal* ( $\lambda$  DE3) [*dcm*]  $\Delta$ *hsdS*

$\lambda$  DE3 =  $\lambda$  *sBamHIo*  $\Delta$ *EcoRI-B int::(lacI::PlacUV5::T7 gene1)* *i21*  $\Delta$ *nin5*

Kindly provided by Prof. Dr. Sven Panke

*Medium and buffer*

Terrific Broth (TB Medium)	12 g Tryptone 4 g Yeast Extract 4 ml Glycerol 17 mM KH <sub>2</sub> PO <sub>4</sub> 72 mM K <sub>2</sub> HPO <sub>4</sub> ad 900 ml ultrapure water
LB Medium	10 g Tryptone 86 mM NaCl 5 g Yeast-Extract 20 mM MgSO <sub>4</sub> *7H <sub>2</sub> O 5.5 mM Glucose ad 1000 ml ultrapure water
PBS (pH 7.4)	137 mM NaCl 2.69 mM KCl 4.3 mM Na <sub>2</sub> HPO <sub>4</sub> 1.5 mM KH <sub>2</sub> PO <sub>4</sub>
Washing buffer	50 mM Tris/HCl pH 8.0 50 mM NaCl 1 mM EDTA
Sonication buffer	50 mM Tris/HCl pH 8.0 50 mM NaCl 1 mM EDTA 0.1 mM Phenylmethylsulfonylfluoride (PMSF)



---

Unfolding buffer	50 mM Tris/HCl pH 8.0 50 mM NaCl 1 mM EDTA 0.1 mM PMSF 5 M Guanidine-HCl 2 mM Glutathione (red) 0.2 mM Glutathione (ox)
Refolding buffer	50 mM Tris/HCl pH 8.0 50 mM NaCl 1 mM EDTA 2 mM Glutathione (red) 0.2 mM Glutathione (ox)
TBST buffer	15 mM Tris 137 mM NaCl 1% Tween 20
WST assay medium	RPMI 1640 10% FCS 1% Penicillin/Streptomycin 6.6% Albumin (Bovine Fraction V, solution 7.5%, Sigma Aldrich (Schnelldorf, Germany))
RPMI 1640	Sigma Aldrich (Schnelldorf, Germany)
Macrophage activation medium	RPMI 1640 10% FCS 1% Penicillin/Streptomycin 50 ng/ml M-CSF
M1 medium	RPMI 1640 5% FCS 1% Penicillin/Streptomycin 100 ng/ml LPS 20 ng/ml IFN $\gamma$

M2 medium	RPMI 1640 5% FCS 1% Penicillin/Streptomycin 10 ng/ml M-CSF 20 ng/ml IL-4
SDS-PAGE running buffer	25 mM Tris 192 mM Glycine 3.5 mM SDS
4xTris-Cl/SDS pH 6.8	0.5 M Tris 14 mM SDS
SDS sample buffer (6x, reducing)	7 ml 4xTris-Cl/SDS, pH 6.8 3 ml Glycerol 350 mM SDS 603 mM Dithiothreitol 0.18 mM Bromphenol blue ad 10 ml water
Western Blot transfer buffer	25 mM Tris 192 mM Glycine 200 ml Methanol ad 1000 ml water (pH 8.3)
MACS Rinsing solution	PBS pH 7.2 2 mM EDTA
MACS buffer	PBS pH 7.2 2 mM EDTA 0.5% BSA
HBS buffer	130 mM NaCl 0.9 mM NaH <sub>2</sub> PO <sub>4</sub> 0.8 mM MgSO <sub>4</sub>

	5.4 mM KCl
	25 mM Glucose
	20 mM HEPES
Freezing buffer	60% HBS buffer
	30% Human serum
	10% DMSO
	(Recipe kindly provided by Novartis AG)

### *Instruments*

auto-MACS	Miltenyi Biotec (Bergisch Gladbach, Germany)
ÄKTA purifier™ system	GE Healthcare (Buckinghamshire, GB)
Hitachi Elite La Chrom HPLC	VWR (Radnor, PA, USA)
+ Diode array detector (VWR Hitachi L-2455U)	
+ Fluorescence detector (VWR Hitachi L-2485U)	
MALDI-MS Autoflex II LRF	Bruker Daltonics Inc (Billerica, MA, USA)
LTQ-Orbitrap Velos Pro	Thermo Scientific (Waltham, MA, USA)
Spectramax 250 microplate reader	Molecular Devices (Sunnyvale, CA, USA)
Ultrasonic homogenizer SONOPULS Germany)	BANDELIN electronic GmbH & Co KG (Berlin,
Flow Cytometry: FACS Calibur	Becton Dickinson (Franklin Lakes, NY, USA)
FluorChem FC2	Protein Simple (Santa Clara, CA, USA)
Genesys 10S UV-Vis	Thermo Scientific (Waltham, MA, USA)
RT-PCR ABI prism 7900HT	Applied Biosystems (Foster City, CA, USA)

## **Methods**

### Synthesis of Plk TFA salt (modified from [23], supporting information)

Boc protected lysine (26 mmol) was added to an ice cooled solution of 60 ml 1 M NaOH and 60 ml tetrahydrofuran (THF). 20 mmol Propargyl chloroformate were added slowly and drop-wise to the solution and the whole mixture was stirred overnight at room temperature. 300 ml ethylacetate were added to extract the excess of propargyl chloroformate and the organic phase was then discarded. The aqueous phase was acidified using 300 ml of 1 M HCl and discarded after the addition of ethylacetate, which was afterwards dried over MgSO<sub>4</sub> and then evaporated with a rotary evaporator. The resulting product was dissolved in 52 ml dichloromethane (DCM) prior to adding 52 ml Trifluoro acetic acid (TFA) drop-wise and stirring for 1 h at room temperature. The solvent was evaporated and the final product was precipitated using diethyl ether and dried under vacuum.

### Cloning

The gene encoding for full length human IL-4 (gene bank reference ID: AF395008.1, amino-acids 25-153) was purchased from Sino Biological Inc. Wild-type IL-4 cDNA was amplified using the forward primer 5' CCCCATATG CACAAGTGCGATATCACCTTACAGG 3' and the reverse primer 5' CCCGGATCC TCAGCTCGAACACTTTGAATATTTCTCTC 3' for PCR amplification. The resulting IL-4 cDNA was subcloned with the restriction endonucleases NdeI and BamHI into the backbone of the pET11a plasmid, resulting plasmid IL-4 PET11a.

Mutant 42(TAG)-IL-4 cDNA was customized designed with NdeI and BamHI restriction endonuclease sites and synthesized and subcloned in the transfer plasmid pUC47 by GenScript. pUC47 plasmid DNA was digested with the restriction endonucleases NdeI and BamHI and the resulting DNA-fragment was subcloned into the backbone of a pET11a construct yielding plasmid 42(TAG)-IL-4 pET11a, containing already the gene for the pyrrolysine tRNA and the lipoprotein promoter lpp and the terminator RRN b/c as described in Eger et al. [11]. Correct insert sequences of all constructs were confirmed by T7-promotor based DNA sequencing.

## Transformation

The plasmids 42(TAG)-IL-4 PET11a and pRSF Duet, containing the gene for the pyrrolysine tRNA synthetase *pylS*, were co-transformed in *BL21(DE3)* for expression. For wild-type IL-4 expression, IL-4 PET11a was transformed in *BL21(DE3)*.

## Expression and purification (from [24] ) of wild-type IL-4

The bacteria *BL21(DE3)* with plasmids were first grown in LB-Medium supplemented with 100 mg/l Carbenicillin overnight. The next morning a 1% dilution of the overnight culture was grown in TB-medium with 100 mg/l Carbenicillin at 37°C. At an  $OD_{600}=0.6$ , 1 mM IPTG were added and induced the expression for 7 hours at 33°C. The reaction was then stopped by centrifugation at 5000xg and once washed with washing buffer prior to freezing at -80°C.

After thawing, the pellet was resuspended in 30 ml of sonication buffer and treated with ultrasound (70 W, 6 times 1 min with 2 min pause). Then the suspension was centrifuged at 25,000xg for 15 min at 4°C. The supernatant was discarded and the pellet was resuspended in 9 ml unfolding buffer per g pellet and left for 1 hour at room temperature. Afterwards, this suspension was added to the 9 times volume of Refolding buffer, left for 4 hours and finally centrifuged at 2500xg for 15 min at 4°C, prior to dialysis against PBS. The purification was done by ion exchange chromatography using a 5 ml Hi Trap SP XL column in an ÄKTA purifier, with 25 mM ammonium acetate pH 5 as running buffer and 25 mM ammonium acetate with 2 M NaCl pH 5 as elution buffer. For the separation a gradient to 60% elution buffer over 45 column volumes was used with collecting 5 ml fractions. For storage the protein was dialyzed against PBS overnight at 4°C, and then frozen at -80°C.

## Expression of Plk IL-4 (see **Table 1** for details)

The bacteria *BL21(DE3)* with plasmids were first grown in LB-Medium supplemented with 100 mg/l Carbenicillin and 34 mg/l Kanamycin overnight. A 1% dilution of the overnight culture was grown in TB-medium with 100 mg/l Carbenicillin and 34 mg/l Kanamycin at 37°C.

At a certain OD<sub>600</sub> 3 mM Plk were added and later 1 mM IPTG was supplemented to induce the expression. The reaction was then stopped by centrifugation at 5000xg and washed once with washing buffer prior to freezing at -80°C.

Prior to usage of a certain protocol for an expression, we performed time course experiments by collecting samples after different time points after induction, to find the necessary expression time at 33°C or 37°C, respectively. For 33°C the influence of presenting Plk was studied as well.

Inclusion body purification of Plk IL-4 (modified from:[24], see **Table 1** for details)

The frozen bacteria were thawed on ice, resuspended in sonication buffer and sonicated under different conditions.

Afterwards, the suspension was centrifuged at 25,000xg for 15 min at 4°C to remove all soluble bacterial proteins, and the supernatant was discarded. The pellet was resuspended in Unfolding buffer and gently stirred for 1h at room temperature. This suspension was then slowly added to Refolding buffer and left for 4 h at room temperature. To remove all bacterial residues the mixture was then centrifuged at 4000xg for 15 min at 4°C and the supernatant was dialyzed against PBS buffer overnight at 4°C.

Purification of Plk IL-4 (see **Table 1** for details)

The purification was done by ion exchange chromatography using a 5 ml Hi Trap SP XL column in an ÄKTA purifier, with 25 mM ammonium acetate pH 5 as running buffer and 25 mM ammonium acetate with 2 M NaCl pH 5 as elution buffer. For the separation a gradient was used with collecting 5 ml fractions.

A reversed phase approach was tried as additional purification using an approx. 17ml ZORBAX SB C3 column and a gradient between Eluent A (ultrapure water, with 0.1%TFA (m/m)) and Eluent B (ACN, with 0.1%TFA (m/m)). The gradient was set up as follows: 5-30% B for 7 column volumes (CV), 30-40% B for 7 CV, 40-95% B for 6 CV + flushing at 95% B and reequilibration to 5% B.

		A	B	C
<b>Expression</b>	<b>Temperature [°C]</b>	33	37	
	<b>Time [h]</b>	17	6	
	<b>OD<sub>600</sub> of Plk addition</b>	0.3	0.4	
	<b>OD<sub>600</sub> of IPTG addition</b>	0.6	0.7	
	<b>Plk type</b>	TFA salt	HCl salt	
	<b>Remarks</b>	Regular flasks	Baffled flasks, 2 mM MgSO <sub>4</sub> , Propylene glycol	
<b>Inclusion body purification</b>	<b>Sonication</b>	70 W, 6 times 1 min with 2 min pause	Increasing from 40 – 70 W during each of 3 times 30 s with 90 s pause	
	<b>Unfolding</b>	9 ml unfolding buffer per 1 g pellet		
	<b>Refolding</b>	Addition of unfolding suspension to 9 times its volume of refolding buffer	Centrifugation 45 min, 100000x g Addition of supernatant to double volume of refolding buffer + dialysis against ≈ 2 l of refolding buffer	
<b>Purification</b>	<b>Ion exchange chromatography gradient</b>	0 – 45% elution buffer over 20 column volumes	0 – 40% elution buffer over 12 column volumes	
	<b>Reversed phase chromatography</b>	No	Yes	No

**Table 1:** Detailed information about 3 different batches of Plk IL-4 expression and purification

### SDS

The samples were mixed with reducing SDS-sample buffer and heated to 95°C for 5 min, then loaded on a 15% polyacrylamide gel, separated and detected with Coomassie blue.

## Western Blot

For Western Blot analysis an SDS page was run as described before, but instead of staining, the proteins were transferred to a nitrocellulose membrane, blocked with albumin and treated with anti-IL-4-antibody (goat, 1:2000 dilution) overnight. After several washing steps using TBST buffer, the second antibody, carrying horseradish peroxidase (1:2000 dilution) was added for 90 minutes and washed again. The membrane was then treated with the luminescent substrate and documented by FluorChem FC2.

## WST

For the WST-assay TF1 (human erythroleukemic cell line) cells were seeded in a 96-well Microtest plate (50.000 cells/well) in WST assay medium supplemented with increasing concentrations of IL-4 (0.039 to 20 ng/ml) and grown for 48 h at 37°C with 5% CO<sub>2</sub>. In the next step 20 µl WST reagent were added per well, incubated for 4 hours and then the UV absorption was measured at 450 nm using SPECTRAmax 250.

## HPLC

A VWR Hitachi Elite La Chrom HPLC system equipped with a diode array detector was used to analyze the wild-type and Plk IL-4 samples. Reversed phase separation was performed using a Nucleosil 300-5 C4 column with a flow rate of 1 ml/min and the protein was detected at 220 nm after loading of 30 µl sample. As a gradient we used a tri-phasic approach, having (i) a linear gradient from 10 to 35% Eluent A (ACN with 0.1% (m/m) TFA) and Eluent B (ultrapure water with 0.1% (m/m) TFA) over 8 min, then (ii) a linear gradient from 35 to 40 % Eluent A over 9 min and finally (iii) the flushing with 100% Eluent A and reequilibration.

The concentration was determined based on a calibration curve prepared using wild-type IL-4.

In case of click reaction analysis a fluorescence detector was additionally used to detect the fluorescent dye at  $\lambda_{\text{ex}} = 488 \text{ nm}$  and  $\lambda_{\text{em}} = 517 \text{ nm}$  for Chromeo 488.



## MALDI-MS

Sample preparation: The sample was desalted using ZipTip<sub>C18</sub>-tips following the manufacturer's instructions, except that the elution step was performed using 60% LC-MS ACN, 0.1% TFA in LC-MS water. Afterwards, the samples were mixed 1+1 with the matrix (saturated solution of sinapic acid in 60% ACN/ 0.3% TFA/ 40% water) and then applied to the MTP 384 target plate.

Matrix-assisted laser desorption ionization (MALDI)-MS spectra were acquired in the linear positive mode by using an Autoflex II LRF instrument. Mass spectra were calibrated externally with a protein standard I.

### Trypsin digest – MS analysis

Plk IL-4 was mixed with NuPAGE LDS sample buffer and 2  $\mu$ l 1 M DTT and heated to 70°C for 10 minutes. Afterwards 2.4  $\mu$ l of a 1 M Iodacetamide solution were added and the mixture was incubated in the dark, at room temperature for 20 minutes. The sample was then loaded on a 15% SDS-PAGE, separated in the dark and then the interesting band was cut out and analyzed.

For in-gel digestion the excised gel bands were destained with 30% ACN, shrunk with 100 % ACN, and dried in a Vacuum Concentrator (Concentrator 5301, Eppendorf, Hamburg, Germany). Digest with trypsin was performed overnight at 37 °C in 0.1 M  $\text{NH}_4\text{HCO}_3$  (pH 8). About 0.1  $\mu$ g of protease was used for one gel band. Peptides were extracted from the gel slices with 5 % formic acid.

NanoLC-MS/MS analyses were performed on an LTQ-Orbitrap Velos Pro equipped with an EASY-Spray Ion Source and coupled to an EASY-nLC 1000 (Thermo Scientific). Peptides were loaded on a trapping column (2 cm x 75  $\mu$ m ID, PepMap C18 3  $\mu$ m particles, 100 Å pore size) and separated on an EASY-Spray column (25 cm x 75  $\mu$ m ID, PepMap C18 2  $\mu$ m particles, 100 Å pore size) with a 30 minute linear gradient from 3% to 30% ACN and 0.1% formic acid. MS scans were acquired in the Orbitrap analyzer with a resolution of 30,000 at m/z 400, MS/MS scans were acquired in the Orbitrap analyzer with a resolution of 7,500 at m/z 400 using HCD fragmentation with 30% normalized collision energy. A TOP5 data-dependent MS/MS method was used; dynamic exclusion was applied with a repeat count of 1 and an exclusion duration of 30 seconds; singly charged precursors were excluded from selection. Minimum signal threshold for precursor selection was set to 50,000. Predictive AGC was used with AGC target a value of 1e6 for MS scans and 5e4

for MS/MS scans. Lock mass option was applied for internal calibration in all runs using background ions from protonated decamethylcyclotrasiloxane ( $m/z$  371.10124).

Mascot Distiller 2.4 was used for raw data processing and for generating peak lists, essentially with standard settings for the Orbitrap Velos (high/high settings). Mascot Server 2.4 was used for database searching with the following parameters: peptide mass tolerance: 10 ppm, MS/MS mass tolerance: 0.02 Da, enzyme: “semiTrypsin” with 3 missed cleavage sites allowed; variable modifications: carbamidomethyl (C), Gln->pyroGlu (N-term. Q), oxidation (M), and pyrrolysine analogue Plk (K).

### Click reaction

The click reaction was performed under different conditions in order to optimize its yield. Therefore, first only the stable conditions are described, and then detailed.

50  $\mu\text{M}$   $\text{CuSO}_4$  and 250  $\mu\text{M}$  THPTA were combined, then 2.5 mM sodium ascorbate were added (concentrations in the final solution), and the whole mixture was incubated at room temperature for 10 min. Afterwards, the reaction partners were added and the reaction was performed for a certain time.

To check if the reaction was successful 15% SDS-PAGEs were performed and to check its yield the samples were analyzed by HPLC. In that case the usual IL-4 peak gained a shoulder for the click product, the area of which was set in relation to the area of the whole peak (compare **Figure 20 A**).

- a) Reaction for wild-type and Plk IL-4 using a reaction time of 1h at room temperature.
- b) Comparison between the use of 50  $\mu\text{M}$  and 1 mM Copper
- c) Optimization by varying time (1 h, 3 h, 7 h) and temperature (37°C, 25°C, 4°C).

Each experiment was accompanied by its copperless counterpart in order to guarantee a specific click reaction.

---

### Isolation of monocytes from buffy coat (modified from[25])

Histopaque-1077 was distributed in 50 ml tubes with 20 ml each, then the buffy coat was diluted 1+1 with RPMI medium and used to overlay the Histopaque carefully. The system was centrifuged at 950xg for 15 min with the brakes off and the developed interphases were collected and washed with RPMI twice, each time centrifuged at 350xg for 7 minutes, with combining 2 pellets after first washing step.

The final pellet was resuspended in medium, counted with Turks solution and the suspension was diluted with medium to give a concentration of 50-70 million cells in 3 ml. A Percoll solution was prepared using 48.5% Percoll, 41.5% water and 10% 1.6 M NaCl. It was then distributed with 10 ml per tube, overlaid with the diluted cell suspension and centrifuged at 580xg with the brakes off. Again the interphases were collected, washed once (*vide supra*) and then combined, resuspended in medium and counted with trypane blue.

The cells were washed with MACS rinsing solution (5 min, 218xg) and resuspended in 80  $\mu$ l MACS buffer per  $10^7$  cells. The CD14 microbeads were added (20  $\mu$ l per  $10^7$  cells) and the mixture was incubated at 2-8°C for 15 minutes. Afterwards, the cells are washed with MACS buffer (10 min 300xg) and resuspended in 500  $\mu$ l MACS buffer up to  $10^8$  cells and transferred to the autoMACS. The cells were automatically sorted using the positive selection program, which is capable of separating bead-labeled (positive) cells and retrieve them specifically.

The cells were washed and resuspended with RPMI (5 min, 218xg), counted with trypane blue and then prepared for freezing and flow cytometry analytics to confirm proper isolation.

### Flow Cytometry

The isolated cells were incubated with FITC labeled Anti-CD14 antibody for 45 min at 4°C (20  $\mu$ l antibody per  $1 \times 10^6$  cells following manufacturer's protocol) and 10.000 were then analyzed using FACSCalibur and recording forward scatter, sideward scatter and fluorescence using an argon-ion laser line at 488 nm and the FL1 detector at 530/30 nm. BD CellQuest Pro (Franklin Lakes, NY, USA) was used as measuring software, and for further analysis we used Flowing Software 2.5.0 (Perttu Terho, Turku Centre for Biotechnology, Turku, Finland).

### Freezing protocol

For freezing, the monocytes were centrifuged (5 min, 300xg) and resuspended in Freezing buffer in a concentration of  $4 \times 10^6$  cells per ml, then aliquoted in 500  $\mu$ l portions ( $2 \times 10^6$  cells) and frozen overnight at  $-80^\circ\text{C}$  protected with a styrofoam box. Afterwards, the tubes were transferred to storage in liquid nitrogen and stayed at least 24 h before usage.

### Thawing and activation (adapted from [20])

The cells were given to RPMI-medium (10% FCS, 1% Penicillin/Streptomycin) in a semi-frozen state and washed once to remove the freezing buffer components. Afterwards, they were resuspended in macrophage activation medium ( $2 \times 10^6$  cells/ml with 1 ml per well in a 24-well plate) for 6 days at  $37^\circ\text{C}$  and 5%  $\text{CO}_2$ .

After 6 days, the cells were adherent and washed with PBS once, before the M1 or M2 medium was added for particular activation. As a control we used M0 macrophages, receiving fresh macrophage activation medium. All activation media were incubated with the cells for 24 h prior to RNA isolation.

### RNA Isolation

The RNA isolation of activated macrophages was performed with the PureLink RNA Mini Kit following the manufacturer's instructions. In short, the cells were lysed using 2-mercaptoethanol, then bound to the membrane with ethanol, washed several times and finally eluted with 15  $\mu$ l RNase free water.

The RNA-content was determined by UV-absorption using Tray Cell Type 105.800 cuvette at 260 nm to calculate the necessary amount of reagent for transcription to cDNA (High Capacity cDNA Reverse Transcriptase Kit, AB). We then used a concentration of 1  $\mu$ g RNA in 10  $\mu$ l solution and added 2  $\mu$ l RT-Buffer, 0.8  $\mu$ l dNTPs, 2  $\mu$ l Primer Random, 1  $\mu$ l reverse Transcriptase (all from the kit) and 4.2  $\mu$ l RNase free water. Alternatively, we first prepared a MasterMix of the reagents prior to addition to the RNA.

The mixture was then tempered for 10 min at 25°C, 120 min at 37°C, 5 min at 85°C and finally frozen at -80°C. The concentration of prepared cDNA was again determined by UV-absorption at 260 nm and used for the qPCR (quantitative polymerase chain reaction) calculations.

## qPCR

The cDNA was thawed and diluted to a concentration of 300 ng/μl with RNase free water, the TaqMan Gene Expression Master Mix (MM) was diluted with water (690 μl MM + 552 μl RNase free water) and mixed with the DNA (414 μl diluted MM + 23 μl DNA). The mixture was combined with the probe (61 μl DNA-MM + 3.2 μl probe) and transferred to the qPCR plates (96-well optical reactron plate with barcode) with using 20 μl per well. The plate was then sealed with qPCR foil and centrifuged shortly to guarantee an even filling. Afterwards, the PCR was performed using RT-PCR ABI prism 7900HT with FAM detector performing following thermal profile:

Stage 1: 50°C, 2 min

Stage 2: 95°C, 10 min

Stage 3: 95°C, 15 s

Stage 4: 60°C, 1 min

(Stages 3 and 4 were repeated 40 times)

The fluorescence was measured at each cycle and the cycle number, when the extrapolated curve cut the threshold was determined by the SDS 2.4 software (Applied Biosystems). We used three M1- and three M2-marker genes, and additionally GAPDH as housekeeping gene.

The analysis was then manually done by the comparative  $C_T$  method [26]

1. Calculation of mean values for GAPDH for each DNA type
2. Calculation of  $\Delta C_T$  by subtraction of the GAPDH mean from each value (matching DNA type)
3. Calculation of mean values for each gene in control (M0)
4. Calculation of  $\Delta\Delta C_T$  by subtraction of the control mean from each value (matching gene)
5. Calculation of fold change for gene expression:  $2^{-\Delta\Delta C_T}$

The fold change in gene expression is then compared between M1 and M2 activated macrophages. The marker genes were mainly chosen from Jaguin et al. [20], with additionally using ALOX 15 [21, 22].

## Results

### *Wild-type IL-4*

Wild-type IL-4 was expressed and purified by mainly following the concept of [24]. The additional purification using ion exchange chromatography (**Figure 3**), resulted in IL-4 with a very high purity, as shown in SDS-PAGE (**Figure 4**), where only minor additional bands were visible and HPLC (**Figure 14**), where the wild-type IL-4 only showed one distinct peak. The identity was proven by a Western Blot (**Figure 5**), which was performed along with an IL-4 reference (R&D Systems), and showed the same fluorescent band for both interleukins. Additionally, the bioactivity was studied by WST assay (**Figure 6**) observing the proliferation of TF1 cells again compared to the reference. Both cytokines developed a very similar proliferation pattern and did not show substantial differences.

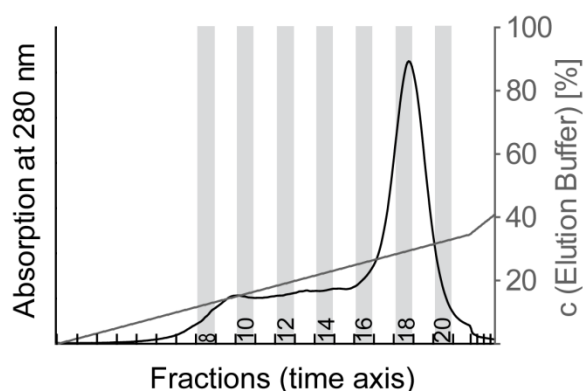


**Figure 3:** ÄKTA graph of the ion exchange chromatography, showing the development of a plateau in the fractions 8 to 16, and a following peak in the fractions 17 to 21, which were then collected for further analysis.

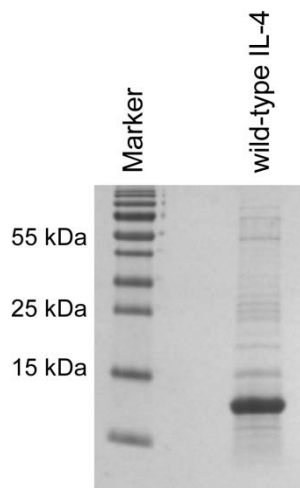


**Figure 4:** SDS PAGE of wild-type IL-4, showing a prominent band at approximately 15 kDa and only minor additional bands, indicating minor impurities.

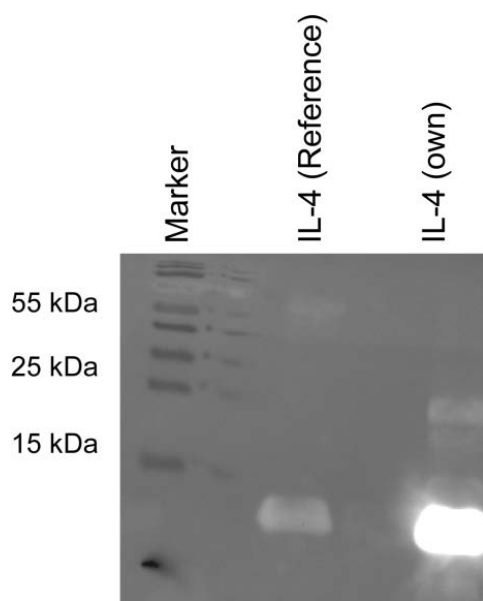


**Figure 5:** Western Blot of our and the reference IL-4, both showing the same fluorescent band.

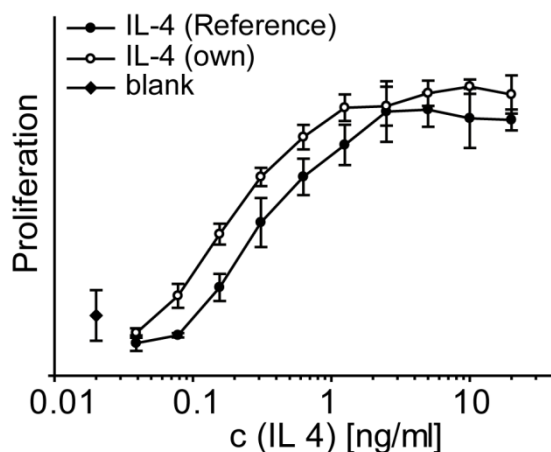


**Figure 6:** Bioactivity assay using WST reagent, showing the proliferation of TF1 cells correlated to the IL-4 concentration. Both IL-4 species (filled circles: reference IL-4, open circles: own IL-4) showed a parallel slope and no substantial differences.

### *Plk IL-4*

The expression and purification of Plk IL-4 was first performed following variant A (**Table 1**), which was chosen after a time course experiment concerning expression time (**Figure 7**).

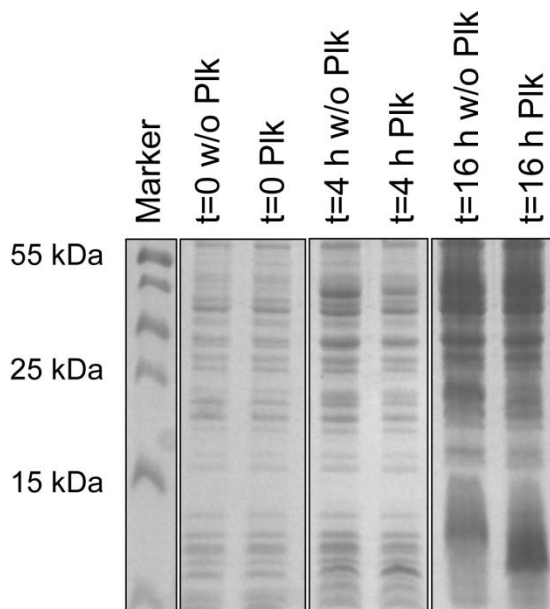


**Figure 7:** SDS PAGE of the time course experiment at 33°C. The basic expression before induction (t=0) did not show visible IL-4 expression. After inducing for 4 hours (t=4 h), a new band appeared at approximately 15 kDa and was more expressed in the presence of Plk. After 16 hours of expression (t=16 h), this band got stronger and was only present, when Plk was in the medium. (w/o = without)



The purification of Plk IL-4 was performed as for wild-type IL-4, but with minor changes, as prior runs were not able to show distinct peaks (data not shown). The ÄKTA graph (**Figure 8**), showed a double peak, which resulted in the collection of 3 different samples and their analysis using SDS PAGE (**Figure 9**). We could thereby identify the fractions 14-16 to be the most suitable ones, concerning their combination of Plk IL-4 content and purity and used those for the following characterization studies.

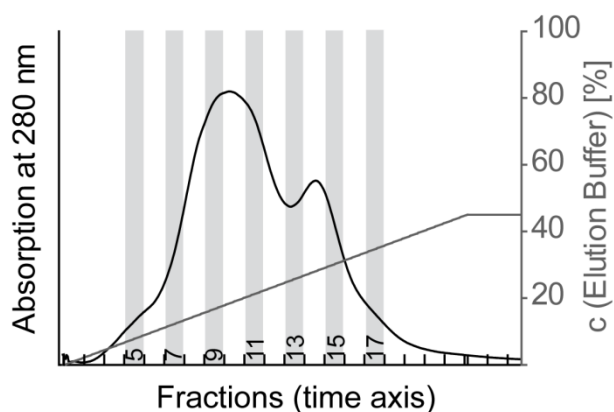


**Figure 8:** ÄKTA graph of the ion exchange chromatography, showing a double peak. We collected fractions 7-11, 12/13 and 14-16 separately, as they represented the first peak (7-11), the intermediate part (12/13) and the second peak (14-16).

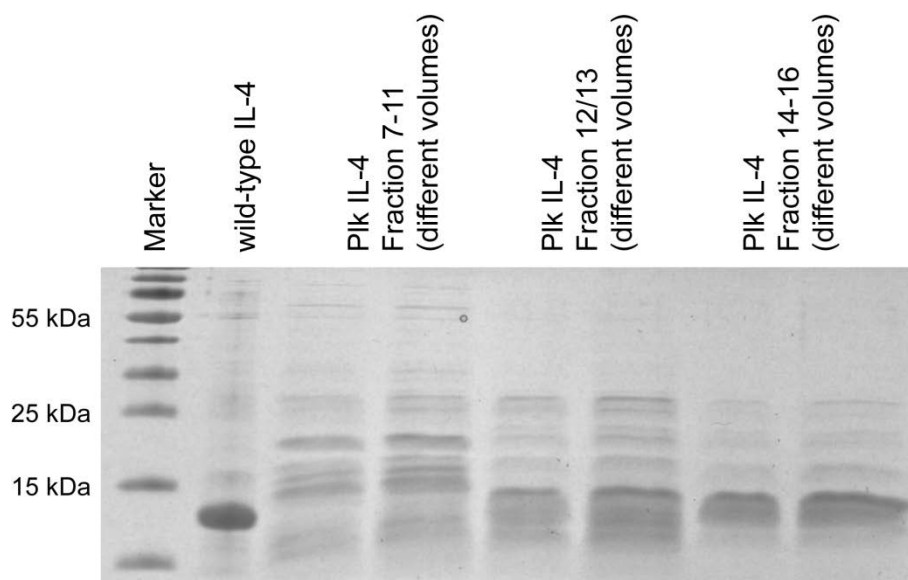


**Figure 9:** SDS PAGE of the chosen ÄKTA fractions in comparison to wild-type IL-4 as a reference. The fractions 7-11, did not show any content of Plk IL-4. The fractions 12/13 did show the right band, but included many impurities. All seven fractions were discarded. The fractions 14-16 contained Plk IL-4 in the best purity.

The first prove of identity was a Western Blot (**Figure 10**), which showed a fluorescent band for both IL-4 variants. A more detailed look at the molecule itself was possible by using MALDI-MS, which resulted in finding the calculated protein mass of 15170 Da (**Figure 11**). We additionally studied the incorporation of Plk at the right position in the protein by NanoLC-MS/MS analysis of trypsin digested samples (**Figure 12**). We performed a WST assay, to observe the proliferation of TF1 cells and explore the bioactivity of Plk IL-4. The assay could find a very good accordance for the developed curves between both cytokines (**Figure 13**).

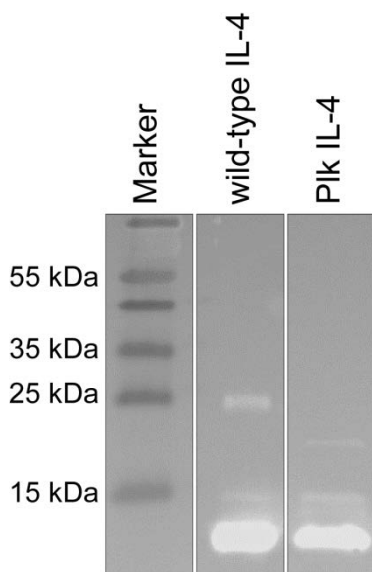


**Figure 10:** Western Blot of wild-type and Plk IL-4, both showing the same fluorescent band.

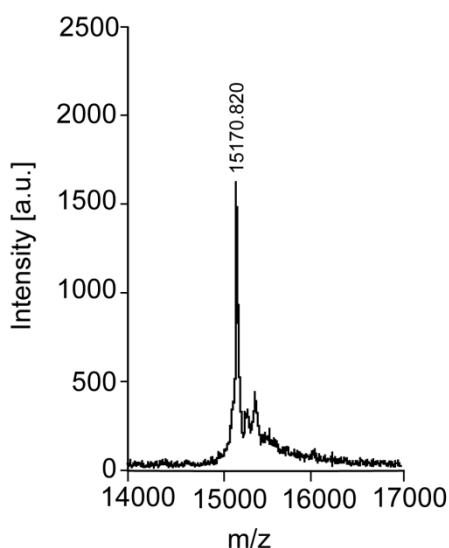


**Figure 11:** MALDI-MS spectrum for Plk IL-4 (calculated mass was 15170 Da), (a.u. = arbitrary units)

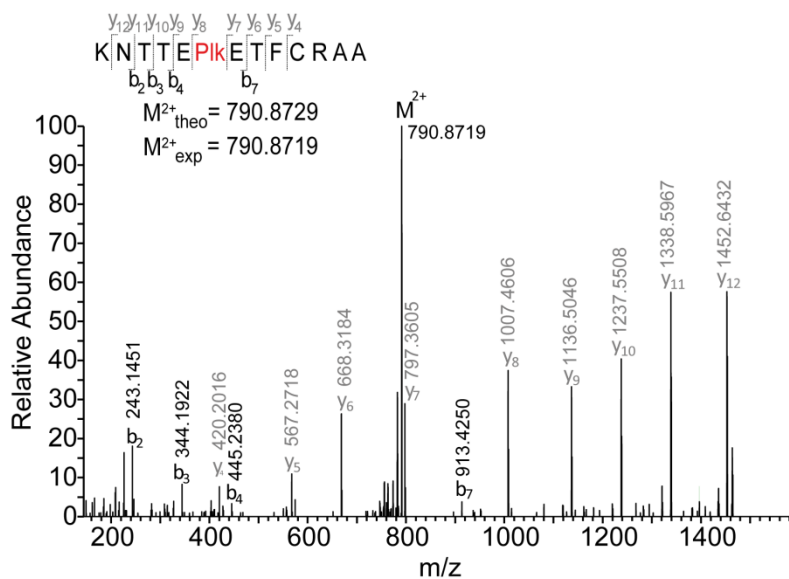


**Figure 12:** HCD MS/MS spectrum and assigned fragment ions of the peptide KNTTEPlkETFCRAA showing the incorporation of Plk at position 6. This peptide was identified with a Mascot Score of 98.

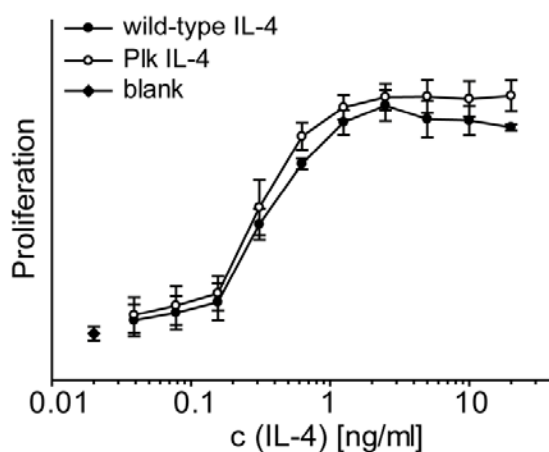


**Figure 13:** Bioactivity assay using WST reagent, showing the proliferation of TF1 cells correlated to the IL-4 concentration. Both IL-4 species (filled circles: wild-type IL-4, empty circles: Plk IL-4) showed a parallel slope and no substantial differences.

After already having seen some impurities in the SDS PAGE (**Figure 9**), the purity of expressed Plk IL-4 was examined by HPLC (**Figure 14**), and we detected additional peaks. The purity, calculated by area-% of the main peak was 51% after this approach. Additionally, the main, and thereby Plk IL-4-peak, is shifted to higher retention times.

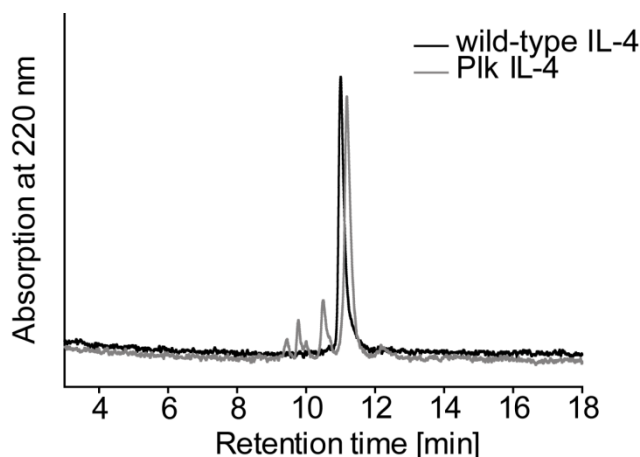


**Figure 14:** HPLC graph of Plk IL-4 and wild-type IL-4, showing additional peaks for Plk IL-4 at earlier retention times and a shift to higher retention times for the main peak.

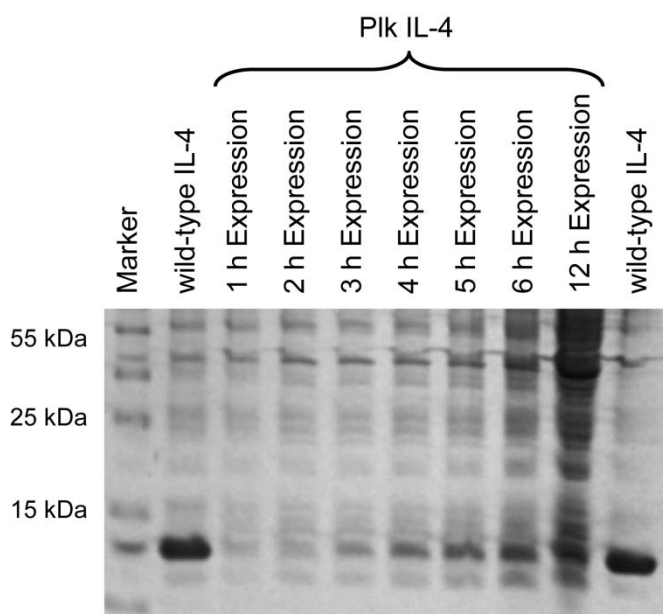


**Figure 15:** SDS PAGE of the time course experiment at 37°C. The band corresponding to Plk IL-4 was identified by comparison to wild-type IL-4. Their strengths increased by increasing the expression time, until the point of 6 hours. After 12 hours, there was a very strongly expressed pattern of different, unwanted proteins.

To overcome the purity issues we changed some parts of both the expression and purification method. In variant B and C (**Table 1**) we used a higher temperature for expression, paired with the use of baffled flasks and a shorter time, which was set to 6 hours after evaluating by a time course experiment (**Figure 15**), in order to enable a more efficient bacterial cultivation and fewer byproducts. The sonication step was done in a milder way and the refolding was done with less volume, to enable an easier ion exchange purification. In variant B we additionally used a

reversed phase step, which resulted in only 39% purity and a different and strong impurity pattern in all used characterization methods (**Figure 16**). Variant C, lacking the last step, was performed next and resulted in the, to this point, highest purity of 69% by choosing the fractions 10 and 11 as a compromise between yield and purity, as some Plk IL-4 containing fractions were discarded (**Figure 17**).

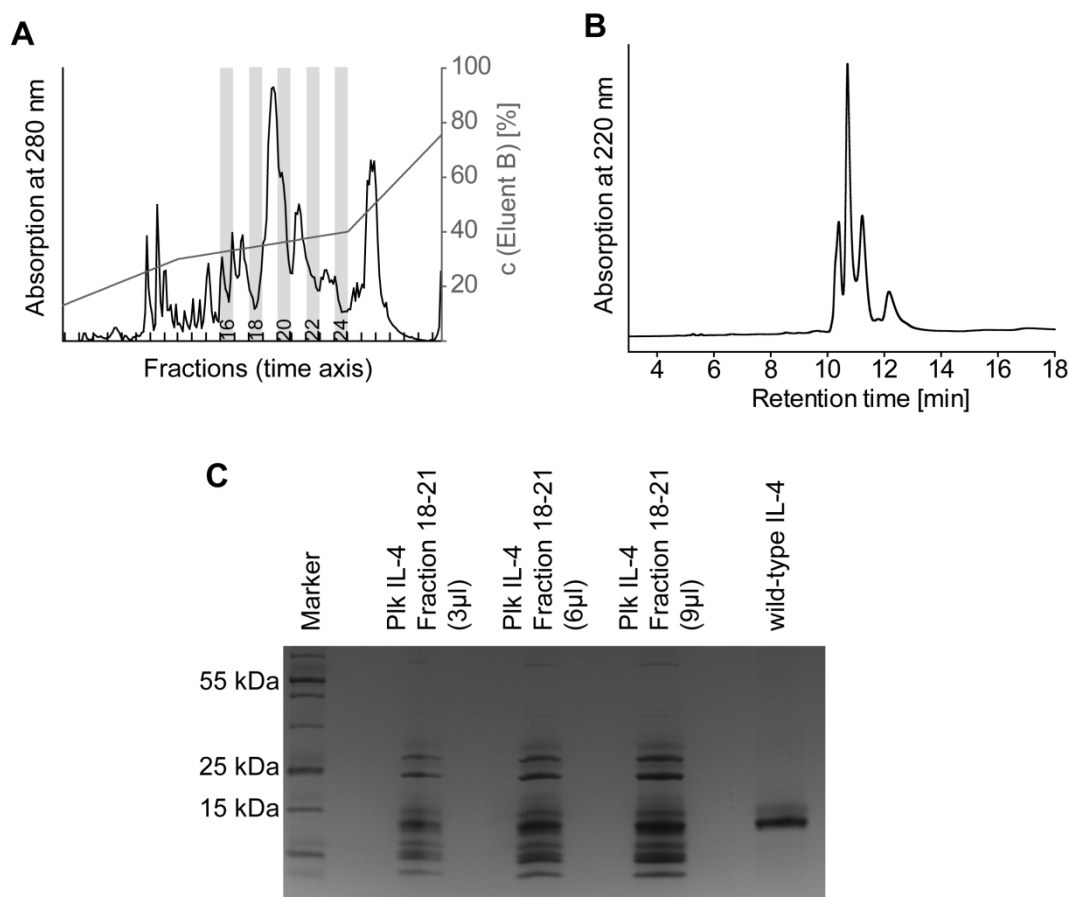


**Figure 16:** Purification of Plk IL-4 following variant B (**Table 1**). The ÄKTA graph of the RP-purification steps, showed many different peaks. The fractions 18-21 were chosen for further analysis, as this has been the gradient, where wild-type IL-4 was detectable (data not shown). The HPLC graph (B), as well as the SDS PAGE (C) both showed strong impurities and a different impurity pattern compared to the ion exchange chromatography alone.

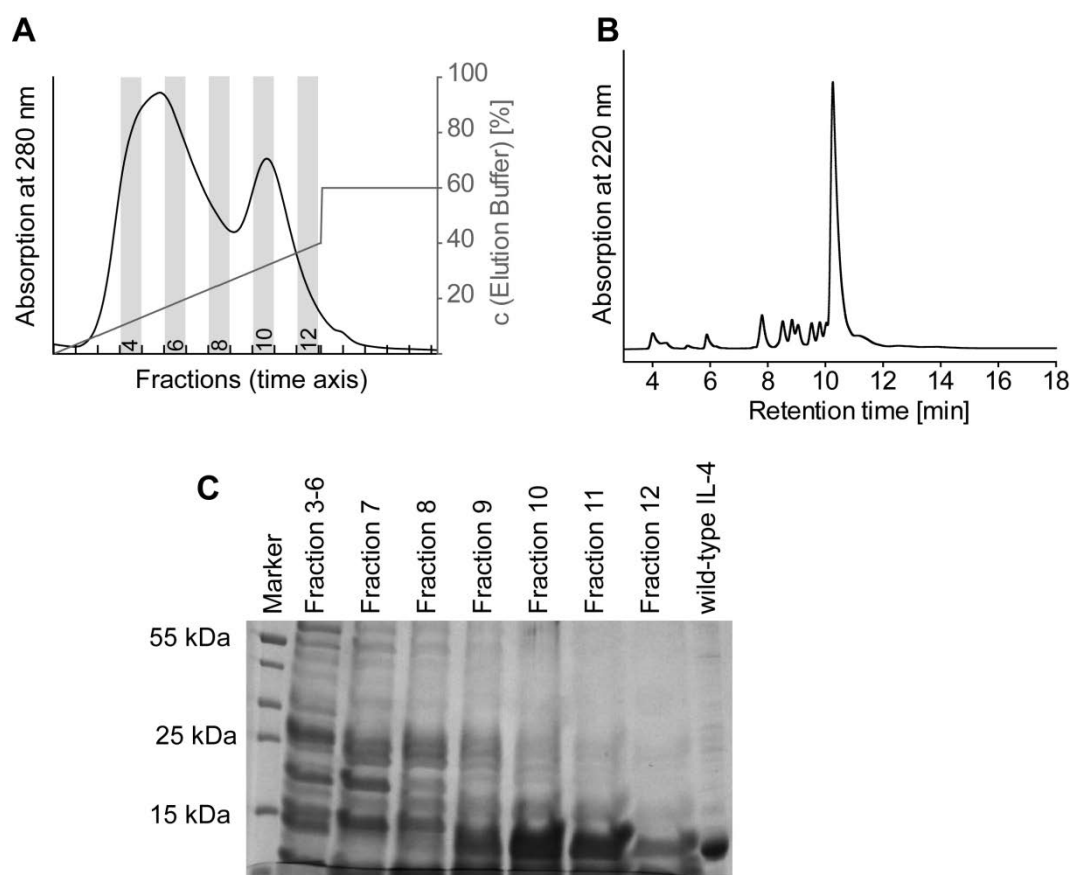


**Figure 17:** Purification of Plk IL-4 following variant C (Table 1). The ÄKTA graph of the ion exchange chromatography steps, showed a double peak. The fractions 3-12 were chosen for further individual analysis. The SDS PAGE (C) identified the fractions 9-12 as Plk IL-4 containing, but only 10 and 11 were subsequently characterized by HPLC (B) and resulted in a purity of 69%.

Another crucial parameter for the usability of Plk IL-4 for the project was its ability to be reacted after the click reaction mechanism (“Clickability”). The first approach for this question was to perform the reaction of a fluorescent dye (Chromeo 488) with both wild-type and Plk IL-4, to see if it was specific to the introduced alkyne group. The chromatogram for Plk IL-4 developed additional fluorescent peaks and a shoulder in the UV graph, whereas the chromatogram of wild-type IL-4 only showed the fluorescent peaks of the dye itself, at lower retention times (Figure 18).

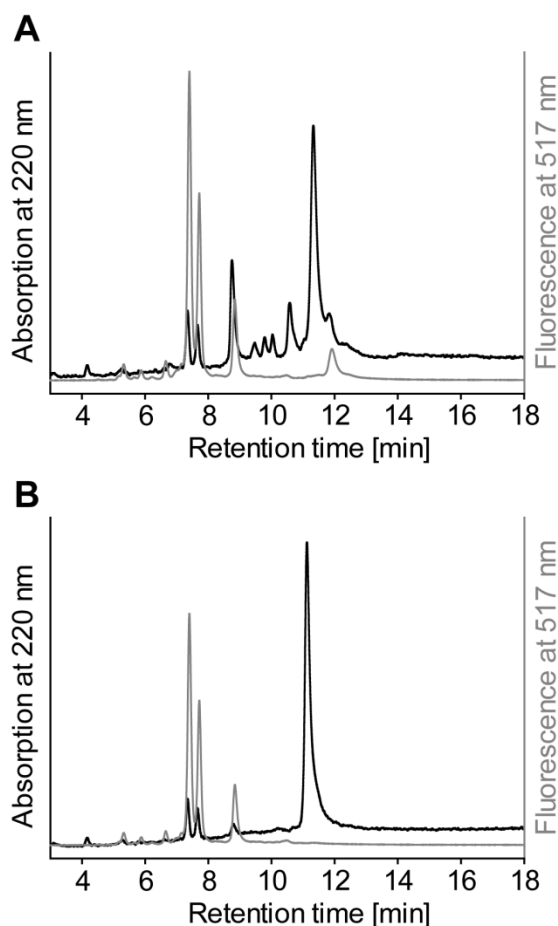


**Figure 18:** HPLC graphs of click reaction products with the fluorescent dye Chromeo 488. (A) For Plk IL-4 it shows an additional shoulder in the UV-curve as well as an additional fluorescent peak at the corresponding retention time. The reaction with wild-type IL-4 (B) resulted in no additional peaks, compared to the pure dye.

In order to enlarge the reaction yield for the click reaction, we were interested in the possible influence of different factors. Initially we tested for the necessary copper concentration by performing the experiment with 1 mM (**Figure 19 A**) and 50  $\mu$ M  $\text{CuSO}_4$  (**Figure 19 B**). The higher copper concentration yielded in a better click ratio, but in an overall reduced area. The following experiments were performed with only 50  $\mu$ M. Next, both the temperature (4 $^\circ$ C, 25 $^\circ$ C and 37 $^\circ$ C) and the reaction time (1 h, 3 h and 7 h) were varied to find the optimal conditions. The efficiency was calculated by dividing the “clicked” ratio by the overall peak ratio (**Figure 20 A**). The results showed no differences in click efficiency for 3 and 7 hours at 4 and 25 $^\circ$ C, but showed a lower value for the highest temperature (**Figure 20 B**). Throughout the performance of many HPLC runs we observed a slight shift of the main peak, but neglected this effect as it was also present for wild-type

IL-4 (data not shown) and therefore due to changings in the column or device and not relevant for our experiments.

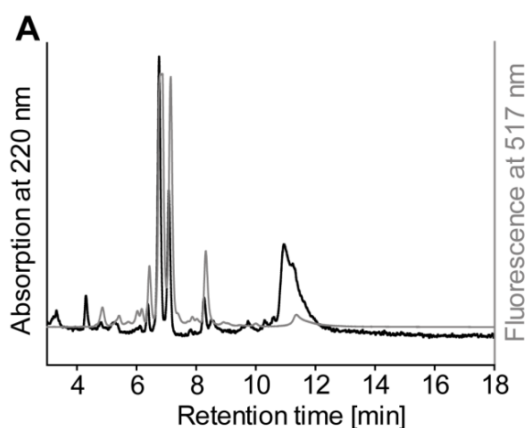


**Figure 19:** HPLC graphs of click reaction products with the fluorescent dye Chromeo 488 in the presence of two different copper concentrations. (A) contained 1 mM copper, whereas (B) contained 50  $\mu$ M copper.

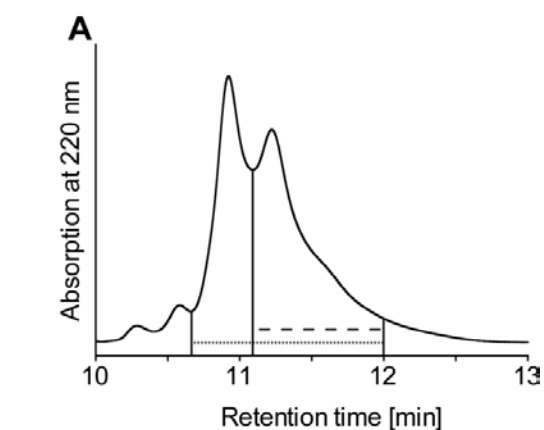
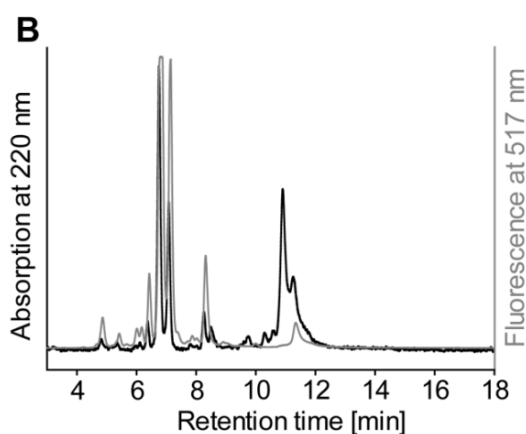
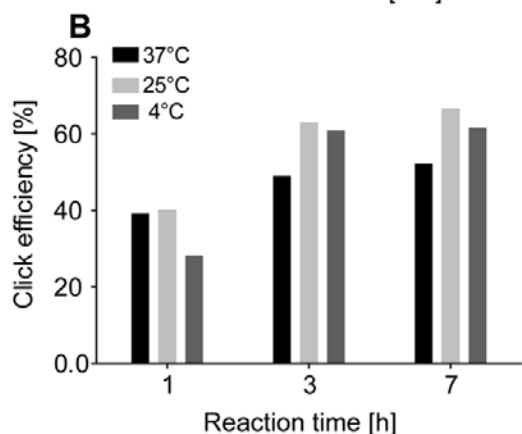


**Figure 20:** (A) Illustration of the division of the zoomed-in main peak of the HPLC chromatogram of click reaction products with the fluorescent dye Chromeo 488. The peak area was divided in the whole peak (dotted line) and the “clicked” part (dashed line) for calculation of click reaction efficiency. (B) Summary of results for the optimization of click reaction by varying the temperature (4°C, 25°C and 37°C) and the reaction time (1 h, 3 h and 7 h).





## Macrophages

The isolation of monocytes from buffy coat was confirmed by flow cytometry using a FITC-labeled anti CD14 antibody. The dot plot of the flow cytometry analysis (**Figure 21 A**) showed two cell populations, with the one in the box showing the monocytes. The fluorescence of the cells in the box region (**Figure 21 B**) showed a very similar pattern and the population was CD14 positive for all isolations.

After their activation and polarization to M1 and M2 macrophages, the gene expression of certain marker genes was tested using qPCR and analyzed by the comparative  $C_T$  method, resulting in an x-fold gene expression compared to non-polarized M0 Macrophages (**Figure 22**). The M1 markers (relB, CCR7, IRF 7) showed a significantly ( $p < 0.05$ ) higher expression for M1 activated macrophages than for M2 (**Figure 22 A-C**). The M2 markers (PPARG and SCARB 1) showed the same effect vice versa (**Figure 22 D,E**). The third M2 marker, ALOX 15, is not shown in the figure as his analysis was not possible using the comparative  $C_T$  method, because the raw data for both M0 and M1 macrophages was undeterminable or above a threshold of 38 cycles several times.

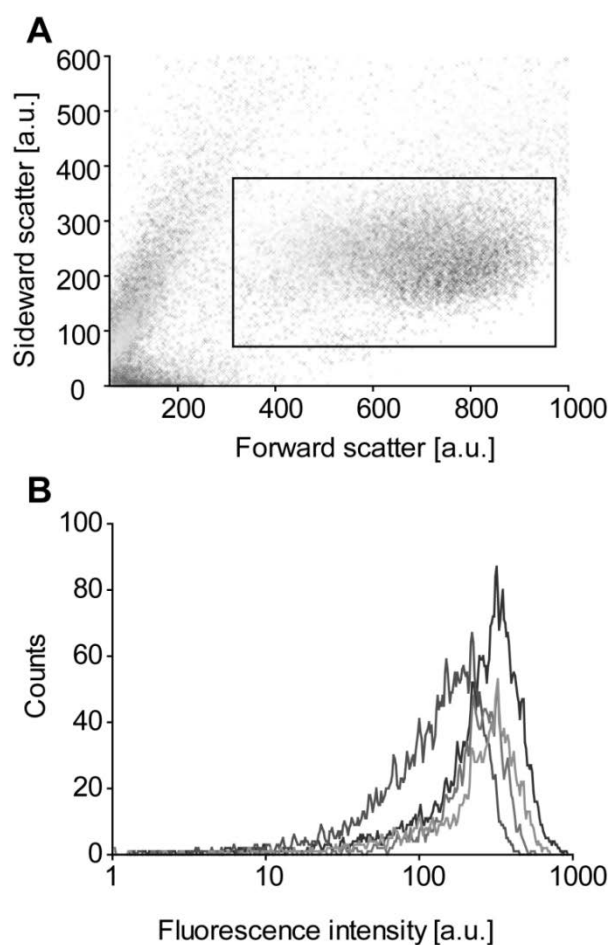


**Figure 21:** Flow Cytometry results of freshly isolated monocytes after treatment with FITC-labeled anti CD14 antibody. (A) Dot plot for morphological characterization, with the box indicating the monocyte region and (B) the recorded fluorescence of the cells in the monocyte region. Both figures are showing four different isolations, marked by gray shades. (a.u. = arbitrary units)

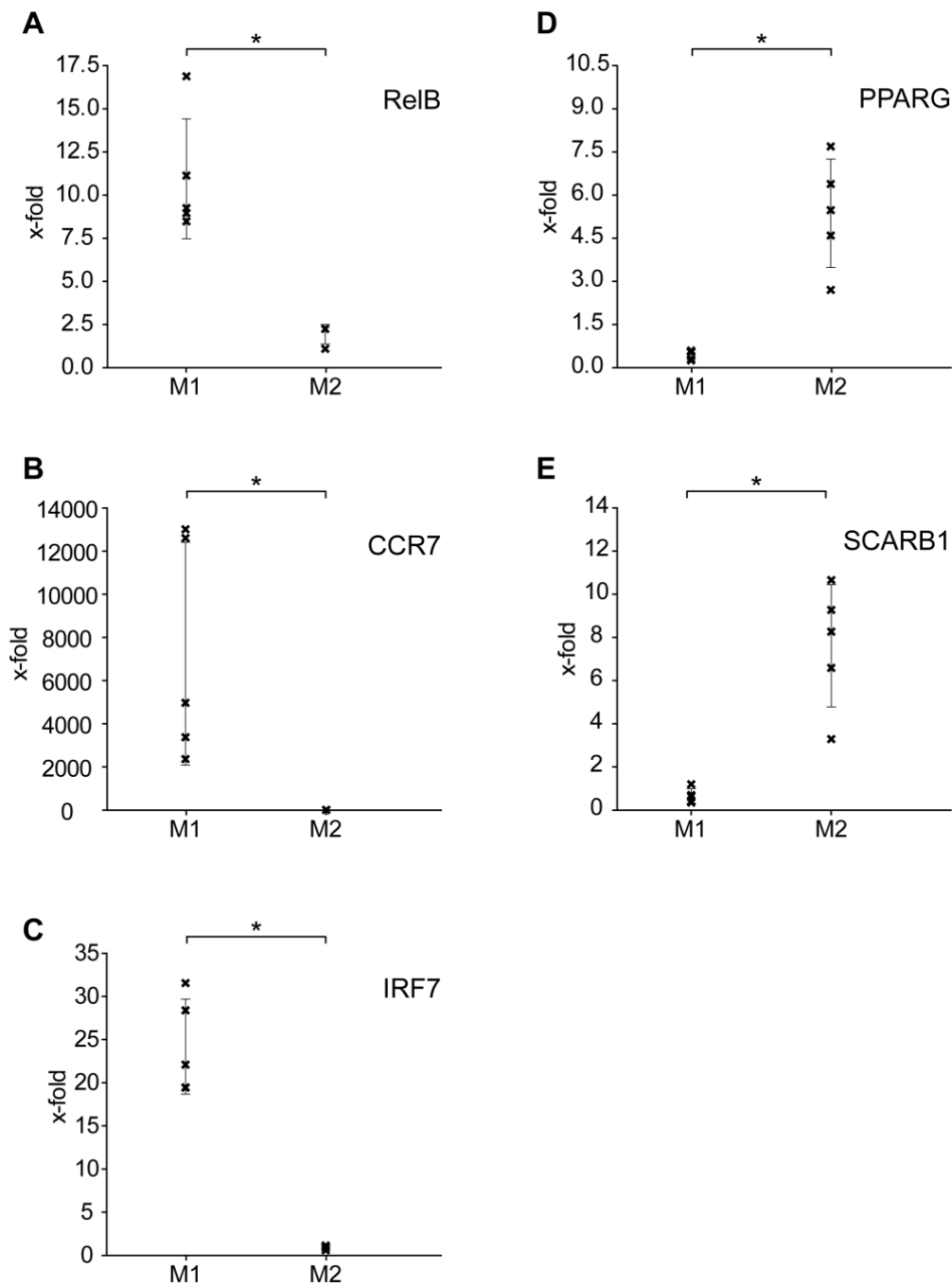


**Figure 22:** X-fold expression of selected genes after polarization to M1 and M2 macrophages, determined by qPCR. Data are expressed relative to levels found in non-polarized M0 macrophages. (A-C) represent M1 marker genes, (D, E) represent M2 Marker genes. Five independent experiments and cell populations are shown for each gene and \* indicates a significant difference with  $p < 0.05$ .

## Discussion

### *Wild-type IL-4*

The expression of wild-type IL-4 was successfully performed by mainly following the protocol from [24], but the purification by ion exchange chromatography was added and resulted in a high purity of the expressed protein. As it additionally showed bioactivity comparable to a reference (**Figure 6**) and the same fluorescent band in the Western Blot (**Figure 5**) its usability was confirmed and we used our own cytokine as reference for further comparisons to Plk IL-4 for bioactivity, identity and purity.

### *Plk IL-4*

The successful expression of Plk IL-4 was proven by several methods. The identity was confirmed by SDS-PAGE (**Figure 7**), where the lack of Plk resulted in the lack of a band at the right size, which is due to the fact, that the protein synthesis was interrupted, when the Plk substrate was not available. An additional confirmation was achieved through a Western Blot, where the modified cytokine was still recognized by the IL-4 antibody and showed the same fluorescent band as wild-type IL-4 (**Figure 10**) and by MALDI-MS (**Figure 11**), where the main mass coincided with the calculated mass. As this did not yet confirm the introduction of Plk at the right position, HCD MS/MS (**Figure 12**) was needed to proof this as well. As other groups already showed that the modification of IL-4 can lead to the increase or loss of its receptor binding and functionality [10, 27], this positioning was crucial for the maintenance of bioactivity as an influence on the receptor binding sites needed to be avoided. Additionally, the right folding after inclusion body purification was fundamental, and both issues were clarified by a bioactivity assay, where we could confirm accordance with wild-type IL-4 (**Figure 13**). Unlike other studies [27], we were able to modify the protein inside, instead of changing the C-terminus, which might offer advantages in terms of activity. Although we were able to produce this bioactive Plk IL-4, the purity remained a main issue, which we characterized by HPLC and tried to overcome by changing the expression and purification steps. Generally, the substitution of lysine by Plk resulted in a slightly shifted main peak (**Figure 14**), due to the thereby increased hydrophobicity, and the appearance of additional smaller peaks, indicating contained impurities, which probably stemmed from the bacterial proteome. The use of a reversed phase purification step resulted in a different impurity pattern

(**Figure 16**) and led to an even worse purity. This might be due to the long exposure to both, ACN [28] and TFA, responsible for low pH and ion pairing. At the moment, the best purity we could reach was 69% (**Figure 17**), which is insufficient and will be issue of future work. There are still many possibilities for improvement in all steps of the process, from the expression, over the inclusion body treatment and its refolding step to the change of the purification method or the introduction of an additional step.

These, so far reached steps are only the basis for the main target of immobilizing the cytokine in a bioactive manner. Therefore, the next step was to examine the ability of Plk IL-4 to react with an azide partner (“Clickability”). For initial experiments we chose Chromeo 488 as partner, as the fluorescent dye is easily detectable parallel to the protein. A common problem in reacting proteins is the number of available functional groups. Although we introduced the alkyne group to overcome this issue, we studied this by comparing Plk and wild-type IL-4 after click conditions, and found the reaction to be specific for the modified IL-4 analogue (**Figure 18**), as the wild-type variant did not develop a shoulder in UV signal, nor additional fluorescent peaks compared to the pure dye. As this was proven we were able to go on to optimize the reaction in terms of efficiency, and tried two different copper concentrations found in the literature [16, 29]. The higher concentration of 1 mM copper sulfate seemed to show the better click ratio, but as the overall area was smaller we assume protein loss (**Figure 19**). The formation of reactive oxygen species by the interaction between copper ions and sodium ascorbate may result in oxidation processes of certain amino acids [30] and the cleavage [31] or cross-linking of proteins [32]. Thus, our finding is in accordance with literature, and the following experiments were performed at 50  $\mu$ M copper to minimize these effects. Our second approach for optimization was the variation of temperature (4°C, 25°C, 37°C) and reaction time (1 h, 3 h, 7 h) (**Figure 20**). As each experiment was only performed once, the explanatory power is low and our results can only give guidance for future experiments that need to study the conditions in detail and in statistically analyzable numbers. Nevertheless, we were able to gain some information, which could help to design the follow-up experiments. This is, on the one hand, the lower efficiency for the lowest reaction time and on the other hand the low increase over time at 37°C, indicating that both mentioned conditions are apparently less suitable than the others.

## *Macrophages*

We were able to successfully isolate monocytes from human blood, by combining the technique of Repnik et al. [25] in a slightly modified way, with magnetic cell sorting (MACS). The initial isolation served as rough purification, by separating the peripheral blood mononuclear cells and removing the lymphocytes by different density gradients. The final purification by MACS allowed the selection of CD14-positive cells by marking them with magnetic beads and resulted in defined monocyte populations. CD14 is expressed relatively specific by monocytes and only minor on other cell types, and plays an important role in the interaction with bacteria [33, 34]. Their identity and purity was confirmed by flow cytometry analysis, showing two cell populations, from which one was the monocyte population (**Figure 21 A**), being further defined by fluorescence with an anti CD14 antibody. The other one was probably mainly cell debris, as it was found at very low forward scatter, indicating smaller size than cells.

As we were interested in having a stock of monocytes we needed to guarantee a safe storage and chose a freezing and thawing program as described in the methods part. In order to make sure the cells were not harmed by this process we compared their morphological development with freshly isolated cells and found no differences apart from a slightly slower start in optical differentiation (data not shown), probably due to the freezing stress. The main parameter for the functionality of frozen monocytes was their possible activation to macrophages first, and to M1 and M2 macrophages afterwards. The polarization to M1 was done using Interferon- $\gamma$  (IFN $\gamma$ ), as it is secreted by cells in case of stress and infection [35] and Lipopolysaccharides [36] as the microbial stimulus. To achieve an M2 population, the cells were exposed to IL-4, which can be presented by T<sub>H</sub>2 cells during adaptive immune response or by granulocytes during inherent reaction [35, 37]. Each batch was checked by qPCR to be classified as usable for further experiments if the activation could be confirmed.

The activation to macrophages was performed by the addition of M-CSF (macrophage colony stimulating factor) as it has been shown before, that the so-prepared macrophages can be activated to M1 and M2 [20] and as it is the ubiquitously produced [19]. The alternative activation using GM-CSF (granulocyte-macrophage colony stimulating factor) would have led to a different macrophage population [19, 38, 39].

The qPCR results all showed the desired significant differences between M1 and M2 macrophages (**Figure 22**), and thereby proved the usability of the chosen marker genes [20-22] by determining the x-fold gene expression compared to non-polarized macrophages. The used method

is based on finding the threshold cycle  $C_T$ , whereas a low cycle number stands for a high expression and vice versa [26]. The only exception was ALOX 15, which was not analyzable using the comparative  $C_T$  method. However, the expression in M2 macrophages was high (low cycle number), which allows for the conclusion that ALOX 15 is usable as marker gene, and permits the interpretation in an “all-or-nothing” way. The strong variations between different cell populations are comparable to those found in literature [20] and, at least for CCR 7 (**Figure 22 B**) the measurement took place close to the detection limit, which might result in unproportionally high values. Although the absolute outcomes differ slightly from the literature, the method is capable to find significant differences, which is sufficient for our purpose.

## **Conclusion**

We are now able to isolate, activate and characterize macrophages, and thereby prepared the basis for following experiments with these cells. Additionally, we showed the successful expression of Plk IL-4, but need to work on its purity and the optimization of the click reaction conditions, in order to make it suitable for the presentation of immobilized cytokine to macrophage populations. The next steps of this project will have to prove the bioactivity of an immobilized IL-4, prior to performing the final setup with macrophages.

## References

- [1] S. Gordon, Alternative activation of macrophages, *Nature reviews. Immunology*, 3 (2003) 23-35.
- [2] S.J. Van Dyken, R.M. Locksley, Interleukin-4- and interleukin-13-mediated alternatively activated macrophages: roles in homeostasis and disease, *Annual review of immunology*, 31 (2013) 317-343.
- [3] A. Mantovani, Macrophage diversity and polarization: in vivo veritas, *Blood*, 108 (2006) 408-409.
- [4] A. Kennedy, U. Fearon, D.J. Veale, C. Godson, Macrophages in synovial inflammation, *Frontiers in immunology*, 2 (2011) 52.
- [5] C.N. Lumeng, J.L. Bodzin, A.R. Saltiel, Obesity induces a phenotypic switch in adipose tissue macrophage polarization, *Journal of Clinical Investigation*, 117 (2007) 175-184.
- [6] C.N. Lumeng, J.B. DelProposto, D.J. Westcott, A.R. Saltiel, Phenotypic switching of adipose tissue macrophages with obesity is generated by spatiotemporal differences in macrophage subtypes, *Diabetes*, 57 (2008) 3239-3246.
- [7] J. Khallou-Laschet, A. Varthaman, G. Fornasa, C. Compain, A.T. Gaston, M. Clement, M. Dussiot, O. Levillain, S. Graff-Dubois, A. Nicoletti, G. Caligiuri, Macrophage plasticity in experimental atherosclerosis, *PloS one*, 5 (2010) e8852.
- [8] F.K. Swirski, M. Nahrendorf, Leukocyte behavior in atherosclerosis, myocardial infarction, and heart failure, *Science*, 339 (2013) 161-166.
- [9] M.R. Walter, W.J. Cook, B.G. Zhao, R.P. Cameron, Jr., S.E. Ealick, R.L. Walter, Jr., P. Reichert, T.L. Nagabhushan, P.P. Trotta, C.E. Bugg, Crystal structure of recombinant human interleukin-4, *The Journal of biological chemistry*, 267 (1992) 20371-20376.
- [10] M. Kraich, M. Klein, E. Patino, H. Harrer, J. Nickel, W. Sebald, T.D. Mueller, A modular interface of IL-4 allows for scalable affinity without affecting specificity for the IL-4 receptor, *BMC biology*, 4 (2006) 13.
- [11] S. Eger, M. Scheffner, A. Marx, M. Rubini, Synthesis of defined ubiquitin dimers, *Journal of the American Chemical Society*, 132 (2010) 16337-16339.
- [12] W. Wan, J.M. Tharp, W.R. Liu, Pyrrolysyl-tRNA synthetase: an ordinary enzyme but an outstanding genetic code expansion tool, *Biochimica et biophysica acta*, 1844 (2014) 1059-1070.
- [13] R. Huisgen, Kinetics and Mechanism of 1,3-Dipolar Cycloadditions, *Angewandte Chemie International Edition in English*, 2 (1963) 633-645.
- [14] V.V. Rostovtsev, L.G. Green, V.V. Fokin, K.B. Sharpless, A Stepwise Huisgen Cycloaddition Process: Copper(I)-Catalyzed Regioselective "Ligation" of Azides and Terminal Alkynes, *Angewandte Chemie International Edition*, 41 (2002) 2596-2599.
- [15] J.E. Moses, A.D. Moorhouse, The growing applications of click chemistry, *Chemical Society reviews*, 36 (2007) 1249-1262.
- [16] S.I. Presolski, V.P. Hong, M.G. Finn, Copper-Catalyzed Azide-Alkyne Click Chemistry for Bioconjugation, *Current protocols in chemical biology*, 3 (2011) 153-162.
- [17] C. Uttamapinant, M.I. Sanchez, D.S. Liu, J.Z. Yao, A.Y. Ting, Site-specific protein labeling using PRIME and chelation-assisted click chemistry, *Nat Protoc*, 8 (2013) 1620-1634.

- [18] G. Raes, R. Van den Bergh, P. De Baetselier, G.H. Ghassabeh, C. Scotton, M. Locati, A. Mantovani, S. Sozzani, Arginase-1 and Yml Are Markers for Murine, but Not Human, Alternatively Activated Myeloid Cells, *The Journal of Immunology*, 174 (2005) 6561-6562.
- [19] D.C. Lacey, A. Achuthan, A.J. Fleetwood, H. Dinh, J. Roiniotis, G.M. Scholz, M.W. Chang, S.K. Beckman, A.D. Cook, J.A. Hamilton, Defining GM-CSF- and macrophage-CSF-dependent macrophage responses by in vitro models, *Journal of immunology*, 188 (2012) 5752-5765.
- [20] M. Jaguin, N. Houlbert, O. Fardel, V. Lecureur, Polarization profiles of human M-CSF-generated macrophages and comparison of M1-markers in classically activated macrophages from GM-CSF and M-CSF origin, *Cellular immunology*, 281 (2013) 51-61.
- [21] A. Schmieder, J. Michel, K. Schonhaar, S. Goerdt, K. Schledzewski, Differentiation and gene expression profile of tumor-associated macrophages, *Seminars in cancer biology*, 22 (2012) 289-297.
- [22] S.J. Wuest, M. Crucet, C. Gemperle, C. Loretz, M. Hersberger, Expression and regulation of 12/15-lipoxygenases in human primary macrophages, *Atherosclerosis*, 225 (2012) 121-127.
- [23] D.P. Nguyen, H. Lusic, H. Neumann, P.B. Kapadnis, A. Deiters, J.W. Chin, Genetic encoding and labeling of aliphatic azides and alkynes in recombinant proteins via a pyrrolysyl-tRNA Synthetase/tRNA(CUA) pair and click chemistry, *Journal of the American Chemical Society*, 131 (2009) 8720-8721.
- [24] A. Kimmenade, M.W. Bond, J.H. Schumacher, C. Laquoi, R.A. Kastelein, Expression, renaturation and purification of recombinant human interleukin 4 from *Escherichia coli*, *European Journal of Biochemistry*, 173 (1988) 109-114.
- [25] U. Repnik, M. Knezevic, M. Jeras, Simple and cost-effective isolation of monocytes from buffy coats, *Journal of Immunological Methods*, 278 (2003) 283-292.
- [26] T.D. Schmittgen, K.J. Livak, Analyzing real-time PCR data by the comparative CT method, *Nature Protocols*, 3 (2008) 1101-1108.
- [27] V. Duppatla, M. Gjorgjevikj, W. Schmitz, H.M. Hermanns, C.M. Schafer, M. Kottmair, T. Muller, W. Sebald, IL-4 analogues with site-specific chemical modification at position 121 inhibit IL-4 and IL-13 biological activities, *Bioconjugate chemistry*, 25 (2014) 52-62.
- [28] K. Gekko, E. Ohmae, K. Kameyama, T. Takagi, Acetonitrile-protein interactions: amino acid solubility and preferential solvation, *Biochimica et Biophysica Acta (BBA) - Protein Structure and Molecular Enzymology*, 1387 (1998) 195-205.
- [29] A.E. Speers, G.C. Adam, B.F. Cravatt, Activity-based protein profiling in vivo using a copper(i)-catalyzed azide-alkyne [3 + 2] cycloaddition, *Journal of the American Chemical Society*, 125 (2003) 4686-4687.
- [30] E.R. Stadtman, C.N. Oliver, Metal-catalyzed oxidation of proteins. Physiological consequences, *The Journal of biological chemistry*, 266 (1991) 2005-2008.
- [31] V. Hong, S.I. Presolski, C. Ma, M.G. Finn, Analysis and optimization of copper-catalyzed azide-alkyne cycloaddition for bioconjugation, *Angew Chem Int Ed Engl*, 48 (2009) 9879-9883.
- [32] Y. Liu, G. Sun, A. David, L.M. Sayre, Model studies on the metal-catalyzed protein oxidation: structure of a possible His-Lys cross-link, *Chemical research in toxicology*, 17 (2004) 110-118.
- [33] D.L. Simmons, S. Tan, D.G. Tenen, A. Nicholson-Weller, B. Seed, Monocyte antigen CD14 is a phospholipid anchored membrane protein, *Blood*, 73 (1989) 284-289.



- 
- [34] M. Lingnau, C. Hoflich, H.D. Volk, R. Sabat, W.D. Docke, Interleukin-10 enhances the CD14-dependent phagocytosis of bacteria and apoptotic cells by human monocytes, *Human immunology*, 68 (2007) 730-738.
- [35] D.M. Mosser, J.P. Edwards, Exploring the full spectrum of macrophage activation, *Nature Reviews Immunology*, 8 (2008) 958–969.
- [36] D.M. Mosser, The many faces of macrophage activation, *Journal of Leukocyte Biology*, 73 (2003) 209-212.
- [37] A. Mantovani, A. Sica, S. Sozzani, P. Allavena, A. Vecchi, M. Locati, The chemokine system in diverse forms of macrophage activation and polarization, *Trends in immunology*, 25 (2004) 677-686.
- [38] S. Hashimoto, T. Suzuki, H.Y. Dong, N. Yamazaki, K. Matsushima, Serial analysis of gene expression in human monocytes and macrophages, *Blood*, 94 (1999) 837-844.
- [39] F. Sallusto, A. Lanzavecchia, Efficient presentation of soluble antigen by cultured human dendritic cells is maintained by granulocyte/macrophage colony-stimulating factor plus interleukin 4 and downregulated by tumor necrosis factor alpha, *The Journal of experimental medicine*, 179 (1994) 1109-1118.



## GENERAL CONCLUSIONS AND OUTLOOK

The development of drug delivery devices for proteins challenges formulation scientists in a variety of ways. Due to the instability of peptide drugs, these are inaccessible for many application routes, as their travel through the gastrointestinal tract would lead to their degradation and additionally, their physicochemical characteristics are not favorable for systemic uptake [1]. Nevertheless, the avoidance of this passage is not sufficient for the delivery of therapeutic proteins. A carrier is necessary for the protection of the proteins during storage and application and equally important, for their delivery to a target in the right manner. The material determines the mechanism of interaction with the therapeutic and influences both loading and release kinetics [2]. Additionally, it has an impact on the interaction with components of the human body [3], which might be desirable for local drug delivery but also might be disadvantageous in case of losing the therapeutic by deposition in certain tissues.

The interaction between the carrier and the therapeutic protein is the pivotal point in developing a new drug delivery device and the possibility to interfere in this mechanism and thereby change the loading, release and mobility pattern would allow for an accurately tailored delivery. Therefore, the subject of this thesis was the understanding of and the influence on this interaction using two different approaches. On the one hand we studied the impact of environmental changes on physical adsorption of drugs to carriers and on the other hand, we chose a covalent coupling of drugs to a carrier. Although both mechanisms were very different and aimed for different delivery kinetics, the main target of finding and exploring protein-protein interactions for the development of drug delivery devices connected them.

Silk fibroin (SF) is a biomaterial with many advantages for a use as carrier and its suitability for biomedical applications has already been shown [4-6]. Its processability under very mild and all-aqueous conditions enables SF to be used with even sensitive proteins, as it avoids most stress factors found for artificial polymers [7, 8]. Due to its extraordinary properties, it offers the preparation of different application forms, for example 3D scaffolds for tissue engineering [9, 10], nanoparticles for triggered delivery [11] and hydrogels [12] or films [13] with variable properties. What was insufficiently described with the rare information being scattered among several publications [14, 15] and in absence of coherent experiments addressing this question was the interaction of drugs, particularly biologics, with SF in solution. Surprisingly, a wide body of data is readily available when loading biologics to solid SF systems [6, 16-19], but the previous step, the exposure of the biologics to SF in solution and before casting into solid systems, has remained

largely unexplored. Therefore, we addressed this question of interaction of biologics and SF in solution and deciphered conditions within which various pharmaceutical parameters (aggregation, drug load of the biopolymer SF, etc.), were tailored by modulating the environment within which the drug and SF were dissolved. Based on studies concerning the *in vivo* spinning processes of spiders and silk worms, the understanding of the main influence factors was possible and transferable to drug delivery applications [20]. The identified factors were (i) the pH, directly influencing the presented charges of the SF molecule and thereby its folding pattern, (ii) the ionic strength and composition, apparently impacting the stability of SF micelles, which resulted in different levels of interaction potential with other SF molecules or different proteins and (iii) the fluid flow/shear forces, aligning the molecules for thread formation *in vivo*. The latter had only minor impact on drug delivery applications, although it favors  $\beta$ -sheet formation which is critical for the following reasons. It impacts the release kinetics, as it directly influences the diffusion coefficient [13] and the formation of the carrier vehicle, as it results in very stable and water-insoluble structures [14]. Additionally, the tendencies for this conformational change cause stability issues as aqueous solutions of SF tend to form hydrogels, especially when not stored properly [14]. This enforces the necessity to control the  $\beta$ -sheet formation and content throughout the production, storage and application of SF drug delivery systems.

In further studies we aimed for the deeper understanding of salt effects on the SF molecule and its interaction with other proteins [21]. Therefore, we thoroughly explored the effects of three Hofmeister salts [22] – NaCl (neutral), NaSCN (chaotropic) and Na<sub>2</sub>SO<sub>4</sub> (cosmotropic) – on the interaction between SF and a positively charged model protein, namely protamine. By using mainly thermodynamic and colloidal characterization methods, we were able to gain mechanistic insights in the interaction and their influence by proper salt choice. The interaction between SF and protamine without salt effects showed a multiphase pattern dependent on the ratio between protamine and SF. At very low amounts of protamine, the ITC showed endothermic signals, corresponding to an unfolding of the SF molecule and the breakdown of its micelles. This was followed by the formation of nanocomplexes and increasingly exothermic signals, indicating the formation of new binding sites for each titration point. Finally, at the maximum heat signal, coacervation processes and precipitation occurred. Afterwards, the signal was reduced with each addition of protamine, indicating that the existing binding sites got saturated. These interpretations were supported by zeta potential experiments, showing charge neutrality at the point of coacervation and NTA experiments, showing the formation of both small nanocomplexes at low and bigger precipitates at higher ratios. Additionally, the hydrophobicity was studied and further

confirmed the hypothesis. When the titration was performed in the presence of NaCl, representing a higher ionic strength without further aspects on protein stability, the reaction was qualitatively comparable. However, quantitatively reduced signals and no endothermic part were observed, which was likely the result of the lower entropy gain by the interaction and its counterion release [23], resulting in a lower ability to impact the SF structure by protamine. When substituting NaCl by the chaotropic NaSCN, the exothermic signal increased throughout the whole titration, indicating the ability of this salt to impact the SF structure and enable protamine to open up more binding sites with each addition, resulting in the highest loading compared to the other salts. The opposite was recorded for the kosmotropic Na<sub>2</sub>SO<sub>4</sub>, abolishing the interaction above a certain threshold-concentration. We were able to show that it was possible to impact and control the stability and interaction of SF by properly changing its environmental conditions and provided an entry point for future studies aiming at an optimization of pharmaceutically relevant questions around the use of SF as a drug delivery carrier.

Although our results were quite encouraging, the translation of these insights into pharmaceutical development requires further studies. The comparison between protamine and polylysine already revealed the system to be more complex and showed that our conclusions from the protamine experiments were not entirely generalizable. To influence a drug delivery systems, all players need to be taken into account and the influences of salt and pH will have to be studied individually. Nevertheless, the studies reported within this thesis provide a valid approach for the individual optimization of the solvent conditions as required for each new biologic. This impact was confirmed by stability tests, resulting in the possibility to prolong the storage of SF solutions when exposed to proper conditions (selected salts for buffering/isotonization), avoiding the  $\beta$ -sheet and thereby hydrogel formation, even at stressful storing conditions of 25°C. To our knowledge this is the first time that solutions of up to 5 % (m/V) SF were successfully stored at room temperature for several months without hydrogel formation or solidification. Although our stability study could only offer preliminary data due to relatively short storage time and since only single samples were used, these results – obtained from experimental conditions deviated from the dynamics of SF in solution including self-assembly and as one of the outcomes described here within - formed the basis of the future use of SF as a biopolymer in liquid state formulations.

The second project used a different approach for the influence of protein-protein interactions by modifying a cytokine to make it available for covalent binding in terms of site specific click chemistry [24-27]. We chose interleukin-4 (IL-4) for this purpose as it is capable of polarizing

macrophages to their M2-state [28]. M2 macrophages have anti-inflammatory properties and are important for repair processes, whereas M1 macrophages as their counterpart are pro-inflammatory and important during immune responses [29, 30]. By the covalent coupling of IL-4, we aimed for an immobilization and thereby for a permanent presentation, which was supposed to lead to a maintained and stable M2 macrophage population. This could be helpful in a variety of diseases where macrophages play a key role in the inflammation processes. These diseases include rheumatoid arthritis and pigmented villonodular synovitis where they could be detected in the synovial fluid and their M1 polarization was responsible for joint damage [31, 32]. Another example is obesity, where mainly M1 macrophages were found in the adipose tissue, which impacted the insulin resistance [33, 34]. Additionally, impaired wound healing [36-38], inflammatory lung diseases [35] and cardiovascular diseases [39, 40] are possible fields of application for a modified macrophage polarization profile.

The concrete approach of covalent binding was so far shown for a modified IL-4 analogue and a fluorescent dye. By introducing an artificial, alkyne-carrying amino acid in the IL-4 sequence we opened this way of reaction to the cytokine [24]. In-depth characterization showed that it was still bioactive when the structure was impacted by the newly introduced amino acid. Although the purity was still insufficient, we could prove the availability for click reaction and set the basis for further studies. As it is supposed to be employed in macrophage polarization to M2-state and the maintenance thereof, the successful isolation of monocytes, their activation to macrophages and finally polarization to M1 and M2 is a necessary framework for future work and all methods were established during this thesis.

The follow-up experiments for this project will have to increase the purity and click efficiency of Plk IL-4 and need to show the maintained bioactivity of the cytokine after click reaction and in an immobilized state. If successful, the immobilized IL-4 analogue will be used to polarize macrophages and it will be studied if this setup is capable of maintaining this polarization over time due to the permanently present cytokine.

With the possible applications being as various as the underlying diseases (*vide supra*), reaching the target tissue will be the future challenge. One can think of the combination with different polymers [2], targeting peptides [41] or the use of bioresponsive systems. By covalently binding the IL-4 analogue to a cleavable linker that is responsive to certain environmental conditions and/or present enzymes, one could develop a system that induces M2 macrophage activation under tailorable conditions. This concept could as well be used to avoid the presence of M1 macrophages and their possibly disadvantageous influences. In certain cases, like impaired

wound healing or the diabetic foot [42], local delivery would be realizable by linking the cytokine to surfaces or 3D-scaffolds for long-term anti-inflammatory effects.

The approach of covalent modification of a protein that has already been shown for SF [43] could allow the adaption of this method to SF in order to use it as a carrier for the IL-4 analogue. Especially concerning the local drug delivery, there are published examples for SF being usable in different forms, including scaffolds [15] and films [13], that could be suitable as a basis for local application.

In conclusion, both mechanisms of impacting the protein-protein interactions showed promising results and might be useful for an application in drug delivery devices. However, these studies were preliminary and further work on this subject is necessary, as outlined above.

## References

- [1] J. Shaji, V. Patole, Protein and Peptide drug delivery: oral approaches, *Indian journal of pharmaceutical sciences*, 70 (2008) 269-277.
- [2] R. Langer, N.A. Peppas, *Advances in biomaterials, drug delivery, and bionanotechnology*, *AIChE Journal*, 49 (2003) 2990-3006.
- [3] O. Pillai, R. Panchagnula, *Polymers in drug delivery*, *Curr Opin Chem Biol*, 5 (2001) 447-451.
- [4] G.H. Altman, F. Diaz, C. Jakuba, T. Calabro, R.L. Horan, J. Chen, H. Lu, J. Richmond, D.L. Kaplan, *Silk-based biomaterials*, *Biomaterials*, 24 (2002) 401-416.
- [5] A.J. Meinel, O. Germershaus, T. Luhmann, H.P. Merkle, L. Meinel, *Electrospun matrices for localized drug delivery: current technologies and selected biomedical applications*, *European journal of pharmaceutics and biopharmaceutics : official journal of Arbeitsgemeinschaft fur Pharmazeutische Verfahrenstechnik e.V.*, 81 (2012) 1-13.
- [6] X. Wang, E. Wenk, A. Matsumoto, L. Meinel, C. Li, D.L. Kaplan, *Silk microspheres for encapsulation and controlled release*, *J Control Release*, 117 (2007) 360-370.
- [7] K. Fu, A.M. Klibanov, R. Langer, *Protein stability in controlled-release systems*, *Nature biotechnology*, 18 (2000) 24-25.
- [8] M. van de Weert, W.E. Hennink, W. Jiskoot, *Protein instability in poly(lactic-co-glycolic acid) microparticles*, *Pharmaceut Res*, 17 (2000) 1159-1167.
- [9] L. Meinel, R. Fajardo, S. Hofmann, R. Langer, J. Chen, B. Snyder, G. Vunjak-Novakovic, D. Kaplan, *Silk implants for the healing of critical size bone defects*, *Bone*, 37 (2005) 688-698.
- [10] S. Hofmann, H. Hagenmüller, A.M. Koch, R. Müller, G. Vunjak-Novakovic, D.L. Kaplan, H.P. Merkle, L. Meinel, *Control of in vitro tissue-engineered bone-like structures using human mesenchymal stem cells and porous silk scaffolds*, *Biomaterials*, 28 (2007) 1152-1162.
- [11] F.P. Seib, G.T. Jones, J. Rnjak-Kovacina, Y. Lin, D.L. Kaplan, *pH-dependent anticancer drug release from silk nanoparticles*, *Advanced healthcare materials*, 2 (2013) 1606-1611.
- [12] F.P. Seib, E.M. Pritchard, D.L. Kaplan, *Self-assembling doxorubicin silk hydrogels for the focal treatment of primary breast cancer*, *Advanced functional materials*, 23 (2013) 58-65.
- [13] D.J. Hines, D.L. Kaplan, *Mechanisms of Controlled Release from Silk Fibroin Films*, *Biomacromolecules*, 12 (2011) 804-812.
- [14] E. Wenk, H.P. Merkle, L. Meinel, *Silk fibroin as a vehicle for drug delivery applications*, *Journal of controlled release : official journal of the Controlled Release Society*, 150 (2011) 128-141.
- [15] L. Uebersax, H.P. Merkle, L. Meinel, *Insulin-like growth factor I releasing silk fibroin scaffolds induce chondrogenic differentiation of human mesenchymal stem cells*, *J Control Release*, 127 (2008) 12-21.
- [16] V. Karageorgiou, M. Tomkins, R. Fajardo, L. Meinel, B. Snyder, K. Wade, J. Chen, G. Vunjak-Novakovic, D.L. Kaplan, *Porous silk fibroin 3-D scaffolds for delivery of bone morphogenetic protein-2 in vitro and in vivo*, *Journal of biomedical materials research. Part A*, 78 (2006) 324-334.
- [17] T. Yucel, M.L. Lovett, D.L. Kaplan, *Silk-based biomaterials for sustained drug delivery*, *J Control Release*, 190 (2014) 381-397.
- [18] Y. Srisuwan, P. Srihanam, Y. Baimark, *Preparation of Silk Fibroin Microspheres and Its Application to Protein Adsorption*, *Journal of Macromolecular Science, Part A*, 46 (2009) 521-525.



- [19] E. Wenk, A.J. Wandrey, H.P. Merkle, L. Meinel, Silk fibroin spheres as a platform for controlled drug delivery, *Journal of Controlled Release*, 132 (2008) 26–34.
- [20] V. Werner, L. Meinel, From silk spinning in insects and spiders to advanced silk fibroin drug delivery systems, *European journal of pharmaceutics and biopharmaceutics : official journal of Arbeitsgemeinschaft fur Pharmazeutische Verfahrenstechnik e.V.*, (2015) 10.1016/j.ejpb.2015.03.016..
- [21] O. Germershaus, V. Werner, M. Kutscher, L. Meinel, Deciphering the mechanism of protein interaction with silk fibroin for drug delivery systems, *Biomaterials*, 35 (2014) 3427-3434.
- [22] W. Kunz, P. Lo Nostro, B.W. Ninham, The present state of affairs with Hofmeister effects, *Current Opinion in Colloid & Interface Science*, 9 (2004) 1-18.
- [23] A.L. Becker, K. Henzler, N. Welsch, M. Ballauff, O. Borisov, Proteins and polyelectrolytes: A charged relationship, *Current Opinion in Colloid & Interface Science*, 17 (2012) 90-96.
- [24] S. Eger, M. Scheffner, A. Marx, M. Rubini, Synthesis of defined ubiquitin dimers, *Journal of the American Chemical Society*, 132 (2010) 16337-16339.
- [25] R. Huisgen, Kinetics and Mechanism of 1,3-Dipolar Cycloadditions, *Angewandte Chemie International Edition in English*, 2 (1963) 633-645.
- [26] V.V. Rostovtsev, L.G. Green, V.V. Fokin, K.B. Sharpless, A Stepwise Huisgen Cycloaddition Process: Copper(I)-Catalyzed Regioselective “Ligation” of Azides and Terminal Alkynes, *Angewandte Chemie International Edition*, 41 (2002) 2596-2599.
- [27] J.E. Moses, A.D. Moorhouse, The growing applications of click chemistry, *Chemical Society reviews*, 36 (2007) 1249-1262.
- [28] S.J. Van Dyken, R.M. Locksley, Interleukin-4- and interleukin-13-mediated alternatively activated macrophages: roles in homeostasis and disease, *Annual review of immunology*, 31 (2013) 317-343.
- [29] A. Mantovani, Macrophage diversity and polarization: in vivo veritas, *Blood*, 108 (2006) 408-409.
- [30] D.M. Mosser, J.P. Edwards, Exploring the full spectrum of macrophage activation, *Nature Reviews Immunology*, 8 (2008) 958–969.
- [31] I. Berger, H. Weckauf, B. Helmchen, V. Ehemann, R. Penzel, B. Fink, L. Bernd, F. Autschbach, Rheumatoid arthritis and pigmented villonodular synovitis: comparative analysis of cell polyploidy, cell cycle phases and expression of macrophage and fibroblast markers in proliferating synovial cells, *Histopathology*, 46 (2005) 490-497.
- [32] A. Kennedy, U. Fearon, D.J. Veale, C. Godson, Macrophages in synovial inflammation, *Frontiers in immunology*, 2 (2011) 52.
- [33] C.N. Lumeng, J.L. Bodzin, A.R. Saltiel, Obesity induces a phenotypic switch in adipose tissue macrophage polarization, *Journal of Clinical Investigation*, 117 (2007) 175-184.
- [34] C.N. Lumeng, J.B. DelProposto, D.J. Westcott, A.R. Saltiel, Phenotypic switching of adipose tissue macrophages with obesity is generated by spatiotemporal differences in macrophage subtypes, *Diabetes*, 57 (2008) 3239-3246.
- [35] B. Pernis, E.C. Vigliani, The role of macrophages and immunocytes in the pathogenesis of pulmonary diseases due to mineral dusts, *American Journal of Industrial Medicine*, 3 (1982) 133-137.

- [36] A. Sindrilaru, T. Peters, S. Wieschalka, C. Baican, A. Baican, H. Peter, A. Hainzl, S. Schatz, Y. Qi, A. Schlecht, J.M. Weiss, M. Wlaschek, C. Sunderkotter, K. Scharffetter-Kochanek, An unrestrained proinflammatory M1 macrophage population induced by iron impairs wound healing in humans and mice, *The Journal of clinical investigation*, 121 (2011) 985-997.
- [37] M.P. Rodero, K. Khosrotehrani, Skin wound healing modulation by macrophages, *International journal of clinical and experimental pathology*, 3 (2010) 643-653.
- [38] T.J. Koh, L.A. DiPietro, Inflammation and wound healing: the role of the macrophage, *Expert reviews in molecular medicine*, 13 (2011) e23.
- [39] F.K. Swirski, M. Nahrendorf, Leukocyte behavior in atherosclerosis, myocardial infarction, and heart failure, *Science*, 339 (2013) 161-166.
- [40] J. Khallou-Laschet, A. Varthaman, G. Fornasa, C. Compain, A.T. Gaston, M. Clement, M. Dussiot, O. Levillain, S. Graff-Dubois, A. Nicoletti, G. Caligiuri, Macrophage plasticity in experimental atherosclerosis, *PloS one*, 5 (2010) e8852.
- [41] S. Majumdar, T.J. Siahaan, Peptide-mediated targeted drug delivery, *Medicinal research reviews*, 32 (2012) 637-658.
- [42] V. Falanga, Wound healing and its impairment in the diabetic foot, *The Lancet*, 366 (2005) 1736-1743.
- [43] H. Zhao, E. Heusler, G. Jones, L. Li, V. Werner, O. Germershaus, J. Ritzer, T. Luehmann, L. Meinel, Decoration of silk fibroin by click chemistry for biomedical application, *J Struct Biol*, 186 (2014) 420-430.

---

## ABBREVIATIONS

ACN	Acetonitrile
AFM	Atomic force microscopy
ALOX 15	Arachidonate 15-lipoxygenase
BSA	Bovine serum albumine
CCR7	C-C chemokine receptor type 7
cDNA	Complementary deoxyribonucleic acid
CMC	Critical micelle concentration
DDS	Drug delivery system
DMSO	Dimethyl sulfoxide
dNTP	Deoxy nucleoside triphosphate
EDTA	Ethylenediaminetetraacetic acid
FAM	6-carboxyfluorescein
FCS	Fetal calf serum
FITC	Fluorescein isothiocyanate
FTIR	Fourier transformed infrared spectroscopy
GAPDH	Glyceraldehyde 3-phosphate dehydrogenase
GM-CSF	Granulocyte-macrophage colony stimulating factor
HBS	HEPES buffered saline
HCD	Higher-energy C-trap dissociation
HEPES	(4-(2-hydroxyethyl)-1-piperazineethanesulfonic acid
HPLC	High Pressure Liquid Chromatography
IFN $\gamma$	Interferon $\gamma$
IgG	Immunoglobulin G
IL-4	Interleukin-4
IPTG	Isopropyl- $\beta$ -D-thiogalactopyranosid
IRF7	Interferon regulatory factor 7
ITC	Isothermal titration calorimetry
LPS	Lipopolysaccharides from E.coli
MACS	Magnetic-activated cell sorting
MALDI	Matrix-assisted laser desorption ionization

## ABBREVIATIONS

---

M-CSF	Macrophage colony-stimulating factor
MS	Mass spectrometry
MWCO	Molecular weight cutoff
NMR	Nuclear magnetic resonance
NTA	Nanoparticle tracking analysis
OD	Optical density
PAGE	Polyacrylamide gel electrophoresis
PBS	Phosphate buffered saline
Plk	Propargyl-protected lysine derivate
PMSF	Phenylmethylsulfonylfluoride
PPAR $\gamma$	Peroxisome proliferator-activated receptor gamma
qPCR	quantitative polymerase chain reaction
relB	Transcription factor RelB
SCARB 1	Scavenger receptor class B member 1
SDS	Sodium dodecyl sulfate
SF	Silk Fibroin
SLS	Static Light Scattering
SO	Sypro Orange
TBTA	Tris[(1-benzyl-1H-1,2,3-triazol-4-yl)methyl]amine
TCEP	Tris(2-carboxyethyl)phosphine
TFA	Trifluoroacetic acid
THPTA	Tris(3-hydroxypropyltriazolyl-methyl)amine
WST	Water soluble tetrazolium

## **Data from this dissertation thesis was published or presented before as follows**

CHAPTER I: FROM SILK SPINNING IN INSECTS AND SPIDERS TO ADVANCED SILK FIBROIN DRUG DELIVERY SYSTEMS:

and

CHAPTER II: THE EFFECTS OF HOFMEISTER SALTS ON SILK FIBROIN AND ITS INTERACTION PATTERN:

### **Publications:**

\*O. Germershaus, \*V. Werner, M. Kutscher, L. Meinel, Deciphering the mechanism of protein interaction with silk fibroin for drug delivery systems, *Biomaterials*, 35 (2014) 3427-3434.

\*shared first authorship

V. Werner, L. Meinel, From silk spinning in insects and spiders to advanced silk fibroin drug delivery systems, *European Journal of Pharmaceutics and Biopharmaceutics*, (2015), 10.1016/j.ejpb.2015.03.016.

### **Poster presentations:**

Kohl, V., Germershaus, O., Kutscher, M., Meinel, L. (2013), Jahrestagung der Deutschen Gesellschaft für Biomaterialien, Erlangen “Silk Fibroin – Protein interactions and their importance for therapeutical use”

Kohl, V., Germershaus, O., Kutscher, M., Meinel, L. (2013), 3rd Conference on “Innovation in Drug Delivery: Advances in Local Drug Delivery”, Pisa (Italy) “Investigations on the mechanism of silk fibroin – protein interactions and its application for controlled drug delivery”

Kohl, V., Germershaus, O., Kutscher, M., Meinel, L. (2013), CRS Germany Local Chapter Meeting, Ludwigshafen "Characterization of Interactions between Silk Fibroin and Protamine"

Kohl, V., Germershaus, O., Kutscher, M., Meinel, L. (2012), Chem-SyStM, Wuerzburg "Mechanism of drug load on silk fibroin biomaterials"

Kohl, V., Germershaus, O., Sakalis, A., Meinel, L. (2012), CRS Germany Local Chapter Meeting, Wuerzburg "Interactions between silk fibroin and selected proteins"

### CHAPTER III: IMMOBILIZING OF INTERLEUKIN-4 FOR PERMANENT M2-ACTIVATION OF MACROPHAGES

Poster presentation:

Werner, V., Wurzel, J., Gutmann M., Lühmann T., Meinel, L. (2014), CRS Germany Local Chapter Meeting, Kiel "Site directed decoration of Interleukin 4"

# CURRICULUM VITAE

*Vera Werner, geb. Kohl*

born June 15, 1987 in Eupen, Belgium

## EDUCATION

---

2011-present **Chair of Pharmaceutics and Biopharmacy, University of Wuerzburg**

*Doctoral studies*

Advisor: Prof. Dr. Dr. Meinel

2010 **License to practice pharmacy**

2010 **Boehringer Ingelheim Pharma GmbH & Co. KG, Biberach/Riss,  
Pharmaceutical Development Germany, Formulation Development**

*Internship (6 months)*

2009-2010 **Apotheke in Hohenroth, Hohenroth**

*Internship (6 months)*

2005-2009 **University of Wuerzburg**

*Studies of Pharmacy*

2005 **Martin-Pollich-Gymnasium, Mellrichstadt, Germany**

*Abitur*

## SCIENTIFIC CONTRIBUTIONS

---

### *Journal publications*

V. Werner, L. Meinel, From silk spinning in insects and spiders to advanced silk fibroin drug delivery systems, *European Journal of Pharmaceutics and Biopharmaceutics*, (2015), 10.1016/j.ejpb.2015.03.016.

\*O. Germershaus, \*V. Werner, M. Kutscher, L. Meinel, Deciphering the mechanism of protein interaction with silk fibroin for drug delivery systems, *Biomaterials*, 35 (2014) 3427-3434.

\*shared first authorship

H. Zhao, E. Heusler, G. Jones, L. Li, V. Werner, O. Germershaus, J. Ritzer, T. Luehmann, L. Meinel, Decoration of silk fibroin by click chemistry for biomedical application, *J Struct Biol*, 186 (2014) 420-430.

M. Kutscher, W.S. Cheow, V. Werner, U. Lorenz, K. Ohlsen, L. Meinel, K. Hadinoto, O. Germershaus, Influence of salt type and ionic strength on self-assembly of dextran sulfate-ciprofloxacin nanoplexes, *International journal of pharmaceutics*, (2015), 10.1016/j.ijpharm.2015.03.022

### ***Poster presentations***

Werner, V., Wurzel, J., Gutmann M., Lühmann T., Meinel, L. (2014), CRS Germany Local Chapter Meeting, Kiel "Site directed decoration of Interleukin 4"

Kohl, V., Germershaus, O., Kutscher, M., Meinel, L. (2013), Jahrestagung der Deutschen Gesellschaft für Biomaterialien, Erlangen "Silk Fibroin – Protein interactions and their importance for therapeutical use"

Kohl, V., Germershaus, O., Kutscher, M., Meinel, L. (2013), 3rd Conference on "Innovation in Drug Delivery: Advances in Local Drug Delivery", Pisa (Italy) "Investigations on the mechanism of silk fibroin – protein interactions and its application for controlled drug delivery"

Kohl, V., Germershaus, O., Kutscher, M., Meinel, L. (2013), CRS Germany Local Chapter Meeting, Ludwigshafen "Characterization of Interactions between Silk Fibroin and Protamine"

Kohl, V., Germershaus, O., Kutscher, M., Meinel, L. (2012), Chem-SyStM, Wuerzburg "Mechanism of drug load on silk fibroin biomaterials"

Kohl, V., Germershaus, O., Sakalis, A., Meinel, L. (2012), CRS Germany Local Chapter Meeting, Wuerzburg "Interactions between silk fibroin and selected proteins"



## ACKNOWLEDGMENTS

I sincerely want to thank Prof. Dr. Dr. Meinel for the possibility to perform my thesis in his group and under his guidance. With the provision of excellent technical equipment and frequent opportunities for discussions and new ideas, he enabled me to develop myself and my project in a successful way.

I would like to express my gratitude to Prof. Dr. Robert Luxenhofer and Prof. Dr. Petra Högger for kindly accepting the review of this thesis.

I am very grateful for the additional support by Prof. Dr. Oliver Germershaus and Dr. Tessa Lühmann, who both always encouraged me and offered me their expertise and time.

Many thanks go to Cornelia Heindl, Dr. Jennifer Ritzer and Stephanie Lamer for performing experiments, which improved my work and results substantially; and to Ilona Zilkowski for the technical help with the NTA equipment.

I am thankful for the support and friendship of my colleagues, who helped me through this thesis with many fruitful discussions.

Finally, I want to thank my husband, family and friends for their constant encouragement and appreciation.

This work was supported by IZKF Wuerzburg, grant number D-218 and “DAAD PAJAKO - Partnerschaften mit Japan und Korea”.